RADIATIVE TRANSFER IN DUSTY NEBULAE

by

Roger Alan Dana

National Aeronautics and Space Administration
Grants NGR05-020-510 and NCA2-OR745-715

SUIPR REPORT NO. 722

November 1977

INSTITUTE FOR PLASMA RESEARCH
STANFORD UNIVERSITY, STANFORD, CALIFORNIA

139

RADIATIVE TRANSFER IN DUSTY NEBULAE

by

Roger Alan Dana

National Aeronautics and Space Administration
Grants NGR05-020-510
and
NCA2-OR745-715

SUIPR REPORT NO. 722

November 1977

Institute for Plasma Research
Stanford University
Stanford, California

ABSTRACT

This study is directed toward two problems of radiative transfer in dusty nebulae; the effects of dust scattering on observable optical and infrared parameters and the accuracy of approximate solutions.

We solve the equation of radiative transfer in a static and homogeneous, but not necessarily uniform, distribution of gas and dust around a central empty core with a point source of energy at its center. While the physics of the gas is well understood, we characterize the dust properties by a phenomenological extinction cross section, albedo and parameters describing the anisotropy of dust scattering. For ultraviolet photons we simultaneously solve ionization equilibrium equations for the gas, and for infrared photons we calculate a self-consistent dust temperature. Ray tracing is used to solve for the angular dependence of the intensity.

The addition of ionized gas adds two serious complications to the solution of the equation of radiative transfer. First, the initial ionization structure and volume of the Strömgren sphere are known only approximately a priori. Second, the gas goes from almost completely ionized to neutral very rapidly at the Strömgren radius. Methods of handling these two complications while solving the boundary value problem of radiative transfer have been developed.

We find that in most cases variation of the albedo (the ratio of the dust scattering cross section to the dust extinction cross section) for ultraviolet photons does not have significant effects on optical observable parameters, and in all cases these effects are much smaller than the effects of the variation of the frequency dependence of the

dust absorption coefficient. Increasing the albedo of the dust strongly affects the emitted infrared spectrum from the dust by reducing the amount of energy the dust can absorb and by reducing the variation of the dust temperature in the nebula. When we compare our solutions with more approximate solutions of radiative transfer, we find that the diffusion approximation, the on-the-spot approximation, and the Eddington approximation are very accurate when the assumptions of the approximation are met.

ACKNOWLEDGMENTS

I would like to sincerely thank Professor Vahé Petrosian for suggesting this problem and for his guidance in its solution. I am also grateful to Dr. Larry Caroff of NASA-Ames Research Center for computer time, for critically reading my thesis and for many helpful comments throughout the course of this work. Thanks are also due to Joshua Knight and Kile Baker for assistance with numerical and programming techniques and for many discussions of broader significance.

I would also like to thank Mrs. Mary Oshima and Ms. Jane Johnston for skillfully typing the manuscript and for cheerful encouragement when needed.

A very special thank you goes to my wife Armella whose encouragement and love made this work possible and meaningful and whose draftsmanship made the figures possible.

Finally, I gratefully acknowledge the financial support for this research from the National Aeronautics and Space Administration through grants NGR05-020-510 and NCA2-OR745-715.

CONTENTS

ILLUSTRATIONS

LIST OF TABLES

1. INTRODUCTION

1.1 Historical Background and Physical Ideas

The study of HII regions is very old. In the seventeenth century Christiaan Heygens described the Orion Nebula. However, the emission mechanisms of gaseous nebula were not understood until after 1925 when quantum theory made it possible to interpret the emission line spectra quantitatively. Even then there was some confusion as to the nature of forbidden lines. It was not until 1927 that S. I. Bowen correctly identified the [OIII] 5007Å, 4959Å doublet that had previously been ascribed to the unknown element "nebulium". Since about 1960 radio observations have been used to map the free-free emission from HII regions. Molecular emission was discovered in 1963. Since 1965 NASA has sponsored a program of infrared observations from high-flying aircraft. In May 1975 the 91 cm Gerard P. Kuiper Airborne Observatory became operational. With this instrument it has become possible to make high quality infrared broad band photometric observations of HII regions.

HII regions are important to astrophysics for four main reasons: First, they are short-lived phenomenon that may yield information on star formation. Second, they trace spiral arms and study of their properties as a function of location may yield information on the formation and maintenance of the spiral arms. Third, they enable the determination of elemental abundances and variations of abundances in the galaxy. And fourth, there exists the possibility of determining the properties of dust grains in HII regions where independent optical and radio observations can be made to determine the

structure of the nebula. Points three and four are also valid for planetary nebulae. In addition, the study of planetary nebulae yields information on post main sequence evolution of stars and the formation of white dwarfs.

The source of ionizing photons that maintain the ionization in a detectable HII region is, in most cases, a hot central star with an effective temperature $T^* \geq 30{,}000^\circ K$. Photoionization adds energy to free electrons that quickly thermalize to an effective temperature $5000^\circ K \leq T_e \leq 10{,}000^\circ K$. If the electron density is less than about 10^4 cm^{-3}, then these electrons excite low-lying energy levels in the ions which depopulate through forbidden lines. Permitted lines in the spectra are produced by recombinations. When the central source is very hot, high degrees of ionization can be achieved by photoionization. The ionization structures of the gas are given by a balance between photoionization and recombination. At the temperatures and densities found in gaseous nebulae, collisional ionizations of hydrogen and helium are negligible.

The infrared radiation comes from two separate sources. First is free-free and free-bound emission from the gas. The luminosity of this emission can be predicted from observed Hβ or radio luminosities. However, the second source, which is usually 10^2 to 10^3 times larger than the predicted infrared emission from the gas, comes from the thermal emission of the dust grains embedded in the nebula. These grains compete with the gas for the absorption of ionizing photons. The energy absorbed by the dust is reradiated as infrared continuum radiation at an effective temperature given by a steady state balance between absorption and emission. The

evidence that the dust grains are mixed with the ionized gas comes first from optical photographs that show dark absorption features inside of HII regions and second from the infrared maps which are usually centered on the radio (which are measuring free-free emission from the ionized gas) maps.

Internal dust alters the observable parameters of a nebula by absorbing and scattering radiation. The dust competes with the gas in absorption of ionizing radiation and, hence, alters the ionization structures of the gas and reduces the volume of the Strömgren sphere. If dust extinction varies with frequency, then the electron temperature structure of the nebula will be qualitatively different from nebulae with only gas.

1.2 Observational Data

HII regions are excited by O and B stars or clusters of stars of population I. Throughout the nebula hydrogen and helium are singly ionized and most of the other elements are primarily in singly or doubly ionized states. The gas density varies typically from 10 to $10^3 cm^{-3}$ with compact objects having densities as high as $10^4 cm^{-3}$. The gas is highly non-uniform with bright knots, rims and condensations observable on most optical photographs. There is also evidence for neutral condensations inside of the ionized reiongs. The mass of ionized gas in HII regions is usually in the range 10^2 to $10^4 M_\odot$ where the lower limit is a strong function of observational selection. The spectra of HII regions contains HI recombination lines and collisionally excited forbidden lines of NII, OII, OIII and NeIII.

Planetary nebulae are isolated shells of gas that have been ejected recently while their central stars evolved into white dwarfs.

The central sources are much hotter ($T^* \sim 100{,}000^{\circ}K$) than HII regions and the gas exhibits higher degrees of ionization, including HeIII, OIII, NeIII, NeIV and NeV. The mass in the shell is usually in the range 0.1 to $1.0M_{\odot}$ (the densities are in the range 10^2 to $10^4 cm^{-3}$) and it is expanding at 25 km/sec typically. The mean lifetime of planetary nebulae is a few times 10^4 years.

A common feature that many HII regions, planetary nebulae and other infrared objects have is the qualitative shape of their infrared spectra. On Figure 1 we have plotted the infrared spectra of DR21 (a compact HII region), W3(OH)/IRS8 (an HII region), NGC7027 (a planetary nebula), and NGC 1068 (a Seyfert galaxy). All of these spectra have a sharply increasing infrared flux in the near infrared ($\lambda < 10\mu$), a roughly power-law section in the mid infrared ($10\mu \leq \lambda \leq 100\mu$) and a Rayleigh-Jeans tail in the far infrared ($\lambda > 100\mu$). The similarity of these spectra indicate two things. First, a similar mechanism of producing the infrared emission is probably operating in all of the objects. Second, the power-law portion indicates that for dust emission models, there must be a range of effective dust temperature in the model and thus that radiative transfer is important in describing the temperature variation. The absorption feature at 10μ that is apparent in the spectra of NGC7027 and NGC1068 is believed to be a feature of silicates. This feature is observed in the spectra of most galactic infrared sources.

1.3 The Model

In order to study and understand the effects of dust extinction (absorption and scattering) on the observable optical and infrared

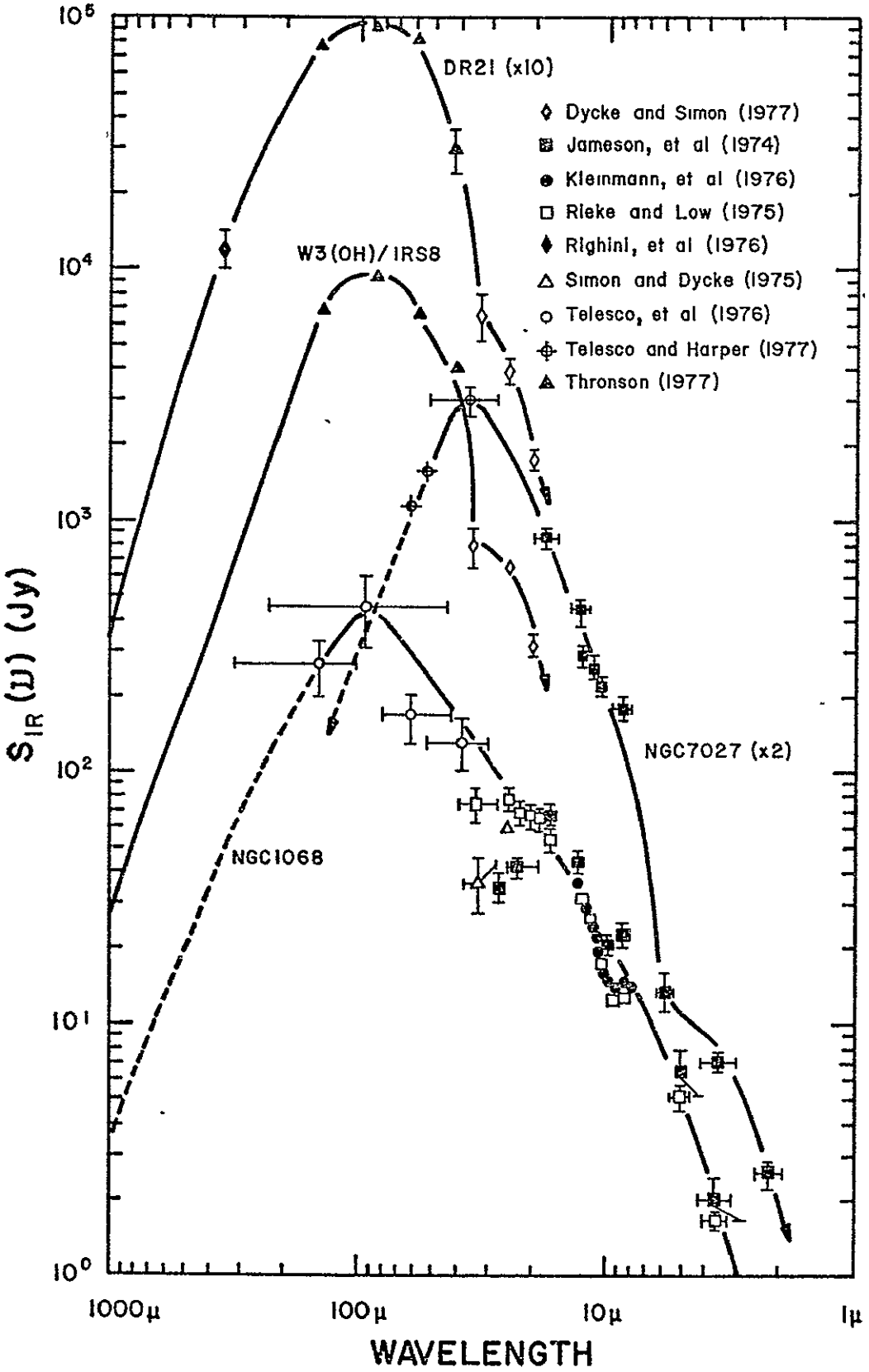

Fig. 1. Infrared Spectra of HII Regions. DR21 is a compact HII region, W3(OH)IRS8 is a HII region, NGC7027 is a planetary nebula, and NGC1068 is a Seyfert galaxy.

parameters of dusty nebulae and to assess the accuracy of more approximate solutions of radiative transfer, we are going to construct a numerical model that not only calculates the ionization structure of the gas but also that is able to handle general anisotropic dust scattering. We will assume a static and homogeneous (but not necessarily uniform) spherical distribution of gas and dust around a central empty core with a point source of energy at its center. We assume spherical geometry because the radio and infrared maps of many nebulae suggest spherical symmetry and also because of the numerical simplifications which result from the symmetry. The static and homogeneous assumptions are harder to justify observationally. Dynamical models of HII regions (c.f. e.g. Yorke 1977) show that the dynamic time scales are much longer than the photon diffusion time scales. Our models are, therefore, a "snapshot" in the evolution of an HII region. We will ignore the ionization shock fronts which exist at the Strömgren radius (i.e. at the transition zone where the gas goes from being almost fully ionized to neutral). Clumpiness can be taken into account in our equations. However, in order to simplify the interpretation of our results, we assume the nebula to be homogeneous. We will also assume that our model HII regions are <u>just</u> ionization bound (i.e. there is no matter outside of the Strömgren sphere) and that there is no radiation incident on the nebulae from outside.

1.4 Method of Solution

It is scattering by dust that requires detailed numerical solutions of the radiative transfer problem because it makes the equation of radiative transfer non-local. We solve the equation of radiative

transfer using the quasi-diffusion method (QDM) described by Leung (1975), which is based on methods of solution developed by Auer (1971) and by Hummer and Rybicki (1971). The equation of radiative transfer can be solved analytically for stellar photons (i.e. photons from the central source which have not interacted with the nebula) because of the point source approximation. We therefore find it convenient to divide the radiation intensity into two parts. First are stellar photons that came directly from the central point source. They remain stellar photons until they interact with the nebula. Second are diffuse photons that are produced in the nebula by scattering or by emission. The total intensity is then just the sum of stellar and diffuse photons. The QDM is then used to solve for the anisotropic diffuse radiation field.

Leung's method (QDM) first defines the Eddington factor, $f_\nu(r)$, and a configuration function, $\zeta_\nu(r)$, which describe the anisotropy of the diffuse radiation field. These functions are used to solve a moment or diffusion equation. The functions $f_\nu(r)$ and $\zeta_\nu(r)$ are initially set equal to the values they would have for isotropic radiation. The solution of the moment equation is used to calculate the scattering source function and ray tracing is used to solve for the angular dependence of the diffuse intensity. With the angular dependence, the functions $f_\nu(r)$ and $\zeta_\nu(r)$ can be updated. This iterative procedure is continued until convergence of the diffuse intensity is achieved.

The addition of ionized gas adds two serious complications to this iterative procedure. First, the initial ionization structure and volume of the Strömgren sphere can only be approximated. Thus

the iteration procedure will change not only the ionization structure but also the outer boundary (or Strömgren radius) of the model . The second complication is the very rapid change in the ionization at the Strömgren radius. Methods of handling these two complications have been a major consideration in the development of our numerical models.

Finally, we will find it convenient to divide the intensity of radiation into three frequency bins ultraviolet photons ($0 < \lambda \leq 912$Å, i.e. photons which can photoionize hydrogen) hereafter referred to as UV photons, optical or OP photons (912Å $< \lambda < 1\mu$), and infrared or IR photons ($1\mu \leq \lambda < \infty$). We separately solve the equation of radiative transfer in each of these frequency bins, simultaneously solving the ionization equilibrium equations for UV photons and calculating the dust temperature and infrared emissions for IR photons.

1.5 Summary of Results

We summarize here some of the major conclusions of this work. We find that the major effect of dust scattering is to transport photons (that otherwise would be absorbed in the inner parts of the nebula) from the inner to the outer parts of the nebula. Consequently, dust scattering can substantially increase the volume of the Strömgren sphere over what it would be for a nebula with the same central source luminosity and dust extinction coefficient but without scattering. We also find that in most cases variation of the albedo (the ratio of the dust scattering cross section to the dust extinction cross section) for UV photons does not have significant effects on optical observable parameters and in all cases, these effects are much smaller than the effects of the variation

of the frequency dependence of the dust absorption coefficient. Increasing the albedo of the dust in the frequency ranges primarily responsible for dust heating decreases the total infrared luminosity of the nebula and the dust temperature at the same relative radius by reducing the amount of energy the dust can absorb. Also increasing albedo reduces the variation of the dust temperature from the inner to the outer radius of the nebula and hence makes the emitted IR spectrum narrower in frequency.

When we compare our QDM solutions with more approximate solutions of radiative transfer, we find that the diffusion approximation and the on-the-spot approximation are very accurate when the assumptions of the approximations are met. In addition, the Eddington approximation, which assumes that the diffuse radiation field is isotropic, gives accurate values for all observable parameters in most cases.

2. MATHEMATICAL FORMULATION

2.1. Equation of Radiative Transfer

The equation of radiative transfer in spherically symmetric nebulae is (c.f. e.g. Chandrasekhar 1960)

$$\mu \frac{\partial I_\nu(r,\mu)}{\partial r} + \frac{(1-\mu^2)}{r} \frac{\partial I_\nu(r,\mu)}{\partial \mu} = - K_\nu(r) I_\nu(r,\mu) + \frac{1}{2} K^s_\nu(r) \int_{-1}^{+1} d\mu' \, P_\nu(\mu,\mu') \, I_\nu(r,\mu') + J_\nu(r) \tag{2.1}$$

where $I_\nu(r,\mu)$ is the photon intensity,* μ is the cosine of the angle between the photon propagation direction and the radial direction, $K_\nu(r)$ is the extinction coefficient, $K^s_\nu(r)$ is the scattering coefficient, $P_\nu(\mu,\mu')$ is the scattering phase function which determines the probability of scattering from the direction μ' into the direction μ for photons of frequency ν, and $J_\nu(r)$ is the emissivity per unit volume, time, solid angle, and frequency interval. For UV and OP photons, the contribution to $J_\nu(r)$ is from recombinations in the gas and for IR photons, $J_\nu(r)$ is given by Kirchhoffs Law as

$$J_\nu(r) = \epsilon_{IR}(r,\nu) N_\nu(T_d) \tag{2.2}$$

where $\epsilon_{IR}(r,\nu)$ is the infrared emissivity of the dust grains and

---

* Throughout this discussion we shall be dealing with number of photons rather than energy of radiation, so that $I_\nu(r,\mu)$ is the number of photons per unit area, time, solid angle, and frequency interval.

$$N_\nu(T_d) = \frac{2\nu^2/c^2}{e^{(h\nu/kT_d)}-1} \tag{2.3}$$

is the photon emission for the dust effective temperature T_d. The phase function $P_\nu(\mu,\mu')$ is normalized so that

$$\frac{1}{2}\int_{-1}^{+1} d\alpha\ P_\nu(\alpha) = 1 \tag{2.4}$$

where α is the cosine of the scattering angle. The phase function will be expanded in terms of Legendre polynomials as

$$P_\nu(\mu,\mu') \approx \sum_{\ell=0}^{L} \omega_\ell P_\ell(\mu)\ P_\ell(\mu')\ , \tag{2.5}$$

where the frequency dependence of the coefficients have been suppressed. The normalization condition [Eq. (2.4)] gives $\omega_0 \equiv 1$. The average cosine of the scattering angle, g_1, and the average of the square of the cosine of the scattering angle, g_2, are defined in terms of the ω_ℓ's as

$$\frac{1}{3}\omega_1 = g_1 = \frac{1}{2}\int_{-1}^{+1} d\alpha\ \alpha\ P_\nu(\alpha) \tag{2.6}$$

$$\frac{2}{15}\omega_2 = g_2 = \frac{1}{2}\int_{-1}^{+1} d\alpha\ \alpha^2\ P_\nu(\alpha)\ . \tag{2.7}$$

2.2. Moments of the Intensity

The n^{th} moment of the intensity is defined as

$$M_\nu^n(r) = \frac{1}{2}\int_{-1}^{+1} d\mu\ \mu^n\ I_\nu(r,\mu)\ . \tag{2.8}$$

Most physical processes in nebulae depend on the mean intensity $J_\nu(r) = M_\nu^0(r)$. In addition, the flux, $H_\nu(r) = M_\nu^1(r)$, and the K-Integral, $K_\nu(r) = M_\nu^2(r)$ are needed to solve equation (2.1). The net number of photons passing outward through a spherical shell of radius r is

$$S_\nu(r) = 4\pi r^2\ [4\pi\ H_\nu(r)]\ . \tag{2.9}$$

Two additional functions will be useful in solving Eq. (2.1). First the Eddington factor [Leung (1975) calls this the anisotropy factor] is defined as

$$f_\nu(r) \equiv K_\nu^D(r)/J_\nu^D(r)\ . \tag{2.10}$$

This is also called the variable Eddington factor (Auer and Mihalas, 1970). Second is a function introduced by Auer (1971),

$$\zeta_\nu(r) = \exp\left\{\int_{r_0}^{r} dt\ t^{-1}\ [3 - 1/f_\nu(t)]\right\} \tag{2.11}$$

where r_0 is the inner radius of the nebula. Leung calls $\zeta_\nu(r)$ the configuration function. The Eddington approximation is equivalent to setting $f_\nu(r) \equiv 1/3$ and $\zeta_\nu(r) \equiv 1$. Throughout this discussion, $f_\nu(r)$ and $\zeta_\nu(r)$ will refer to the diffuse radiation field only.

The point source approximation for stellar photons is expressed as

$$I_\nu^*(r,\mu) = 2\, J_\nu^*(r)\, \delta(\mu-1) \ , \qquad (2.12)$$

and the moments of the stellar intensity are,

$$J_\nu^*(r) = H_\nu^*(r) = K_\nu^*(r) \ . \qquad (2.13)$$

2.3. Combined Moment Equation

The intensity in Eq. (2.1) is first divided into the diffuse and stellar parts, noting that only the diffuse radiation field has sources in the nebula. Integrating Eq. (2.1) over μ from -1 to +1 using the weighting functions 1 and μ, gives the zeroth and first moments, respectively. The zeroth moment equations are

$$dS_\nu^*(r)/dr = - \kappa_\nu(r)\, S_\nu^*(r) \qquad (2.14)$$

for stellar photons, and

$$\frac{1}{r^2}\ \frac{d}{dr}\left[r^2\, H_\nu^D(r)\right] = - \kappa_\nu^a(r)\, J_\nu^D(r) + \kappa_\nu^s(r)\, J_\nu^*(r) + j_\nu(r) \qquad (2.15)$$

for diffuse photons, where $\kappa_\nu^a(r)$ and $\kappa_\nu^s(r)$ are the absorption and scattering coefficient, respectively ($\kappa_\nu = \kappa_\nu^a + \kappa_\nu^s$) . The solution to Eq. (2.14) is

$$S_\nu^*(r) = S_\nu^*(r_0)\, e^{-\tau_\nu} \qquad (2.16)$$

where $S_\nu^*(r_0)$ will be determined from the boundary conditions, and the extinction optical depth τ_ν is defined as

$$\tau_\nu(r) = \int_{r_0}^{r} \kappa_\nu(r')\, dr' \ . \tag{2.17}$$

Equation (2.16) combined with Eqs. (2.9), (2.12), and (2.13) completely describes the transfer of stellar photons once $\kappa_\nu(r)$ is known. The remainder of this chapter will be concerned with solving for the diffuse radiation field.

The first moment equation for diffuse photons is

$$\frac{d}{dr} K_\nu^D(r) + \frac{1}{r}\left[3\, K_\nu^D(r) - J_\nu^D(r)\right] = - \left[\kappa_\nu(r) - g_1 \kappa_\nu^s(r)\right] H_\nu^D(r) + g_1 \kappa_\nu^s(r)\, J_\nu^*(r) \ . \tag{2.18}$$

Substituting Eqs. (2.10) and (2.11) into Eq. (2.18) and using Eq. (2.15) to eliminate $H_\nu^D(r)$ gives the combined moment equation

$$\frac{1}{r^2}\frac{d}{dr}\left\{\frac{r^2}{\zeta_\nu(r)\left[\kappa_\nu(r) - g_1\kappa_\nu^s(r)\right]}\ \frac{d}{dr}\left[f_\nu(r)\ \zeta_\nu(r)\ J_\nu^D(r)\right]\right\} = \kappa_\nu^a(r)\ J_\nu^D(r) + \frac{1}{r^2}\ \frac{d}{dr}\left[\frac{g_1 \kappa_\nu^s(r) r^2\ H_\nu^*(r)}{\kappa_\nu(r) - g_1 \kappa_\nu^s(r)}\right] + J_\nu(r) \ . \tag{2.19}$$

Subsequently, Eq. (2.19) will be referred to as the JAY equation. Given the source function and the functions $f_\nu(r)$ and $\zeta_\nu(r)$, this is a linear second-order differential equation for $J_\nu^D(r)$ that is easy to solve once the boundary conditions have been specified (see Appendix A). Before discussing the rest of the quasi-diffusion method (QDM), some simplifying notation and normalized fluxes will be introduced. (On the first time through, the reader should skip directly to section 2.5)

2.4. Optical Depth and Normalized Fluxes

The dust in this model is characterized primarily by its extinction optical depth, $d\tau$, at the Lyman limit ($\nu = \nu_0$, $h\nu_0 = 13.6$ eV) as

$$d\tau = K_{\nu_0}(r)\, dr = n_d(r_0)\, \mathcal{A}_d(r)\, \sigma_{d,0}\, dr \tag{2.20}$$

where $n_d(r_0)$ is the dust number density at the inner surface of the nebula, $\mathcal{A}_d(r)$ describes the radial variation of the dust density ($\mathcal{A}_d(r_0) = 1$), and $\sigma_{d,0}$ is the extinction cross section of the dust evaluated at the Lyman limit. The total extinction optical depth of the dust at the Lyman limit is

$$\tau(r) = n_d(r_0)\, \sigma_{d,0} \int_{r_0}^{r} dr'\, \mathcal{A}_d(r') , \tag{2.21}$$

which, for a power-law dependence of $\mathcal{A}_d(r)$,

$$\mathcal{A}_d(r) = (r_0/r)^{\alpha} , \tag{2.22}$$

gives

$$\tau = \begin{cases} \dfrac{R_0}{1-\alpha}\left[(R/R_0)^{1-\alpha} - 1\right] & \alpha \neq 1 \\ R_0 \ln (R/R_0) & \alpha = 1 \end{cases} \tag{2.23}$$

where

$$R = n_d(r_0)\, \sigma_{d,0}\, r , \quad R_0 = R(r_0) . \tag{2.24}$$

Once the function $\mathcal{A}_d(r)$ (or α for power-law density variations) has been specified, the dust optical depth is characterized by the parameter R_0. For uniform nebulae, the value of R_0 has little effect on the

properties of the model as long as $R_0 \ll \tau_1$ ($\tau_1 = \tau(r_1)$ where r_1 is the outer radius of the nebula). However, if $\alpha > 1$, then $R_0/(\alpha-1)$ is the value of τ as $r \to \infty$, and the properties of the model become dependent on the value of R_0.

The frequency dependence of the dust extinction optical depth is defined by the function $f_d(\nu)$ as

$$\tau_\nu(r) = f_d(\nu)\, \tau(r) , \quad f_d(\nu_0) \equiv 1 . \tag{2.25}$$

One other parameter, the albedo, is needed to completely specify the dust properties in this model. The albedo is defined as

$$\omega_\nu \equiv \kappa_\nu^s / \kappa_\nu . \tag{2.26}$$

Only the dust number density is allowed to vary with radius so that ω_ν, $f_d(\nu)$ and $\sigma_{d,0}$ are constant throughout the nebulae.

The normalized mean intensity (and similarly, all moments of the intensity), denoted by a hat, is defined as*

$$\hat{J}_\nu(r) = \frac{16\pi^2\, J_\nu(r)}{\left[n_d(r_0)\sigma_{d,0}\right]^2 S_0} \tag{2.27}$$

where $\hat{J}_\nu$ has units of 1/Hz and S_0 is the number of ionizing photons per second coming from the central point source, i.e.

$$S_0 = \int_{\nu_0}^{\infty} d\nu [16\pi^2\, r_0^2\, H_\nu^*(r_0)] . \tag{2.28}$$

---

* For nebulae without dust, the factor $n_d(r)\sigma_{d,0}$ in Eq. (2.24) and in other equations throughout this discussion is replaced by $n(r)\sigma_0$ where $n(r)$ is the hydrogen number density and σ_0 is the hydrogen photoionization cross section at the Lyman limit.

The normalized net flux through a spherical shell is defined as

$$\hat{S}_\nu(r) = \frac{16\pi^2 R^2 H_\nu(r)}{\left[n_d(r_0)\sigma_{d,0}\right]^2 S_0} \tag{2.29}$$

so that for stellar photons,

$$\int_{\nu_0}^{\infty} d_\nu \hat{S}^*_\nu(r_0) \equiv 1 . \tag{2.30}$$

In a similar manner, the normalized emission "source function" (the source function is usually defined as $J_\nu(r)/\kappa_\nu(r)$) is defined as

$$\hat{\Sigma}^E_\nu(r) = \frac{16\pi^2 R^2 J_\nu(r)}{\left[n_d(r_0)\ \sigma_{d,0}\right]^3 d_d(r)\ S_0} \tag{2.31}$$

and the normalized extinction, absorption and scattering coefficients are

$$\begin{aligned} \hat{\kappa}_\nu &= \kappa_\nu(r)/n_d(r)\ \sigma_{d,0} \\ \hat{\kappa}^a_\nu &= \kappa^a_\nu(r)/n_d(r)\ \sigma_{d,0} \\ \hat{\kappa}^s_\nu &= \kappa^s_\nu(r)/n_d(r)\ \sigma_{d,0} \equiv \omega_\nu . \end{aligned} \tag{2.32}$$

For nebulae without gas, $\hat{\kappa}_\nu = f_d(r)$. However, $\hat{\kappa}^s_\nu = \omega_\nu$ in all cases because gas does not scatter radiation, resonance scattering of Lyman-α radiation is, in fact, absorption followed immediately by an isotropic emission (see §3 9).

Although the reason for defining these normalized functions may appear obscure at the moment, it will be seen later that once the dust parameters are specified, the properties of the model are determined by one parameter, namely $\hat{S}_0$. The value of this parameter determines the total extinction optical depth of the dust and determines the relative importance of gas and dust.

Finally, in terms of these normalized parameters the JAY equation takes the form

$$\frac{d}{d\tau}\left\{\frac{R^2/\zeta_\nu}{\hat{\kappa}_\nu - g_1\,\omega_\nu}\,\frac{d}{d\tau}\left[f_\nu(\tau)\zeta_\nu(\tau)\hat{J}^D_\nu(\tau)\right]\right\} = \hat{\kappa}^a_\nu\,R^2\,\hat{J}^D_\nu(\tau) + \frac{d}{d\tau}\left[\frac{g_1\,\omega_\nu\,\hat{S}^*_\nu(\tau)}{\hat{\kappa}_\nu - g_1\,\omega_\nu}\right] - \omega_\nu\,\hat{S}^*_\nu(\tau) - \hat{\Sigma}^E_\nu(\tau)\,, \tag{2.33}$$

where only $g_1\omega_\nu$ does not depend on optical depth, or equivalently on radius.

2.5. Ray Equation

Once the JAY equation has been solved, the QDM uses its solution to calculate the scattering source function. This section describes how ray tracing is used to solve for the angular dependence of the diffuse radiation field. The diffuse intensity $I^D_\nu(r,\mu)$ is calculated along a ray characterized by its distance of closest approach to the center of the nebula (see Fig. 2). This calculation is necessary because the diffuse intensity is, in general, highly anisotropic. For a similar treatment, see Hummer and Rybicki (1971).

If we transform into (r,b) coordinates, (where $r \geq b$), then

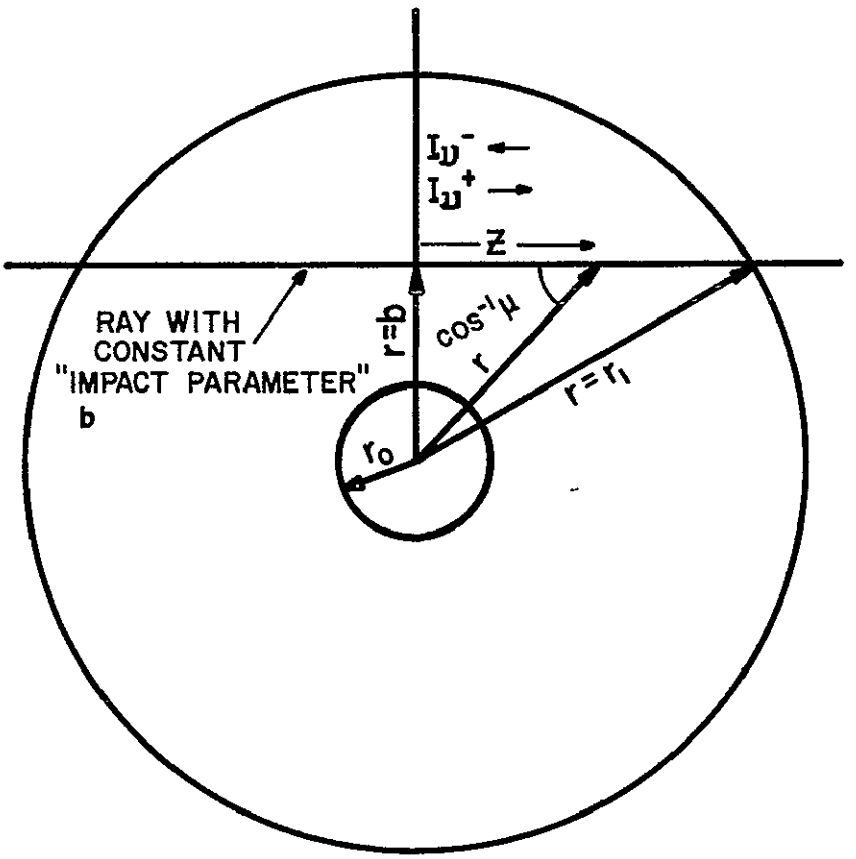

Fig. 2. Geometry of Ray Tracing

$$\mu = \pm \sqrt{1 - b^2/r^2} \tag{2.34}$$

and due to the symmetry, only values of (r,b) for which $z \geq 0$ need to be considered. Because μ is double valued, I_ν^D is separated into I_ν^+ for $0 \leq \mu \leq 1$ and I_ν^- for $-1 \leq \mu < 0$. $I_\nu^+(I_\nu^-)$ denotes the diffuse intensity along a ray going in the outward (inward) direction. By this division, only positive values of μ need to be considered.

Along a ray, Eq. (2.1) for diffuse photons becomes

$$\mu \partial I_\nu^+ / \partial r = - K_\nu(r) I_\nu^+ + J_\nu(r) + \Sigma_\nu^s(r,\mu) \tag{2.35}$$

and

$$\mu \partial I_\nu^- / \partial r = K_\nu(r) I_\nu^- - J_\nu(r) - \Sigma_\nu^s(r,\mu) , \tag{2.36}$$

where Σ_ν^s is the scattering "source function",

$$\Sigma_\nu^s(r,\mu) = \frac{1}{2} K_\nu^s(r) \int_{-1}^{+1} d\mu' \, p_\nu(\mu,\mu')[I_\nu^D(r,\mu') + I_\nu^*(r,\mu')] , \tag{2.37}$$

and from Fig. 2, it is easy to see that $\mu \, \partial/\partial r = \partial/\partial z$.

It is now convenient to define an intensity-like function, U_ν, and a flux-like function, V_ν, as

$$U_\nu = \frac{1}{2}(I_\nu^+ + I_\nu^-) \tag{2.38}$$

$$V_\nu = \frac{1}{2}(I_\nu^+ - I_\nu^-) . \tag{2.39}$$

Alternately adding and subtracting Eqs. (2.35) and (2.36) gives

$$\mu \, \partial U_\nu / \partial r = - K_\nu(r) V_\nu \tag{2.40}$$

and

$$\mu \partial V_\nu / \partial r = - K_\nu(r) U_\nu + J_\nu(r) + \Sigma^s_\nu(r,\mu) \tag{2.41}$$

from which V_ν can be eliminated to obtain a second order differential equation in U_ν,

$$\mu \frac{\partial}{\partial r} \left[\frac{\mu}{K_\nu(r)} \frac{\partial}{\partial r} U_\nu(r,\mu) \right] = K_\nu(r) U_\nu(r,\mu) - J_\nu(r) - \Sigma^s_\nu(r,\mu) , \tag{2.42}$$

or in terms of normalized parameters

$$\mu \frac{\partial}{\partial \tau} \left[\frac{\mu}{\hat{K}_\nu} \partial \hat{U}_\nu / \partial \tau \right] = \hat{K}_\nu \hat{U}_\nu - \hat{\Sigma}^E_\nu(\tau)/R^2 - \hat{\Sigma}^s_\nu(\tau,\mu) . \tag{2.43}$$

Subsequently, this shall be referred to as the RAY equation. Like the JAY equation, once the source functions are given, this is a linear second order boundary value problem that is easily solved for $U_\nu(r,\mu)$ using the difference equations in Appendix A. From the solution, $J^D_\nu(r)$ and all higher moments, $f_\nu(r)$, and $\zeta_\nu(r)$ can be calculated.

The scattering "source function" in normalized units is obtained by combining Eq. (2.5) for $L = 2$, with Eqs. (2.12) and (2.37) to give

$$\hat{\Sigma}^{s}_{\nu}(\tau,\mu) = \omega_{\nu} \sum_{\ell=0}^{2} \omega_{\ell} P_{\ell}(\mu) \frac{1}{2} \int_{-1}^{+1} d\mu' P_{\ell}(\mu') \left[\hat{I}^{D}_{\nu}(r,\mu') + 2\hat{J}^{*}_{\nu}(r)\delta(\mu'-1)\right]$$

$$= \omega_{\nu}\left\{\left[\hat{J}^{D}_{\nu}(\tau) + \hat{J}^{*}_{\nu}(\tau)\right] + 3g_{1}\mu\left[\hat{H}^{D}_{\nu}(\tau) + \hat{J}^{*}_{\nu}(\tau)\right]\right. \tag{2.44}$$

$$\left. + \frac{15}{4} g_{2} (3\mu^{2}-1) \left[\hat{J}^{*}_{\nu}(\tau) - \frac{1}{2} \hat{J}^{D}_{\nu}(\tau) + \frac{3}{2} \hat{K}^{D}_{\nu}(\tau)\right]\right\}.$$

When evaluating $\hat{\Sigma}^{s}_{\nu}(r,\mu)$, $\hat{J}^{D}_{\nu}(\tau)$ is taken from the solution of the JAY equatic and $\hat{H}^{D}_{\nu}(\tau)$ and $\hat{K}^{D}_{\nu}(\tau)$ are taken from the previous iteration (see § 1.4). On the first iteration, $\hat{K}^{D}_{\nu}(\tau)$ is given by the Eddington approximation and $\hat{H}^{D}_{\nu}(\tau)$ is set equal to zero. This iteration procedure is explained in detail in section 6.2. $\hat{J}^{*}_{\nu}(\tau)$ is obtained from the solution of Eq. (2.14) combined with Eq. (2.9) giving

$$\hat{J}^{*}_{\nu}(\tau) = \hat{S}^{*}_{\nu}(\tau)/R^{2} . \tag{2.45}$$

Computations have shown that this iteration procedure is rapidly converging and stable. It will be shown later that the relative strengths of $\hat{\Sigma}^{s}_{\nu}(r,\mu)$ and $\hat{\Sigma}^{E}(r)/R^{2}$ are determined by the parameter $\hat{S}_{0}$. For convenience in calculating fluxes, the RAY equation is solved on an (r,b) grid, where experience has shown that the most accurate solutions are obtained when the b grid is equal to the r grid. However, ten b grid points are added for $b < r_{0}$ in order to accurately calculate moments of $I^{D}_{\nu}(r,\mu)$ at $r = r_{0}$.

The moments of $I^{D}_{\nu}(r,\mu)$ are calculated from U_{ν} using the relations

$$\hat{J}_\nu^D(\tau) = \int_0^1 d\mu\ \hat{U}_\nu(R,\mu) = R^{-1} \int_0^R dB\ B(R^2-B^2)^{-1/2}\ \hat{U}_\nu(R,B), \qquad (2.46)$$

$$\hat{H}_\nu^D(\tau) = \int_0^1 d\mu\ \mu\hat{V}_\nu(R,\mu) = R^{-2} \int_0^R dB\ B\ \hat{V}_\nu(R,B)\ , \qquad (2.47)$$

and

$$\hat{K}_\nu^D(\tau) = \int_0^1 d\mu\ \mu^2\ \hat{U}_\nu(R,\mu) = R^{-3} \int_0^R dB\ B\ (R^2-B^2)^{1/2}\ \hat{U}_\nu(R,B) \qquad (2.48)$$

where $B = n_d(r_0)\ \sigma_{d,0}\ b$. To calculate $\hat{J}_\nu^D$ and $\hat{K}_\nu^D$, it is assumed that $U_\nu(R,B)$ varies linearly between two adjacent B values. $\hat{H}_\nu^D$ is calculated from Eq. (2.40) using a three-point approximation for the radial derivative of $U_\nu(R,B)$. Again a linear approximation for the variation of $U_\nu(R,B)$ with B is used.

2.6. Boundary Conditions

In order to make the boundary conditions clear, we will reiterate the basic structural assumptions of the model.

1. Spherically symmetric nebula around a central empty core with a point source at the origin.
2. No radiation is incident from outside of the nebula.
3. There is no mass outside of the Stromgren sphere.

The spectrum of the central source must be specified. For example it can be taken to be a black body of arbitrary temperature, or for stars which have an effective temperature in the range 30,000° to 50,000° K, the spectra given by the model atmospheres of Auer and Mihalas (1972) have

been used. In normalized units, the solution of the equation of radiative transfer for stellar photons (Eq. 2.14) is

$$\hat{S}^{*}_{\nu}(\tau) = \hat{S}^{*}_{\nu}(0)\ e^{-\tau_{\nu}} \tag{2.49}$$

where Eq. (2.30) gives the normalization condition for $\hat{S}^{*}_{\nu}(0)$. This form for the stellar flux will allow the Strömgren sphere radius to be defined in terms of the normalized flux, $\hat{S}_{\nu}$, rather than having to rely on a less consistent (from model to model) ionization structure criterion (e.g. defining the Strömgren radius as the point where hydrogen is 90% neutral).

The JAY and RAY equations for diffuse radiation are two-point boundary value problems with mixed boundary conditions. For the JAY equation, the inner boundary condition is expressed physically as the fact that there is no source of diffuse photons inside of the central core i.e. $\hat{S}^{D}_{\nu}(\tau = 0) = 0$. The less physical boundary conditions on $\hat{J}^{D}_{\nu}$ are obtained from Eq. (2.18) as

$$\frac{R^2}{\zeta_{\nu}} \frac{d}{d\tau} \left[f_{\nu}(\tau)\zeta_{\nu}(\tau)\ \hat{J}^{D}_{\nu}(\tau) \right] \Bigg|_{\tau=0} = g_1\ \omega_{\nu}\ \hat{S}^{*}_{\nu}(0) \tag{2.50}$$

(JAY equation inner B.C.)

$$\frac{R^2}{\zeta_{\nu}} \frac{d}{d\tau} \left[(f_{\nu}(\tau)\zeta_{\nu}(\tau)\hat{J}^{D}_{\nu}(\tau) \right] \Bigg|_{\tau=\tau_1} \tag{2.51}$$

$$= g_1\omega_{\nu}\ \hat{S}^{*}_{\nu}(\tau_1) - [\hat{k}_{\nu} - g_1\omega_{\nu}]\ f^{B}_{\nu}\ R^2\ \hat{J}^{D}_{\nu}(\tau_1)$$

(JAY equation outer B.C.)

where the boundary factor, f_ν^B, is defined as

$$f_\nu^B \equiv \hat{H}_\nu^D(\tau_1)/\hat{J}_\nu^D(\tau_1) \ . \tag{2.52}$$

For an isotropic radiation field, $f_\nu^B \equiv 1/2$. This value is used on the first iteration and for the Eddington approximation. For the QDM, f_ν^B is evaluated from the solution of the ray equation. Note should be made of the fact that, because $U_\nu(r_1,\mu) = V_\nu(r_1,\mu)$, only the function U_ν is needed to evaluate f_ν^B .

The boundary conditions for the RAY equation are physically simple. At the symmetry line (r=b) , $I_\nu^+ = I_\nu^-$ and at the outer boundary $I_\nu^- \equiv 0$. Using Eq. (2.40), the inner boundary condition becomes

$$d\ U_\nu/dz\big|_{r=b} = 0 \quad \text{for} \quad r > r_0 \tag{2.53}$$

(RAY equation inner B.C.)

and

$$d\ U_\nu/dz\big|_{r=r_0} = 0 \quad \text{for} \quad r \le r_0 \tag{2.54}$$

where d/dz is used because $\mu(r=b) = 0$. The outer boundary condition is

$$\left[\mu \partial U_\nu/\partial r + K_\nu\ U_\nu\right]\Big|_{r=r_1} = 0 \ . \tag{2.55}$$

(RAY equation outer B.C.)

3. PHYSICAL PROCESSES IN THE GAS

3.1. Basic Assumptions

All of the physical processes used in this chapter are discussed in detail in the excellent book by Donald E. Osterbrock, Astrophysics of Gaseous Nebulae (Osterbrock 1974) hereafter referred to as AGN. We review some of the basic processes briefly. For densities found in most gaseous nebulae (i.e. 10^2 to 10^4 H atoms per cm^3), plasma effects are negligible and, for most atomic processes (except for forbidden transitions) electron collisional transitions are unimportant. The gas in this model is composed of $n(r)$ hydrogen atoms per cm^3, $Yn(r)$ helium atoms (where $Y \approx 0.1$) and a small amount of trace elements (we include the following elements O, N, C, Ne, Ar and S). It is assumed, because the abundance of the trace elements is small compared to H and He, that they do not affect either the mean intensity or the electron density inside of the Strömgen sphere. For computational convenience, it is assumed that all photoionization cross sections are zero for frequencies $\nu > 10\ \nu_0$.

Two other basic assumptions are made about the gas. First, all atoms are photoionized from the ground state. The mean life-time of a hydrogen atom against photoionization, τ_{ION}, is given by

$$\tau_{ION}^{-1} \approx \int_{\nu_0}^{\infty} d\nu\ \sigma_H(\nu)\ 4\pi\ J_\nu \qquad (3.1)$$

where $\sigma_H(\nu)$ is the photoionization cross section for hydrogen. For many nebulae (and all of the model nebulae that we have calculated),

10^3 sec $\leq \tau_{ION} \leq 10^6$ sec. However, the mean life-time for spontaneous radiative transitions of hydrogen excited states is 10^{-4} sec to 10^{-8} sec for all states except 2^2S for which it is ≈ 0.1 sec. All of these mean life-times are much smaller than τ_{ION}. The second assumption is that all recombinations are to $n = 1$ or $n = 2$ states. This is done for two reasons By the assumptions of Case B (AGN §4.2), recombinations to states with $n \geq 3$ eventually lead to population of the $n = 2$ state. Also, the recombination rates to $n \geq 3$ states are much smaller than the rates to $n = 1$ or $n = 2$ states. This assumption allows us to reduce the number of frequencies that we must consider and thus, to do a more detailed and accurate calculation of the important aspects of the problem.

Finally, the electron temperature can be calculated (see AGN Chapter 3) and it has been shown (Hjellming 1966 and Rubin 1968) that the variation of $T_e(r)$ can be quite strong, especially at the Strömgren radius. However, the effect of dust is to damp out the variations of T_e (Balick 1975 and Sarazin 1977). For this reason, our models assume an isothermal electron temperature ($T_e = 10^{4\,\circ}$K). This assumption will have little effect on the ionization structures of hydrogen and helium because of the weak temperature dependence ($\approx T_e^{-1/2}$) of the recombination coefficients, but will affect the intensities of certain lines.

3.2. Ionization and Recombination

The ionization equilibrium equation for any two successive stages of ionization i and $i+1$ for any element X may be written in terms of the total mean intensity, the electron density, $n_e(r)$, and atomic constants as

$$\frac{n(X^{i+1})}{n(X^i)} = \frac{\int_{\nu_i}^{\infty} d\nu\ \sigma_{X^i}(\nu)\ 4\pi\ J_\nu(r) + \delta n(H^+)}{n_e\ \alpha_{X^{i+1}} + \delta' n(H^0)} \qquad (3.2)$$

where

$$\sum_{i=0}^{N} n(X^i) = n(X)\ , \qquad (3.3)$$

$n(X)$ is the total number density of the element X, N is the number of ions with photoionization potentials, $h\nu_i$, less than $10h\nu_0$, $\sigma_{X^i}(\nu)$ is the photoionization cross section of the species X^i, $\alpha_{X^{i+1}}$ is the recombination coefficient for the reaction $X^{i+1} + e \rightarrow X^i + \nu$ and δ and δ' are the charge exchange coefficients for O and N (AGN p. 36). We have neglected dielectric recombination because, in general, it has less than a 10% effect on the ionization structures (Sarazin 1977), and we have neglected collisional ionization because of the relatively low ($T_e \approx 10^4\ ^\circ K \ll h\nu_0/k$) electron temperatures found in most gaseous nebulae. As was mentioned in §3.1, $J_\nu(r)$ and n_e are both calculated inside the Stromgen sphere assuming the presence of H, He, and dust. Table I gives the photoionization cross sections and the recombination coefficients for the heavy elements. The frequency integral in Eq. (3.2) and all other frequency integrals in this discussion are calculated assuming that the integrand varies as a power law between two frequency grid points. This assumption is necessary because the ionization edges of the gas result in large variations in $J_\nu(r)$ as a function of frequency, especially at the Strömgren radius.

TABLE I. PHOTOIONIZATION CROSS SECTIONS† AND RECOMBINATION COEFFICIENTS

TRANSITION	$\sigma_{th}(\times 10^{-18}\,cm^2)$	REF	ν_{th}/ν_0	β	s	$\alpha_{rec}(\times 10^{-13}\,cm^3/s)$	REF
$O^o(^3P)$-$O^+(^4S)$	2.94	3	1.002	2 661	1 0		
$O^o(^3P)$-$O^+(^2D)$	3.85	3	1.242	1.242	1 5	3 1	1
$O^o(^3P)$-$O^+(^2P)$	2.26	3	1.367	4.311	1.5		
$O^+(^4S)$-$O^{+2}(^3P)$	7.32	3	2 583	3.837	2 5	20 0	1
$O^{+2}(^3P)$-$O^{+3}(^2P)$	3.65	3	4 040	2.014	3.0	51 0	1
$O^{+3}(^2P)$-$O^{+4}(^1S)$	1.27	3	5.693	0 831	3.0	96.0	1
$O^{+4}(^1S)$-$O^{+5}(^2S)$	0.78	2	8.376	2 6	3.0	12 0	1
$C^o(^3P)$-$C^+(^2P)$	12.19	3	0 828	3.317	2.0	4.7	1
$C^+(^2P)$-$C^{+2}(^1S)$	4.60	3	1.793	1.950	3.0	23.0	1
$C^{+2}(^1S)$-$C^{+3}(^2S)$	1.60	2	3.521	2.6	3 0	32.0	1
$C^{+3}(^2S)$-$C^{+4}(^1S)$	0 68	2	4.743	1.0	2 0	75.0	1
$N^o(^4S)$-$N^+(^3P)$	11.42	3	1.069	4.287	2.0	4.1	1
$N^+(^3P)$-$N^{+2}(^2P)$	6.65	3	2 177	2.860	3 0	22.0	1
$N^{+2}(^2P)$-$N^{+3}(^1S)$	2.06	3	3.489	1.626	3 0	500.0	1
$N^{+3}(^1S)$-$N^{+4}(^2S)$	1.08	2	5.697	2.6	3.0	65.0	1
$N^{+4}(^2S)$-$N^{+5}(^1S)$	0.48	2	7.199	1.0	2.0	150.0	1
$Ne^+(^1S)$-$Ne^+(^2P)$	5.35	3	1 586	3.769	1.0	2.2	1
$Ne^+(^2P)$-$Ne^{+2}(^3P)$	4.16	3	3.012	2 717	1 5		
$Ne^+(^2P)$-$Ne^{+2}(^1D)$	2.71	3	3.256	2 148	1.5	15.0	1
$Ne^+(^2P)$-$Ne^{+2}(^1S)$	0.52	3	3.529	2.126	1.5		
$Ne^{+2}(^3P)$-$Ne^{+3}(^4S)$	1.80	3	4.666	2.277	2.0	44.0	1
$Ne^{+2}(^3P)$-$Ne^{+3}(^2D)$	2.50	3	5.060	2.346	2 5	91.0	1
$Ne^{+2}(^3P)$-$Ne^{+3}(^2P)$	1.48	3	5.253	2.225	2.5	150.0	1

TABLE I. (Contd)

TRANSITION	$\sigma_{th}(\times 10^{-18} cm^{+2})$	REF	ν_{th}/ν_0	β	s	$\alpha_{rec}(\times 10^{-13} cm^3/s)$	REF
$N_e^{+3}(^4S)-N_e^{+4}(^3P)$	3.11	3	7 141	1 963	3.0	230.0	1
$N_e^{+4}(^3P)-N_e^{+5}(^2P)$	1.40	3	9 282	1.471	3.0	280 0	1
$S^{\circ}(^3P)S^{+}(^4S)$	12.6	6	0 762	1 0	0 264		
$S^{\circ}(^3P)-S^{+}(^4S)$	10.6	6	1.471	1.0	2.33	4.1	1
$S^{\circ}(^3P)-S^{+}(^4S)$	2.56	5	7.354	1.0	3.19		
$S^{+}(^4S)-S^{+2}(^3P)$	8.20	6	1 716	1 0	0.837	18 0	1
$S^{+2}(^3P)-S^{+3}(^2P)$	4.37	6	2.561	1.0	0.721	27.0	1
$S^{+3}(^2P)-S^{+4}(^1S)$	0.290	6	3.478	1 0	-1.95	57 0	1
$S^{+4}(^1S)-S^{+5}(^2S)$	11.8	6	5.345	1.0	2 24	120 0	1
$S^{+5}(^2S)-S^{+6}(^1S)$	7.56	6	6.475	1 0	2.23	170.0	1
$Ar^{\circ}(^1S)-Ar^{+}(^2P)$	30.0	4	1.159	3.0	2.0	3.82	4
$Ar^{+}(^2P)-Ar^{+2}(^3P)$	30.0	4	2.032	2.5	2.0	23.8	4
$Ar^{+3}(^4S)-Ar^{+4}(^3P)$	2.67	4	2.996	2 0	1.0	118.0	4
$Ar^{+3}(^4S)-Ar^{+4}(^3P)$	0.591	4	4.398	3 0	2.0	84.0	4
$Ar^{+4}(^3P)-Ar^{+5}(^2P)$	0.450	4	5.518	4.61	2.0	146.3	4
$Ar^{+5}(^2P)-Ar^{+6}(^1S)$	8.0	4	6.693	0 4	2.0	120.0	4

† Photoionization Cross Sections

$$\sigma_{X^i}(\nu) = \sigma_{th}[\beta(\nu/\nu_{th})^{-S} + (1-\beta)\ (\nu/\nu_{th})^{-(S+1)}]$$

(σ_{th} and ν_{th} are the threshold cross section and frequency)

References

1. Aldrovandi and Pe'quignot (1973)
2. Flower (1968)
3. Henry (1970)
4. Kirkpatrick (1972)
5. Weisheit (1974)
6. Weisheit and Collins (1976)

The ground state recombination coefficient is related to the photoionization cross section by the equation (AGN p. 239 ff)

$$\alpha^{1}_{X^{i+1}}(\nu) = \frac{4\pi\,\omega_i}{\omega_{i+1}}\,(\nu/c)^2\,\left(\frac{h^2}{2\pi\,M_e k\,T_e}\right)^{3/2}\,\sigma_{X^{i}}(\nu)\,e^{h(\nu_i-\nu)/k\,T_e} \qquad (3.4)$$

$(\nu \geq \nu_i)$

where ω_i and ω_{i+1} are the statistical weights of the states i and $i+1$, and M_e and T_e are the electron mass and temperature, respectively. The frequency dependence of $\alpha^{1}_{X^{i+1}}(\nu)$ is $\sigma_{X^{i}}(\nu)e^{-h\nu/kT_e}$ where $\sigma_{X^{i}}(\nu)$, for H and He, is a decreasing function of frequency and $h\nu/kT_e \ll 1$. The spectrum of ionizing radiation from the central source goes approximately as $\nu^2\,e^{-h\nu/kT^*}$ where $T^* \geq 3 \times 10^4\,^{\circ}K$. Thus $\alpha^{1}_{X^{i+1}}(\nu)$ for H and He has a much narrower characteristic width in frequency than does the central source and we shall approximate $\alpha^{1}_{X^{i+1}}(\nu)$ as

$$\alpha^{1}_{X^{i+1}}(\nu_{eff}) = \alpha^{1}_{X^{i+1}}\,\delta(\nu-\nu_{eff}) \qquad (3.5)$$

where

$$\nu_{eff} \equiv \int_{\nu_i}^{\infty} d\nu\;\nu\,\alpha^{1}_{X^{i+1}}(\nu)/\alpha^{1}_{X^{i+1}} \qquad (3.6)$$

and

$$\alpha^{1}_{X^{i+1}} = \int_{\nu_i}^{\infty} d\nu\;\alpha^{1}_{X^{i+1}}(\nu) \qquad (3.7)$$

This approximation is valid as long as $\nu_{eff}/\nu_1 - 1 \ll 1$. We shall refer to this radiation as a "line".

3.3. Hydrogen

For hydrogen we define the ionized fraction as

$$x = n(H^+)/n(H)$$
$$(1-x) = n(H^0)/n(H) \ . \tag{3.8}$$

The photoionization cross section and recombination coefficient (Hummer and Seaton 1963) are

$$\sigma_H(\nu) = \sigma_0 \ f_H(\nu), \sigma_0 = 6.3 \times 10^{-18} \ cm^2$$
$$f_H(\nu) = \begin{cases} (\nu_0/\nu)^3 & \text{for } \nu \geq \nu_0 \\ 0 & \text{for } \nu < \nu_0 \end{cases} \tag{3.9}$$
$$\alpha_H = 4.13 \times 10^{-18} \ cm^3/sec \ (T_e = 10^4 \ ^\circ K) \ .$$

Recombination to the ground state is the only source of UV photons from hydrogen, and for $T_e = 10^4 \ ^\circ K$, equations (3.5) - (3.7) give $\nu_{eff} = 1.06 \ \nu_0$. The ground states recombination coefficient is given by Eqs. (3.4) and (3.5) with $\omega_0 = 2$ and $\omega_1 = 1$. Under the assumptions of §3.1, there are 3 OP lines produced by recombinations to $n \geq 2$ states. Each recombination to an excited state produces a Balmer continuum (Ba-C) line. In a manner similar to the treatment of the $n = 1$ recombination line, we will treat the spectrum of the Ba-C as a δ-function. However, because these photons cannot ionize hydrogen, we will set the Ba-C effective frequency equal to $0.25\nu_0$.

Of the recombinations to excited states, two-thirds eventually populate the 2^2P state and one-third populate the 2^2S state. The

2^2P state depopulates through the emission of a Lyman-α (Ly-α) photon at $\nu = 0.75\nu_0$. Our model includes resonance scattering of Ly-α photons (see §3.9). We assume that this does not alter, however, the ground state criterion for photoionizations. For hydrogen, the resonance scattering cross section (at line center) is $\sigma_H(\text{Ly-}\alpha) \approx 9300\ \sigma_0$ for $T_e = 10^4\ ^\circ K$. The $2^2S - 1^2S$ forbidden transition produces a 2-photon continuum with the most probable distribution $\nu_1 = \nu_2 = 1/2\ \nu_{\text{Ly-}\alpha}$. The emission rates of these OP photons are

$$\begin{aligned} \varepsilon_{\text{Ba-C}} &= xn(r)\ n_e\ \alpha_H^B \\ \varepsilon_{\text{Ly-}\alpha} &= 2/3\ \varepsilon_{\text{Ba-C}} \\ \varepsilon_{\text{2-photon}} &= 2 \times \frac{1}{3}\ \varepsilon_{\text{Ba-C}} \end{aligned} \qquad (3.10)$$

where $\alpha^B_{X^{i+1}}$ is defined as

$$\alpha^B_{X^{i+1}} = \sum_{n=2}^{\infty} \alpha^n_{X^{i+1}} \ , \qquad (3.11)$$

and $\alpha^n_{X^{i+1}}$ is the recombination coefficient to the state n.

3.4. Singly Ionized Helium

The fraction of He atoms that are singly ionized, y^+, and the fraction that are neutral, y^0, are defined as

$$\begin{aligned} y^0 &= n(He^0)/n(He) = n(He^0)/Yn(r) \\ y^+ &= n(He^+)/n(He) = n(He^+)/Yn(r) \ . \end{aligned} \qquad (3.12)$$

In the ionization equilibrium equation [Eq. (3.2)], the ionization potential of He^0 is 24.6 eV or $\nu_i = 1.807\ \nu_0$, and the photoionization cross section and recombination coefficient (Hummer and Seaton 1964) are

$$\sigma_{He^0}(\nu) = \sigma_{He^0,0}\, f_{He^0}(\nu) ,$$

$$f_{He^0}(\nu) = \begin{cases} e^{-0.73(\nu/\nu_0 - 1.807)} & \nu \geq 1.807\ \nu_0 \\ 0 & \nu < 1.807\ \nu_0 \end{cases}$$

$$\sigma_{He^0,0} = 7.35 \times 10^{-18}\ cm^3 \qquad (3.13)$$

$$\alpha_{He^+} = 4.31 \times 10^{-14}\ cm^3/sec \quad (T_e = 10^4\ ^\circ K) .$$

The addition of helium ($\approx$ 10% by number) to a nebula has a strong effect on the hydrogen ionization structure because H and He compete for UV photons with frequencies $\nu \geq 1.807\ \nu_0$. This effect is lessened if $T_* \leq 4 \times 10^4\ ^\circ K$ or if dust preferentially absorbes photons with $\nu > 1.807\ \nu_0$ so that the helium Stromgren sphere is smaller than the hydrogen sphere.

Recombinations of singly ionized helium can produce one of four UV lines and one of three OP lines. Ground state recombinations produce photons at an effective frequency $\nu_{eff} = 1.87\ \nu_0$ ($T_e = 10^4\ ^\circ K$) at a rate given by Eqs. (3.4) and (3.5) with $\omega_0 = 1$ and $\omega_1 = 2$. Three-fourths of the recombinations to excited levels are to the triplet state 2^3S and one-fourth are to the singlet states 2^1P and 2^1S. The 2^3S state is metastable with a half-life of $\approx 10^4$ sec. It decays to the 1^1S state via emission of a single photon forbidden line at 19.8 eV ($\nu = 1.456\ \nu_0$). If $n_e \geq 5 \times 10^3\ cm^{-3}$, the dominant mode of depopulation is through collisional excitation to the 2^1S or 2^1P states. For many HII regions, $n_e \leq 10^3\ cm^{-3}$ so this process will not be considered. Although the

life-time of the 2^3S state only marginally meets the life-time criterion of §3.1, a detailed analysis of excited state populations is beyond the scope of this work. Of the singlet state recombinations, one-third are to the 2^1S state and two-thirds are to the 2^1P state. The 2^1S state depopulates (life-time $\approx$ 0.02 sec) by a two photon continuum with $h\nu_1 + h\nu_2 = 20.7$ eV. The probability that a UV photon is produced is 0.56 and the most probable frequency of the photon is $\nu = 1.183\ \nu_0$. Finally, the 2^1P state emits a He Ly-α photon at $\nu = 1.522\ \nu_0$ that is reasonantly scattered by helium (at the line center, $\sigma_{He^0}(\text{Ly-}\alpha) \approx 2600\ \sigma_{He^0,0}$ for $T_e = 10^{4\,\circ}$K). Each of the excited state recombinations discussed above produces a Ba-C line with slightly different frequencies. These OP lines are at frequencies $\nu = 0.241\ \nu_0$, $0.285\ \nu_0$ and $0.351\ \nu_0$ corresponding to recombination to the states 2^1P, 2^1S, and 2^3S, respectively.

3.5. Doubly Ionized Helium

The atomic structure of He^{++} is hydrogenic with $Z = 2$. The photoionization cross section is, therefore,

$$\sigma_{He^+}(\nu) = \sigma_{He^+,0}\ f_{He^+}(\nu)$$

$$f_{He^+}(\nu) = \begin{cases} (4\nu_0/\nu)^3 & \nu \geq 4\nu_0 \\ 0 & \nu < 4\nu_0 \end{cases} \qquad (3.14)$$

$$\sigma_{He^+,0} = \sigma_0/4 = 1.575 \times 10^{-18}\ \text{cm}^3,$$

and the recombination coefficient (Seaton 1960) is

$$\alpha_{He^{++}} = 2.176 \times 10^{-12}\ \text{cm}^3/\text{sec}\ . \qquad (3.15)$$

The fraction of helium that is doubly ionized, y^{++}, is defined as

$$y^{++} = n(He^{++})/n(He) = n(He^{++})/Yn(r) \ . \qquad (3.16)$$

The ionization potential of He^{+} is 54.4 eV or $\nu_1 = 4\ \nu_0$. Even the hottest O stars produce few photons with $\nu \geq 4\nu_0$ so that doubly ionized helium will only play a significant role in the properties of gaseous nebulae if $T^* \sim 10^5\ ^\circ K$ (i.e. planetary nebulae).

Recombinations of He^{++} produce four UV lines and no OP lines with the assumptions of §3.1. Ground state recombinations produce photons at an effective frequency $\nu_{eff} = 4.06\ \nu_0$ ($T_e = 10^4\ ^\circ K$) at a rate given by Eqs. (3.4) and (3.5) with $\omega_1 = 2$ and $\omega_2 = 1$ Recombinations to excited states produce a Ba-C photon with $\nu = \nu_0$. Two-thirds of these recombinations result in Ly-α photons with frequency $\nu = 3\nu_0$ that are resonance scattered by He^{+} ($\sigma_{He^+}(\text{Ly-}\alpha) \approx 9300\ \sigma_{He^+,0}$ at line center). One-third of the recombinations result in population of the 2^2S state that depopulates through a two-photon continuum. The most probable distribution in frequency is $\nu_1 = \nu_2 = 1/2\ \nu_{He^+,\text{Ly-}\alpha}$. The emission coefficients are given in Table II.

3.6. Recombination Source Term and Extinction Coefficient

The recombination source term for UV and OP photons that appears in the JAY and RAY equations has the general form

$$J_\nu(r) = n(r)\ n_e(r)\ \Re(r)/4\pi \qquad (3.17)$$

where

$$n_e(r) = \left[x + Y(y^{+} + 2y^{++})\right]\ n(r) \ , \qquad (3.18)$$

TABLE II. RECOMBINATION LINES OF HYDROGEN AND HELIUM

SOURCE	LINE	ν/ν_0	EMISSION††
H^0	1^1S Rec†	1.06	α_H^1
H^0	Ly-α	0.75	$2/3\ \alpha_H^B$
H^0	$2^1S - 1^1S$	0.375	$2 \times \frac{1}{3} \times \alpha_H^B$
H^0	Ba-C	0.25	α_H^B
He^0	1^1S Rec	1.87	$\alpha_{He^+}^1$
He^0	Ly-α	1.522	$1/4 \times 2/3\ \alpha_{He^+}^B$
He^0	$2^3S - 1^1S$	1.456	$3/4\ \alpha_{He^+}^B$
He^0	$2^1S - 1^1S$†††	1.183	$1/4 \times 1/3\ (0\ 56)\ \alpha_{He^+}^B$
He^0	2^3S Rec	0.351	$3/4\ \alpha_{He^+}^B$
He^0	2^1S Rec	0.285	$1/4 \times 1/3\ \alpha_{He^+}^B$
He^0	2^1P Rec	0.241	$1/4 \times 2/3\ \alpha_{He^+}^B$
He^+	1^1S Rec	4.06	$\alpha_{He^{++}}^1$
He^+	Ly-α	3.0	$2/3\ \alpha_{He^{++}}^B$
He^+	$2^1S - 1^1S$	1.5	$2 \times 1/3\ \alpha_{He^{++}}^B$
He^+	Ba-C	1.0	$\alpha_{He^{++}}^B$

† Recombination to the 1^1S state.

†† Normalized by $n_e n(X^1)$.

††† The 44% of the $2^1S - 1^1S$ transition photons which are not in the UV have been neglected.

the recombination term, $\mathcal{R}$, is

$$\mathcal{R}(r) = x\left[\alpha_H^1(\nu) + \alpha_H^B \Delta_H\right] + Yy^+\left[\alpha^1_{He^+}(\nu) + \alpha^B_{He^+}\Delta_{He^+}\right] + Yy^{++}\left[\alpha^1_{He^{++}}(\nu) + \alpha^B_{He^{++}}\Delta_{He^{++}}\right] \tag{3.19}$$

and the $\alpha^1_{X^{1+1}}(\nu)$ terms are approximated by δ-functions at appropriate effective frequencies. For UV photons, the Δ terms are (see Table II)

$$\Delta_H = 0$$

$$\Delta_{He^+} = \nu_0^{-1}\left\{3/4\ \delta(\nu/\nu_0 - 1.456) + \frac{1}{4}\left[2/3\ \delta(\nu/\nu_0 - 1.522) + \frac{1}{3}(0.56)\ \delta(\nu/\nu_0 - 1.183)\right]\right\} \tag{3.20}$$

$$\Delta_{He^{++}} = \nu_0^{-1}\left[2 \times \frac{1}{3}\delta(\nu/\nu_0 - 1.5) + 2/3\ \delta(\nu/\nu_0 - 3.0) + \delta(\nu/\nu_0 - 1.0)\right]$$

and for OP photons,

$$\Delta_H = \nu_0^{-1}\left[2 \times \frac{1}{3}\delta(\nu/\nu_0 - 0.375) + 2/3\ \delta(\nu/\nu_0 - 0.75) + \delta(\nu/\nu_0 - 0.25)\right]$$

$$\Delta_{He^+} = \nu_0^{-1}\left\{3/4\ \delta(\nu/\nu_0 - 0.351) + \frac{1}{4}\left[\frac{2}{3}\delta(\nu/\nu_0 - 0.241) + 1/3\ \delta(\nu/\nu_0 - 0.285)\right]\right\} \tag{3.21}$$

$$\Delta_{He^{++}} = 0\ .$$

In normalized units, the "source function" [Eq. (2.31)] is

$$\hat{\Sigma}^{E}_{\nu}(\tau) = \left[\frac{R^2 \mathcal{A}_g^2(\tau)}{\mathcal{A}_d(\tau)}\right] \frac{[x + Y(y^{+} + 2y^{++})]}{\hat{S}_0 \alpha^{B}_{H}} \mathcal{R}(\tau) \tag{3.22}$$

where

$$n(r) = n(r_0)\mathcal{A}_g(r) , \quad \mathcal{A}_g(r_0) = 1 \tag{3.23}$$

and

$$\hat{S}_0 \equiv \frac{S_0[n_d(r_0)\sigma_{d,0}]^3}{4\pi\, n^2(r_0)\, \alpha^{B}_{H}} . \tag{3.24}$$

The value of the dimensionless parameter $\hat{S}_0$, mentioned previously in §2.4, determines much of the physics of the model by specifying the relative roles of gas emission and dust extinction. When $\hat{S}_0 \ll 1$, then $\hat{\Sigma}^{E}_{\nu}(r)$ is large and recombination photons dominate dust heating. Alternatively, when $\hat{S}_0 \gg 1$, recombination photons have little effect on the dust thermal structure. Once the dust parameters have been specified, it is $\hat{S}_0$ that determines the total dust extinction optical depth of the nebula (see Appendix B).

The extinction coefficient for UV photons is

$$\begin{aligned} K_{\nu}(r) = {} & n_d(r)\, \sigma_{d,0} f_d(\nu) + n(r)[(1-x)\sigma_0\, f_H(\nu) \\ & + Y\, y^{0} \sigma_{He^{0},0}\, f_{He}(\nu) + Y y^{+} \sigma_{He^{+},0}\, f_{He^{+}}(\nu)] \end{aligned} \tag{3.25}$$

where the radial functions x, y^0, and y^+ vary slowly until they reach their respective Strömgren radii. In normalized units, Eq. (3.25) is

$$\begin{aligned} \hat{K}_{\nu}(\tau) = {} & f_d(\nu) + [\mathcal{A}_g(R)/\mathcal{A}_d(R)] \times \left\{\frac{1-x}{\epsilon} f_H(\nu)\right. \\ & \left. + Y\left[\hat{He}^{0} \frac{y^{0}}{\epsilon} f_{He^{0}}(\nu) + \hat{He}^{+} \frac{y^{+}}{\epsilon} f_{He^{+}}(\nu)\right]\right\} \end{aligned} \tag{3.26}$$

where

$$\hat{He}^{0} = \sigma_{He^{0},0} / \sigma_{0}$$
$$\hat{He}^{+} = \sigma_{He^{+},0} / \sigma_{0} \qquad (3.27)$$

and

$$\varepsilon \equiv \frac{n_d(r_0)\sigma_{d,0}}{n(r_0)\sigma_0} \quad . \qquad (3.28)$$

The parameter ε determines the "width" of the hydrogen and helium transition zones (i.e. regions where the functions x and y^{+} go from 1 to 0) by specifying the optical depth of the gas relative to that of dust. The functions $(1-x)/\varepsilon$, y^{0}/ε and y^{+}/ε are all independent of ε except near their respective Strömgren radii. For normal interstellar dust-to-gas mixtures, $\varepsilon \approx 2 \times 10^{-4}$ (and as described before for nebulae without dust, $\varepsilon = 1$) .

Equations (3.25) and (3.26) are valid for OP photons if we note that f_{H} , $f_{He^{0}}$, and $f_{He^{+}}$ are zero except for Ly-α photons.

3.7. Solution of the Ionization Equations

In dimensionless form, Eq. (3.2) can be written for hydrogen and helium as

$$x(X^{i}) = x(X^{i+1})[x+Y(y^{+}+2y^{++})] \; A_{X^{i+1}} \; R^{2} \mathcal{D}_{g}(R)/u(X^{i}) \qquad (3.29)$$

where

$$u(X^{i}) = \int_{\nu_1}^{\infty} d\nu \; f_{X^{1}}(\nu)[\hat{S}^{*}_{\nu}(\tau) + R^{2} \hat{J}^{D}_{\nu}(\tau)]$$

$$+ R^{2} \sum_{J=1}^{N^{1}} f_{X^{1}}(\nu_J) \hat{J}^{D}_{\nu_J}(\tau) \; , \qquad (3.30)$$

and the summation is over the number, N^i, of "lines" that can ionize the ion X^i (e.g. for hydrogen, this summation is over all 9 UV lines). The coefficients $A_{X^{i+1}}$ are

$$A_H = \epsilon\, \alpha_H / \hat{S}_0\, \alpha_H^B$$

$$A_{He^+} = \epsilon\, \alpha_{He^+} / \hat{S}_0\, \alpha_{He^+}^B\, \hat{He}^0$$

$$A_{He} = \epsilon\, \alpha_{He^{++}} / \hat{S}_0\, \alpha_{He^{++}}^B\, \hat{He}^+ \qquad (3.31)$$

Inside of the hydrogen Strömgren radius, $1 - x \ll 1$ and Eq. (3.29) is a linear equation for $(1 - x)/\epsilon$. Near the Strömgren radius, where x varies rapidly with τ, the quadratic form of Eq. (3.29) is solved. This rapid radial variation of x has been a challenge to all who have constructed models of HII regions. Kirkpatrick (1977) has developed an elegant method of handling the variation accurately when the equation of radiative transfer is approximated as an initial value problem. However, because the exact solution to radiative transfer is a two-point boundary value problem, we have developed a less elegant method (in fact, a brute force method) in order to improve the accuracy of the ionization structure at the hydrogen Stromgren radius (see §6.4).

As can be seen from Eqs. (3.29) and (3.30), the function u only approaches zero at the Strömgren radius so that $x \to 0$ as $\tau \to \infty$. It is therefore more convenient and consistent to define the Strömgren radius as the point where

$$\hat{S}_{tot} = \int_{\nu_0}^{\infty} d\nu [\hat{S}^{*}_{\nu}(\tau_1) + R^2 f^{B}_{\nu} \hat{J}^{D}_{\nu}(\tau_1)] + R^2 \sum_{J=1}^{9} f^{B}_{\nu_J} \hat{J}^{D}_{\nu_J}(\tau_1) < 10^{-10} \quad . \quad (3.32)$$

It should be remembered that $\hat{S}_{tot}$ approaches unity as $\tau_1 \rightarrow 0$. It is not exactly unity because of the small contribution by $\hat{J}^{D}_{\nu}(\tau=0)$.

The helium Strömgren radius is defined when $y^0 \rightarrow 1$. Inside of this point, to avoid solving coupled quadratic equations for y^+ and y^{++}, there are two possible alternatives. First, the $y^+ + 2y^{++}$ term from n_e can be calculated from the ionization structure in the previous iteration. Second, it can be assumed that y^0 and y^{++} are never both non-zero at the same radius. It has been found that the first method leads to a slightly less rapid rate of convergence of the ionization structures.

3.8. Observables

A useful quantity in comparing model HII regions with observations is the fraction of ionizing radiation "destroyed" by the gas. The gas "destroys" ionizing radiation whenever a recombination takes place that does not produce a UV photon. This fraction, f_{gas}, under the assumptions of §3.1, is

$$f_{gas} = S_0^{-1} \int_{r_0}^{r_1} dr\, 4\pi\, r^2\, n(r) n_e(r) \left[x\, \alpha^{B}_{H} + Y\, y^{+} \left(\frac{1}{4} \times \frac{1}{3} \times 0.44\right) \alpha^{B}_{He^{+}} \right] \quad (3.33)$$

where all recombinations to excited states of hydrogen destroy UV protons, whereas only recombinations to the 2^1S state of He^0 (where the two

photon emission process has a 44% probability of not producing a UV photon) can destroy UV photons. In normalized units,

$$f_{gas} = \hat{S}_0^{-1} \int_{R_0}^{R_1} dR\, d_g^2(R)\, R^2 \eta_e \left[x + 0.04\, Y\, y^+ \alpha^B_{He^+} / \alpha^B_H \right], \qquad (3.34)$$

and

$$\eta_e = x + Y(y^+ + 2y^{++}) \ . \qquad (3.35)$$

Equation (3.34) can be used to approximately determine τ_1 and $\hat{S}_0$ for any spherically symmetric dusty nebula, if the radial variations of the gas and dust densities and the spectrum of the central source are known. If the dust is optically thick over most of the spectrum of the central source then the total stellar luminosity L^* is equal to the total observed IR luminosity L_{IR}, and assuming a spectrum, S_0 can be calculated. If the dust is optically thin, then it might be possible to observe L^* and the spectrum directly. Because it is possible to express $\hat{S}_0$ approximately as an explicit function of τ_1 (see Appendix B), then setting $x \approx y^+ = 1$ inside the hydrogen Strömgren sphere allows Eq. (3.34) to be expressed as a simple function of τ_1. In addition, f_{gas} is approximately proportional to the ratio $L_{H\beta}/L_{IR}$ (i.e. the integral in Eq. (3.33) is proportional to the $H\beta$ volume emission measure) where the constant of proportionality is the ratio of the effective $H\beta$ recombination coefficient (AGN p. 66ff) to α^B_H. Thus Eq. (3.34) relates an observational quantity to an explicit function of τ_1.*

---

* It should be noted that this analysis is not dependent on the determination of the gas or dust densities. This is consistent with our

The ratio of the intensity of helium to hydrogen recombination lines is directly observable and is (in the absence of intrinsic reddening)

$$L_{He^{+1}} = \int_{R_0}^{R_1} dR\, \mathcal{G}_g^2(R)\, R^2 \eta_e y^{+1} \Big/ \int_{R_0}^{R_1} dR\, \mathcal{G}_g^2(R)\, R^2 \eta_e\, x \ . \qquad (3.36)$$

$L_{He^+} \approx 1$ when the hydrogen and helium Strömgren spheres coincide. For O stars, $L_{He^{++}}$ is on the order of 10^{-8}.

Finally, we have defined the average ionization of the ion X^{+i} as

$$\langle x(X^{+1}) \rangle \equiv \int_{R_0}^{R_1} dR\, \mathcal{G}_g^2(R)\, R^2 \eta_e x(X^{+1}) \Big/ \int_{R_0}^{R_1} dR\, \mathcal{G}_g^2(R)\, R^2 \eta_e \ . \qquad (3.37)$$

This quantity is proportional to the volume emission measure of recombination lines emitted by the ion X^{1-1}.

3.9. Lyman-Alpha Lines

Radiative transfer of resonantly scattered Lyman-α lines is included in our calculations with a slight modification of Eq. (2.1) and subsequently the JAY and RAY equations. Resonance scattering is defined to be an absorption (using the doppler broadened absorption cross section evaluated at line center) followed immediately by an isotropic emission. Equation (2.1) for H Lyman-α photons is, for example,

---

comments of §3.6 that once the dust parameters are specified, it is the combined parameter $\hat{S}_0$ which determines the physics of the model and not the values of the individual parameters which combine to form $\hat{S}_0$. At this point, however, if the size of the nebula is known, $n_d(r_0)\sigma_{d,0}^0$ can be calculated from Eq. (2.24) once τ_1 is specified.

$$\frac{dI^D_{\nu_L}}{d\ell} = -\left[n_d(r)\ \sigma_{d,0}\ f_d(\nu_L) + (1-x)n\ (r)\ \sigma_H\ (\nu_L)\right] I^D_{\nu_L}$$

$$+ \frac{1}{2}\ n_d(r)\sigma_{d,0}\ f_d(\nu_L)\ \omega_{\nu_L} \int_{-1}^{+1} d\mu'\ P_{\nu_L}(\mu,\mu')\ I^D_{\nu_L}$$

$$+ (1-x)\ n\ (r)\ \sigma_H\ (\nu_L)\ J^D_{\nu_L}(r) \qquad (3.38)$$

where $\nu_L = 0.75\ \nu_0$ is the frequency of the H Lyman-α line, $d\ell$ is along the photon propagation direction, and the last term represents the isotropic emission. This equation differs from that of recombination lines because the gas source term depends directly on $J^D_\nu(r)$.

4. PHYSICAL PROCESSES IN THE DUST

4.1 Basic Concepts

The parameterization of the dust has been discussed in Section 2.4. To reiterate, the dust is parameterized by $n_d(r)$, $\sigma_d(\nu)$ and ω_ν and, in the case of anisotropic scattering, by g_1 and g_2. All of these quantities are, in fact, averages over a distribution of dust particle properties. If the distribution of particle properties is represented by a function $f(a)$, a being the particle's radius, then the mean radius is

$$\bar{a} \equiv \int_0^\infty da\ a\ f(a) \Big/ \int_0^\infty da\ f(a) \tag{4.1}$$

and, for example, the mean extinction cross section is

$$\bar{\sigma}_d(\nu) \equiv \int_0^\infty da\ \sigma_d(\nu,a)\ f(a) \Big/ \int_0^\infty da\ f(a) \tag{4.2}$$

In a real nebula, $f(a)$ may also be a function of position, time and particle composition. Keeping this in mind, we will continue to use "mean" particle parameters knowing that these averages can obscure some of the physics of the dust. For example, we characterize the dust emissivity by generalized Mie theory so that the emissivity is

$$e_{IR}(\lambda) = \pi a^2 (2\pi a/\lambda)^J \tag{4.3}$$

where J is in the range $0 \leq J \leq 2$, and the mean dust radius is in the range $0.1\mu \leq a \leq 1\mu$ for normal galactic grains. If we average Eq. (4.3) over a particle distribution then an additional factor

the order of unity would appear and a would be replaced by $\bar{a}$.

For UV and OP photons the frequency dependencies of $\sigma_d(\nu)$ and ω_ν are given by power laws and for IR photons, both generalized Mie theory and a more realistic extinction coefficient from Knacke and Thomsen (1973) have been used.

4.2 Dust Energy Balance and Dust Temperature

The dust particles absorb UV, OP and IR radiation and radiate this energy in the infrared at temperatures from $\sim 1000^{\circ}K$ down to a theoretical limit of $3^{\circ}K$. Assuming that the heating processes are radiative only, the dust energy balance equation is

$$\int_0^\infty d\nu n_d(r)\sigma_d(\nu)\ (1-\omega_\nu)\ B_\nu(T_d) = \int_0^\infty d\nu h\nu\ n_d(r)\sigma_d(\nu)\ (1-\omega_\nu)J_\nu(r) \quad (4.4)$$

where T_d is the effective temperature of the dust grains at the radius r and $B_\nu(T_d)$ is the Planck function at the temperature T_d. The left-hand side of Eq. (4.4) represents the infrared emission and, in practice, for arbitrary $\sigma_d(\nu)$ the integral extends only over IR photon frequencies. The right-hand side calculates the absorption of UV, OP and IR radiation.

To evaluate the dust temperature from Eq. (4.4), it is convenient to write the energy absorption term in the form

$$W_{FR}(\tau) = \nu_0^{-1}\int_{\nu_1}^{\nu_2} d\nu\ \nu f_d(\nu)(1-\omega_\nu)[\hat{S}^*_\nu(\tau) + R^{2\hat{}}\hat{J}^D_\nu(\tau)], \quad (4.5)$$

where, $W_{FR}(\tau)$ is proportioned to the right-hand side of Eq. (4.4) and depending on the limits ν_1 and ν_2, $W_{FR}(\tau)$ is also proportioned to the energy absorbed from the UV, OP or IR frequency ranges. In actual calculations, (ν_1,ν_2) have the values $(\nu_0,10\nu_0)$, $(0.0912\nu_0,\nu_0)$ and $(\sim 0,\ 0.0912\nu_0)$ for UV, OP and IR photons respectively. For the lines, Eq. (4.5) integrates to

$$W_L(\tau) = R^2\nu_0^{-1}\sum_{J=1}^{15}\nu_J\,\hat{J}^D_{\nu_J}(\tau)(1-\omega_{\nu_J})f_d(\nu_J), \tag{4.6}$$

and is summed over all 15 UV and OP lines. $F(\tau)$ is the sum of the W functions:

$$F(\tau) = W_{UV}(\tau) + W_{OP}(\tau) + W_{IR}(\tau) + W_L(\tau). \tag{4.7}$$

The left-hand side of Eq. (4.4) has the form

$$I(T_d) = \int_0^\infty \frac{dx\ x^3 f_{IR}(x)}{e^{(T_0 x/T_d)} - 1},\quad T_0 = h\nu_0/k,\ x = \nu/\nu_0\ . \tag{4.8}$$

$f_{IR}(x)$ is the frequency dependence of the infrared emissivity $[f_{IR}(\nu)=(1-\omega_\nu)f_d(\nu)]$ and $T_0=157890.0^\circ K$. Eq. (4.4) now has the form

$$I(T_d) = \hat{I}F(\tau)/R^2 \tag{4.9}$$

and the dimensionless constant $\hat{I}$, which scales the temperature, is

$$\hat{I} = \left(\frac{c^2}{32\pi^2 \nu_0^3}\right) S_0 [n_d(r_0)\sigma_{d,0}]^2 Q_J \ , \qquad (4.10)$$

where Q_J gives the efficiency of IR emission relative to $\sigma_{d,0}$

$$Q_J = \sigma_{d,0}/[\pi a^2 (2\pi a \nu_0/c)^J] \ . \qquad (4.11)$$

For non-Mie theory emissivities, Q_0 is used in Eq. (4.10). Q_0 is the ratio of the extinction to the geometric cross sections and is the order of unity for interstellar grains (Spitzer 1968, p. 60). As we have seen in Section 3.8, S_0 is determined from the luminosity of the central source and $n_d(r_0)\sigma_{d,0}$ can be determined observationally so that Q_J is the only free parameter in Eq (4.10) and can be varied to scale the dust temperature of the model. In the next section, we shall see that $\hat{I}$ also determines the "strength" of the infrared emission.

For generalized Mie theory, $I(T_d)$ is given by

$$I(T_d) = (T_d/T_0)^{4+J} \Gamma(4+J)\zeta(4+J) \qquad (4.12)$$

where $\Gamma(4 + J)$ is the gamma function and $\zeta(4 + J)$ is the Riemann zeta function. If $f_{IR}(x)$ has an arbitrary functional form, then Eq. (4.8) must be used to tabulate T_d as a function of I. The right-hand side of Eq. (4.9) is given by radiative transfer and a table look-up or Eq. (4.12) are used to calculate $T_d(\tau)$

4.3 Infrared Source Term

The source term of IR photons for the Jay and Ray equations is given in terms of the IR absorption coefficient by Kirchoff's law (Eqs. 2.2 and 2.3). Using the normalization condition, (Eq. 2.31), the source function for the Jay and Ray equations is

$$\hat{\Sigma}^{E}_{\nu}(\tau) = \frac{\hat{S}_{IR} R^2 f_d(\nu)(1-\omega_\nu)(\nu/\nu_0)^2}{e^{[h\nu/kT_d(\tau)]}-1} \qquad (4.13)$$

The parameter $\hat{S}_{IR}$ (with units of 1/Hz), which determines the "strength" of the IR photon emission, is given by

$$\hat{S}_{IR} = 1/\nu_0 \hat{I} \ . \qquad (4.14)$$

So far, $\hat{S}_{IR}$ and $\hat{I}$ are valid for any nebula regardless of the existence of gas. For nebulae with gas $\hat{S}_{IR}$ is more conveniently expressed in terms of the gas density and dust-to-gas ratio as

$$\hat{S}_{IR} = \left[\frac{6\pi M_H \nu_o^2}{\alpha_H^B c^2}\right] \frac{R_{DG}[10^3 cm^{-3}/n(r_0)]\ [2\pi/0.912]^J}{\hat{S}_0} \ . \qquad (4.15)$$

M_H is the mass of a hydrogen atom and the "dust-to-gas" ratio, R_{DG}, is defined as

$$R_{DG} = \left[\frac{M_d/M_g}{0.01}\right]\left[\frac{1 gr/cm^3}{\rho}\right]\left[\frac{0.1\mu}{a}\right]^{J-1} \qquad (4.16)$$

where M_d/M_g is the dust-to-gas mass ratio and ρ is the density of a grain ($\rho \approx 1$ gr/cm^3). For non-Mie theory, Eqs. (4.15) and (4.16) are evaluated for $J = 0$. With $\hat{S}_{IR}$ and $\hat{I}$ in the form of Eq. (4.15), it is the parameter R_{DG} which can be freely adjusted. Combining Eqs. (3.28), (4.11) and (4.16), it is easy to see that

$$\epsilon = (2 \times 10^{-4})(2\pi/0.912)^J R_{DG}/Q_J \quad . \tag{4.17}$$

From Eqs. (4.9) and (4.13) it can be seen that $\hat{S}_{IR}$ (or equivalently $\hat{I}$) determines not only the "strength" of the IR emission but also the spectrum. By noting that neither Q_J nor R_{DG} depend on S_0, it is easy to see that the variation of these parameters will change the qualitative shape of the emitted infrared spectrum while keeping the total IR luminosity, L_{IR}, constant. We will return to this point in the next section.

The observed flux of infrared photons is

$$S_{IR} = \hat{F} R^2 (\nu/\nu_0) \left(\hat{H}_\nu^D + \hat{J}_\nu^*\right) \tag{4.18}$$

where

$$\hat{F} = h\nu_0 S_0/4\pi D^2 \quad . \tag{4.19}$$

D is the distance to the nebula. $S_{IR}(\nu)$ is usually expressed in Janskys (JY) where one Jansky is 10^{-23}ergs/cm^2-sec-Hz. S_0 is obtained from the total luminosity of the source which, in turn, is obtained from a measured luminosity times $4\pi D^2$. Thus the quantity

S_0/D^2 is usually independent of distance. $\hat{I}$ is also independent of distance if $n_d(r_0)\sigma_{d,0}$ is calculated from an observed angular size.

4.4 Generalized Mie Theory

For many HII regions that are heated by O or B stars, the dominant source of dust heating is from UV and OP photons. Also, in many nebulae the infrared spectrum is much broader in frequency than a single black body indicating that the dust must not be optically thick over most of the spectrum, if $\tau_\nu \gg 1$ for IR frequencies, then we would only see into the nebula to a depth where $\tau_\nu \sim 1$ and the spectrum would necessarily be much narrower. In these cases it may be physically reasonable to assume that the dust is optically thin to all IR photons. This assumption is very useful for the purposes of understanding this model because it allows the investigation of the effects of radiative transfer in the UV and OP frequency ranges on the dust temperature structure while preserving the quantitative features of the IR spectrum

When the dust is optically thin to IR photons, the observed spectrum is

$$4\pi D^2 S_{IR}(\nu) = \int_{r_0}^{r_1} dr 4\pi r^2 [4\pi J_\nu(r)] \tag{4.20}$$

which in terms of $\hat{S}_{IR}$ and $\hat{F}$ is

$$S_{IR}(\nu) = \hat{F}\,\hat{S}_{IR}(\nu/\nu_0)^{3+J} \int_0^{\tau_1} \frac{d\tau R^2}{e^{(h\nu/kT_d)}-1} \tag{4.21}$$

$T_d(r)$ is calculated from Eqs. (4.7), (4.9) and (4.12) with $W_{IR} \equiv 0$.

The total infrared luminosity of the source is

$$L_{IR} = 4\pi D^2 \int_0^\infty d\nu \; S_{IR}(\nu). \tag{4.22}$$

Substituting Eq. (4.21) into (4.22) and changing the order of integration, L_{IR} is equal to

$$L_{IR} = 4\pi D^2 \hat{F} \int_0^{\tau_1} d\tau \; F(\tau), \tag{4.23}$$

independent of $\hat{S}_{IR}$ (or equivalently, of $\hat{I}$). It can be explicitly seen that variation of $\hat{S}_{IR}$ and $\hat{I}$ through the parameters Q_J or R_{DG} does not change L_{IR}. In addition, while S_{IR} affects the qualitative shape of the IR spectrum, its value cannot be obtained observationally. Thus Q_J or R_{DG} can only be obtained by "fitting" an observational IR spectrum with the results of the model.

Eq. (4.21) assumes that the nebulae just fills the beam of the observing telescope. In general, however, the flux is measured as a function of aperture size where the aperture of the telescope is less than the size of the object. In the optically thin case, the IR flux from within a circle of radius b, centered on the nebula, is

$$4\pi D^2 \, S_{IR}(b,\nu) = \begin{cases} 4\pi \left[\int_0^{r_0} dt \int_{r_0}^{r_1} dr + \int_{r_0}^{b} dt \int_{t}^{r_1} dr \right] rt(r^2-t^2)^{-\frac{1}{2}} \, J_\nu(r) & b > r_0 \\ 4\pi \int_0^{b} dt \int_{r_0}^{r_1} dr \; rt(r^2-t^2)^{-\frac{1}{2}} \, J_\nu(r) \; . & b \le r_0 \end{cases} \tag{4.24}$$

Changing the order of integration, Eq. (4.24) reduces to

$$4\pi D^2 S_{IR}(b,\nu) = 4\pi\left[\int_{r_0}^{r_1} dr\, r^2 J_\nu(r) - \int_{\max(b,r_0)}^{r_1} dr\, r\sqrt{r^2 - b^2}\, J_\nu(r)\right], \quad (4.25)$$

where $\max(b,r_0)$ picks the larger of (b,r_0). When $b = r_1$, Eq. (4.25) reduces to Eq. (4.20).

5. APPROXIMATE SOLUTIONS OF RADIATIVE TRANSFER

5.1. Introduction

Approximate solutions of radiative transfer have been used exclusively in previous models of the ionization structure of H II regions. Hummer and Seaton (1963) were the first workers to calculate accurate models using the on-the-spot approximation (OSA) for planetary nebulae (without dust). Tarter (1967) developed a more elegant solution using the "outward only" approximation. For models of H II regions with dust, Balick (1975) has used the OSA and Sarazin (1977) has used the "outward only" approximation. All of these solutions are unable to handle dust scattering explicitly. In this chapter we will discuss approximate solutions of radiative transfer in some detail including the OSA, the diffusion approximation (valid for nebulae with little or no gas), and a "modified Eddington approximation". In Chapter 7, we will make detailed comparisons of the results of these approximate solutions with the QDM solution in order to assess the accuracy of the approximations.

Petrosian and Dana (1975, Paper I) and Dana and Petrosian (1976, Paper II) have developed semi-analytic approximate solutions of radiative transfer which are accurate to within 50%, and which are convenient for the initial modeling of dusty nebulae. The important results of these papers will be presented here.

5.2. On-the-Spot Approximation

The existence of a Stromgren sphere requires that all ionizing photons be absorbed in the nebulae, i.e. the number of diffuse ionizing photons emitted per second must equal the number of diffuse photons

absorbed per second. Thus, for UV photons,

$$\int dV J_\nu(r) = \int dV K^a_\nu(r)\ J^D_\nu(r)\ , \qquad (5.1)$$

where the integrals are over the entire volume of the nebula. The essence of the on-the-spot approximation is to assume that, in the absence of dust scattering, Eq. (5.1) is valid locally so that

$$J_\nu(r) = K^a_\nu(r)\ J^D_\nu(r)\ . \qquad (5.2)$$

We shall distinguish between two different forms of Eq. (5.2). First, the generalized on-the-spot approximation (GOSA) assumes that the diffuse intensity is absorbed by both gas and dust. Second, the on-the-spot approximation (OSA) assumes that the diffuse intensity is absorbed by the gas only.

For recombination photons to the ground state, the effective frequency is very close to the ionization limit of H^0, He^0, and He^+ where the respective photoionization cross sections are the largest. The gas opacity is therefore large for these photons and they should be absorbed close to where they were emitted. This is also true for Lyman-α photons which are resonantly scattered and hence cannot travel far before they are absorbed by dust. Equation (5.2) is not valid, however, if dust scatters UV photons or if the nebula is density bound (i.e. there is insufficient gas or dust in the nebula to absorb all UV photons).

5.2.1. Generalized On-the-Spot Approximation

From Eq. (2.15) with $K^s_\nu \equiv 0$, it can be seen that Eq. (5.2) implies that $S^D_\nu(\tau) \equiv 0$, and that the normalized mean intensity, $\hat{J}^D_\nu(\tau)$,

is given by the ratio of Eq. (3.22) to Eq. (3.26). With $\hat{J}_\nu^D$ given by GOSA and $\hat{J}_\nu^*$ given by Eqs. (2.45) and (2.49), the ionization structure and dust temperature functions $W_{UV}(\tau)$ and $W_L(\tau)$ can be calculated. Other solutions of radiative transfer must be used, however, for OP and IR photons. A GOSA solution has been included in our numerical model that has the same gas and dust properties as the QDM solution.

5.2.2. Semi-Analytic Approximate Solution

We have developed semi-analytic OSA models of dusty H II regions containing hydrogen and helium. These models use frequency and angle averaged cross sections and intensities. Approximate analytic expressions are derived for evaluation of the variation of the fraction of ionizing radiation absorbed by gas and the ratio of the volume emission measures of He II to H II regions with the spectrum of the central source, helium abundance, and absorption properties of dust. For nebulae containing hydrogen and helium, we have derived simple coupled differential equations for the net flux of ionizing photons and for the fraction of ionizing photons capable of ionizing helium. These initial value problems are easily solved numerically to give $\hat{S}^*(\tau)$ [Eq. (2.16)] and the ionization structures of hydrogen and helium. In the absence of helium or in the absence of dust, these equations have analytic solutions. Appendix B gives the derivations and important results of the OSA models.

5.3. Diffusion Approximation

The diffusion approximation has often been used in models where scattering dominates radiative transfer. The approximation assumes a single isotropic point source surrounded by an isotropic medium in which $\kappa^s \gg \kappa_\nu^a$ and the scattering is isotropic. The medium can either be

infinite or be surrounded by a "free surface" i.e. a surface on which no photons enter from outside. The solution of the diffusion approximation is valid a few scattering mean free paths away from the central source and away from the free surface.

The inner boundary condition is

$$S_\nu(\tau=0) = S_\nu^* \tag{5.3}$$

and for an infinite medium, the outer boundary condition is

$$\lim_{r \to \infty} J_\nu(r) = 0 . \qquad \text{(Infinite Medium)} \tag{5.4}$$

At a free surface, it is assumed that $J_\nu(r)$ vanishes at an extrapolation distance d (Davison 1957, §8.5) outside of the surface where d is obtained from the exact solution of Milne's problem (infinite half-space). The free surface boundary condition is

$$J_\nu(r_1+d) = 0 , \; d \approx 0.7104/\kappa_\nu , \qquad \text{(Free Surface)} \tag{5.5}$$

where $1/\kappa_\nu$ is the extinction mean free path. The key assumption in this approximation is that $d/r_1 \ll 1$.

We will assume a uniform medium. However, this assumption is not mathematically necessary and nonuniform nebulae will have a different numerical factor in the "diffusion constant" which comes from the value of

$$\int dV' \exp -\left\{ \int_{\vec{r}'}^{\vec{r}} d\ell \, \kappa(\vec{\ell}) \right\} / \ell^2 , \tag{5.6}$$

$$\vec{\ell} = \vec{r} - \vec{r}' ,$$

integrated over the volume of the nebula.

The diffusion equation for $J_\nu(r)$ is

$$-\nabla^2 J_\nu(r) = K_D^2 J_\nu(r) , \quad K_D = \sqrt{3K^s K^a} . \tag{5.7}$$

K^s and K^a are functions of frequency but are assumed uniform throughout the medium. In spherical coordinates, the solution to Eq. (5.7) is

$$J_\nu(r) = \frac{1}{r}\left(Ae^{\tau_D} + Be^{-\tau_D}\right) , \quad \tau_D = K_D \tau . \tag{5.8}$$

The ratio A/B can be obtained from the outer boundary conditions on $J_\nu(r)$ [Eqs. (5.4) or (5.5)]. The net flux through a spherical shell is given by Fick's law

$$S_\nu(r) = -\left(4\pi r^2/3K^s\right) \hat{r}\cdot\vec{\nabla}[4\pi J_\nu(r)] . \tag{5.9}$$

Equation (5.9) is derived assuming that the medium is infinite (i.e. it is not valid within a few mean-free-paths of surfaces) and assuming that $J_\nu(r)$ is a slowly varying function of position. A nice derivation of Fick's law is given in Lamarch (1966, §5.4). Upon substituting Eq. (5.8) into (5.9) and using the inner boundary condition [Eq. (5.3)], the flux is

$$S_\nu(r) = S_\nu^* \left[(1+\tau_D)e^{-\tau_D} - \varepsilon(1-\tau_D)e^{\tau_D}\right] \Big/ (1-\varepsilon) , \tag{5.10}$$

where

$$\varepsilon = \begin{cases} \exp\left[-2\sqrt{3\omega(1-\omega)}\,(\tau_1 + 0.7104)\right] . & \text{(Free Surface)} \\ 0 & \text{(Infinite Medium)} \end{cases} \tag{5.11}$$

If τ_D is frequency independent, then S_ν^* is replaced by S_0 .

5.4. Modified Eddington Approximation (MEA)

Hummer and Rybicki (1971) introduced a modified Eddington factor which they used as an initial estimate of $f_\nu(r)$ [Eq. (2.10)]. In this approximation, we solve the JAY equation with

$$f_\nu(r) = \begin{cases} 1 - (2/3)e^{-\tau} & \text{Continuum frequencies} \\ 1/3 & \text{Lines} \end{cases} \tag{5.12}$$

for all iterations. This approximation has the correct form for the continuum $f_\nu(r)$ at both the inner boundary where J_ν^D is isotropic and at the outer boundary where J_ν^D is radially outward $(f_\nu \to 1)$. Because the lines are emitted isotropically, their intensity remains fairly isotropic throughout the nebula.

6. COMMENTS ON PROGRAM SCATER

6.1. Introduction

Program SCATER is the numerical model that has been constructed to solve the problem of radiative transfer in dusty nebulae. The program currently resides in the NASA-Ames Research Center's CDC7600 computer and is available for public use. SCATER is currently about 6000 cards long and requires ~ 25,000 words of small core memory and ~ 75,000 words of large core memory. While SCATER was being written, an effort was made to make the code as efficient as possible (within the author's limited knowledge of code optimization) and most Eddington approximation models can be run with less than 30 seconds of CPU time. However, because the program was written for a general dusty nebula with or without gas, and because it was written over a period of about a year, there are many parts of the program which are not necessary and/or efficient when the program is applied to a specific nebula. Also, the program is not complete as it does not calculate a self-consistent electron temperature or the forbidden line emission from the gas. It is estimated that this additional physics would require 2 to 3 months of additional programming and testing. Inasmuch as this thesis is a users' manual and guide to SCATER, we will deal briefly in this chapter with the iteration procedure, timing, and accuracy of the numerical model.

6.2. Iteration Scheme

Figure 3 gives a brief flow chart of the iteration scheme of program SCATER. Most of the "bookkeeping" details are necessary because the program uses the same subroutines for UV, OP, and IR photons. This

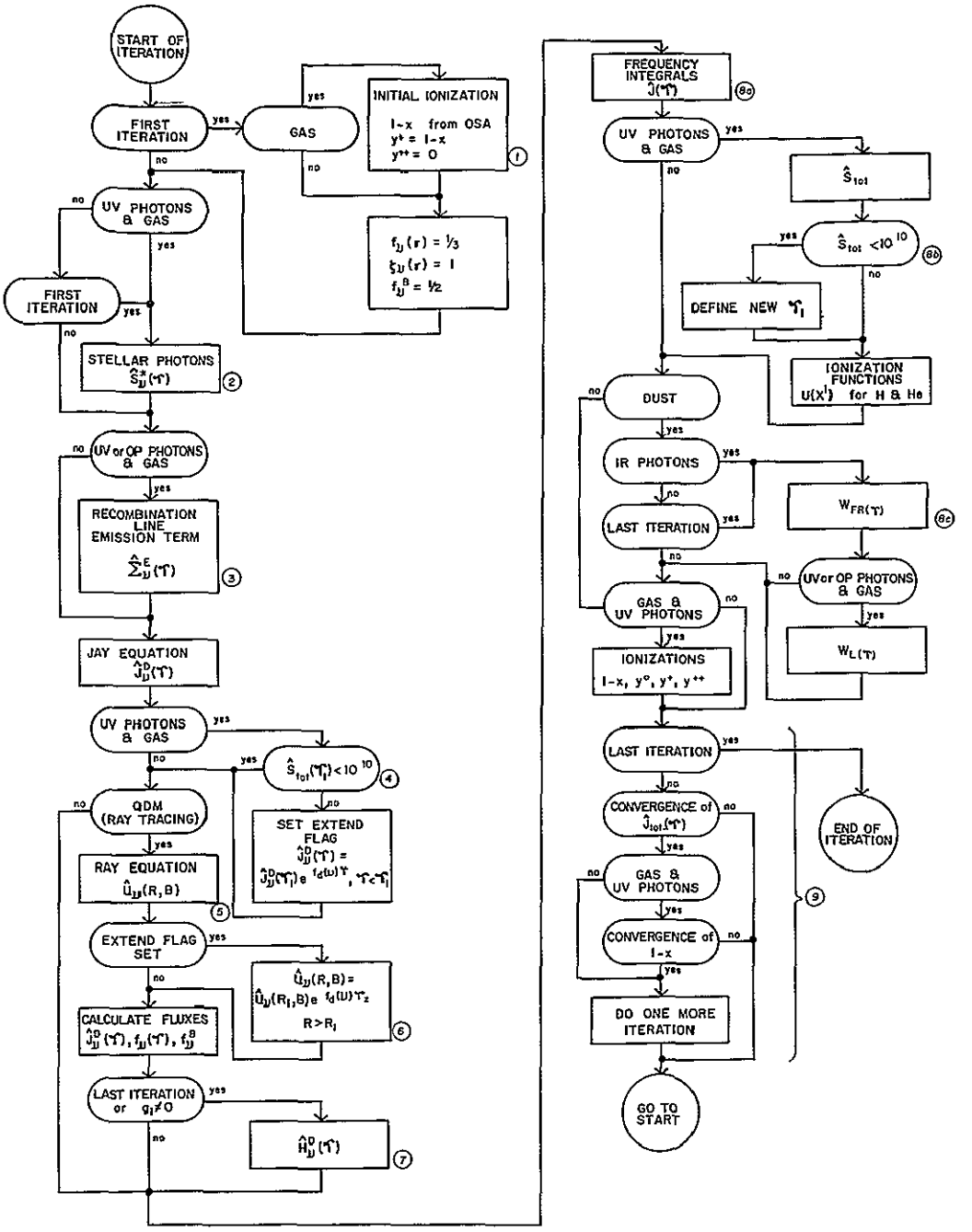

Fig. 3. Flow Chart of the Iteration Scheme of Program Scater
Circled numbers refer to comments in the text

iteration procedure is necessary because the source functions $\hat{\Sigma}^{E}_{\nu}(\tau)$ [Eq. (3.22)] and $\hat{\Sigma}^{S}_{\nu}$ (R,B) [Eq. (2.43)] depend on the total intensity and must be updated each iteration. In addition, if there is gas, the extinction coefficient is also dependent on the total intensity and the iteration procedure is much less rapidly converging.

The following numbered comments refer to the numbered sections of Fig. 3.

1. On the first iteration, the Eddington approximation or the modified Eddington approximation [Eq. (5.12)] is used to evaluate $f_{\nu}(\tau)$ [Eq. (2.10)], $\zeta_{\nu}(\tau)$ [Eq. (2.11)] and f^{B}_{ν} [Eq. (2.52)]. If there is gas, then the initial hydrogen ionization is given by the OSA analytic model (see Appendix B) using $\hat{S}_{O}$ and the absorption optical depth. If $\omega_{\nu} \geq 0.5$ for UV photons, then using $\omega_{\nu} = 0.5$ for the absorption optical depth in the OSA model produces a better guess for the value of τ_{1} at the Strömgren radius.

2. Once the initial ionization structure has been calculated, the stellar flux as a function of τ and ν can be calculated. If there is no gas or if OP or IR photons are being considered then the stellar flux does not depend on the ionization structure (extinction is by dust only) and is calculated only on the first iteration.

3. The UV and OP recombination lines source term is calculated from the ionization structure, and the JAY equation can be solved for $\hat{J}^{D}_{\nu}(\tau)$, $\tau \leq \tau_{1}$.

4. For nebulae with gas and for UV photons, the Strömgren radius condition [Eq. (3.32)] on the flux is checked at the old value of τ_{1} . If $\hat{S}_{tot}(\tau_{1})$ is too large, an extend flag is set (meaning that the

Stromgren sphere will be moved outward) and $\hat{J}^D_\nu(\tau_1)$ is calculated for $\tau > \tau_1$ assuming radially outward flow and extinction by dust only.

5. The new value of $\hat{J}^D_\nu(\tau)$ is used to update the scattering source function $\hat{\Sigma}^S_\nu(R,B)$. Using $\hat{\Sigma}^E_\nu(\tau)$ calculated in step 3, the RAY equation is solved within the old Strömgren sphere.

6. If the extend flag is set, $\hat{U}_\nu(R,B)$ [Eq. (2.38)] is extended beyond the Strömgren sphere assuming dust extinction and no sources for $R > R_1$. τ_Z is the dust extinction optical depth along a ray starting at the old Strömgren radius. For $B > R_1$, it is assumed that $\hat{U}_\nu(R,B) = 0$.

7. Because $\hat{H}^D_\nu(\tau)$ is calculated from the derivative of $\hat{U}_\nu(R,B)$ [Eqs. (2.40) and (2.47)], the program avoids its calculation unless it is required in the scattering source function (i.e. $g_1 \neq 0$) or it is the last iteration and the diffuse flux is desired for comparison with $\hat{S}^*_\nu(\tau)$.

8a. At this point, frequency integrals are calculated assuming that the integrands vary as power-laws between two adjacent frequency grid points. The total integrated mean intensity, $\hat{J}(\tau)$, is calculated in each frequency bin and is equal to

$$\hat{J}(\tau) = \int_{\nu_1}^{\nu_2} d\nu \left[\hat{S}^*_\nu(\tau)/R^2 + \hat{J}^D_\nu(\tau)\right] + \sum_{J=1}^{m} \hat{J}_{\nu_J}(\tau) , \qquad (6.1)$$

where m is the number of lines in the bin and is equal to zero for IR photons or for nebulae without gas.

8b. For nebulae with gas and for UV photons, $\hat{S}_{tot}(\tau)$ is calculated. A new value of τ_1 is defined as the first value of τ for which $\hat{S}_{tot} < 10^{-10}$. The ionization functions for hydrogen and helium are calculated for $\tau \leq \tau_1$ [Eq. (3.30)]

8c. The dust energy functions, $W_{FR}(\tau)$ [Eqs. (4.5) and (4.6)], are evaluated on the last iteration for UV and OP photons. If the dust is not optically thin to infrared photons, then $W_{IR}(\tau)$ and the dust temperature are calculated on each iteration of the IR intensity.

9. $\hat{J}(\tau)$ is compared with its values on the previous iteration. For UV photons and nebulae with gas, 1-x [Eq. (3.8)] is also compared with its previous values. If both of these functions have converged to within a specified error limit throughout the nebula, the program does one more iteration.

6.3. Timing and Array Sizes

The timing of program SCATER is critically important if it is going to be used to fit the spectra of observed objects. The fitting process requires many runs as several parameters are usually varied. In general, the ODM solutions take too much times to be of value in the fitting process. However, either the Eddington approximation or the modified Eddington approximation run in a reasonable amount of time and are accurate (see Chapter 7).

Because of the large variation in optical depth scales associated with various frequencies and because of the $1/r^2$ dependence of the diffuse mean intensity at the center of the nebulae, it is not practical to use an optical depth distance scale. We therefore used a uniform distribution of radial grid points, with extra radial points added at the center of the nebulae to handle the $1/r^2$ dependence and for models with gas, extra radial grid points are also added at the Strömgren radius. We used 100 radial grid points and 110 impact parameters*. Each frequency

* Dr. Alan Tokunaga of NASA-Ames has doubled the size of the radial

band has up to 40 grid points. In the continuum, the frequency grid points are determined by spectrum of the central source and by the edges of the gas.

In order to make useful comparisons, a standard model without dust scattering has been run to calculate the ionization structure of hydrogen. Without scattering or helium, only one frequency grid point is calculated for UV diffuse photons (i.e. the $H1^2S$ recombination line). Each model calculated only UV photons and executed 30 iterations. The times of execution (not including compiling times) were 8.638 seconds for QDM, 3.264 seconds for the Eddington approximation, and 3.256 seconds for the GOSA. The QDM time can be reduced to 6.815 seconds if the Eddington approximation is used for the first 15 iterations while the program "finds" the Strömgren radius. The difference in time between the QDM and the Eddington approximation is approximately proportional to $1/2 \times (\text{no. of frequencies})^2$, i.e. the time required to solve for $\hat{U}_\nu$ on the (R,B) grid for each frequency. Additional time is also required to calculated $\hat{J}^D_\nu(\tau)$ and $f_\nu(\tau)$ using Eqs. (2.46) and (2.48). Thus, if scattering ($\omega_\nu = 1.0$) is included, the QDM time increases to 187.7 seconds while the Eddington approximation time is only 7.964 seconds.

6.4. Stromgren Sphere

The rapid radial variation of the ionization structure at the Strömgren radius causes serious problems of the accuracy and rate of

---

* (Contd.)
arrays in SCATER as part of his effort to use the program to fit the infrared spectrum of S140.

convergence of the numerical model. Interior to the Strömgren radius, the ionization structure is rapidly converging and accurate. To deal with these problems, extra radial grid points are added where the hydrogen ionization varies most rapidly. However, because the exact position of the Strömgren radius is not known a priori, these points are added several iterations into the UV calculation when the value of τ_1 is no longer changing.

The new radial grid points are added symmetrically around the grid point where the variation of 1-x from the previous iteration is maximum. Depending on the number of unused grid points in the radial arrays, 2, 8, 18, or 32 points are added between the first through fourth grids, respectively away from the point of maximum variation. The functions $f_\nu(\tau)$ and $\hat{H}_\nu(\tau)$ are estimated at the new grid points using a cubic splines fit through the old points. The ionization functions are estimated assuming a power-law dependence between the old grid points. A better "fitting" function could be used that might speed up the convergences of 1-x . Once this procedure is completed, the B grid is adjusted so the B grid is equal to the R grid and a new iteration is started.

6.5. Accuracy

During the construction of program SCATER, each subroutine was carefully tested and comparisons were made with analytic results whenever possible. In addition, there are two models that can be run to test the differential equation solvers and dust physics and to test the gas physics.

For pure dust nebulae with $\omega_\nu \equiv 1$, the total net flux through a spherical shell must remain constant throughout the nebula. To within

1 to 2%, over most of the nebula the model kept the flux constant where the difference is attributed to the linear approximation of $\hat{U}_\nu(R,B)$ between B grid values. This effect can be corrected (e.g. Mathis 1972) but the error is well within acceptable astrophysical error limits.

For pure hydrogen nebulae, direct comparison can be made to Hummer and Seaton's (1963) on-the-spot calculations. Using our built-in GOSA model, we find close agreement between the hydrogen ionization, 1-x , and the optical depth of hydrogen at the Lyman limit, except at the Strömgren radius. Because Hummer and Seaton take into account the frequency dependence of H 1^2S recombination spectrum and because of differing radial grids, close agreement is not expected at the Strömgren radius where diffuse photons are the dominant source of ionization. In addition, our model calculates f_{gas} [Eq. (3.33)] to be $\sim 2\%$ below the exact value of unity in this case. This error is attributed primarily to the rapid variation of $n_e(r)$ [Eq. (3.18)] at the Strömgren radius.

7 VARIATION OF PARAMETERS AND COMPARISONS WITH OTHER CALCULATIONS

7.1 Introduction

Although we have calculated model dusty nebulae using program SCATER for a wide range of the parameters, we will limit this discussion to those questions which have not been addressed in previous calculations. 1) What are the effects of dust scattering on the internal structure and observable parameters of dusty nebulae? 2) How accurate are approximate solutions of radiative transfer? The internal structure of gaseous nebulae without dust is well understood theoretically from the work of Hummer and Seaton (1963,1964), Hjellming (1966) and Rubin (1968). More recently, Balick (1975) and Sarazin (1977) have analyzed in great detail the effects of dust absorption on the ionization and thermal structure of dusty HII regions. Neither of the calculations, however, include scattering. Approximate models of dusty HII regions that analyze the effects of UV absorbing dust have been calculated by Mathis (1970, 1971), Petrosian, Silk and Field (1972), Krügel (1975), Natta and Panagia (1976) and by Papers I and II.

In this discussion we will consider two types of models. Type I models have a constant Strömgren radius while the dust parameters are varied. In these models, S_0 (in practice, $\hat{S}_0$) is "tuned" to keep the Strömgren radius fixed. Type II models have a constant value of S_0 (or $\hat{S}_0$) while the dust parameters are varied.

We define our standard model to consist of a uniform nebula at a distance of 1 kpc with a constant dust-to-gas ratio. The stellar spectrum is a $40{,}000^{\circ}$K (log g = 4.0) model atmosphere from Auer and Mihalas (1972). Once the dust parameters have been specified, $\hat{S}_0$

determines the properties of the gas (see Section 3.6). We have chosen $\hat{S}_0 = 4.13$ which corresponds to (but is not uniquely defined by) a single zero-age main sequence central source with radius given by Panagia (1973), hydrogen number density of $10^3 cm^{-3}$, and $\epsilon \times 10^{-4}$. When $\omega_0=0$, $Y = 0.1$, and $f_d(\nu) = 1$ for UV photons, this $\hat{S}_0$ gives $\tau_1 \approx 1.5$.

Table III summarizes the physical parameters that must be specified to completely determine the properties of our model. If the model nebula contains no ionized gas, then the parameters $\hat{S}_0$, Y, ϵ and $G_g(r)$ do not need to be specified. Conversely, if the model nebula contains no dust, then the parameters $f_d(\nu)$, ω_ν, g_1, g_2 and $\hat{S}_{IR}$ do not need to be specified. However, $\epsilon = 1$ and $G_d(r) = G_g(r)$ in this case. The values of the parameters for our standard model (model A in the next section) are also indicated. The value of R_0 is entirely arbitrary and was picked for numerical convenience.

7.2 Variation of Albedo and Extinction Coefficient

We will consider the effects of the variation of the albedo and of radiative transfer on the mean intensity and Eddington factor using type II models (constant central source luminosity). The same quantitative effects that we will discuss are also seen in type I models (constant τ_1).

Also in this section we will discuss the effects of the variation of the albedo and the frequency dependence of the extinction coefficient on the ionization structures of the gas for type I models. The observational question we are trying to answer is If I have line intensities from a resolved HII region, how do dust parameters affect

TABLE III

PHYSICAL PARAMETERS

Parameter	Defined	Model A	Comments
$\hat{S}_0$	3.24+	4.13	Determines τ_1 and "relative strength" of dust and gas physics
ε	3.28	2×10^{-4}	Determines "width" of Strömgren radius
Y	§3.1	0.1	n(He)/n(H), He abundance relative to H
$G_d(r)$	2.30	1.0	Radial variation of dust and
$G_g(r)$	3.23	1.0	gas densities
R_0	2.24	0.1	Radius of central core in optical depth units
$\hat{S}^*_\nu(0)$	§2.4	T^*_{AM}=++ 40,000 °K	Normalized spectrum of the central source
$f_d(\nu)$	2.25	1.0	Frequency dependence of the dust extinction coefficient
ω_ν	2.26	0.0	Albedo of the dust
g_1	2.6	0.0	Average cosine of the scattering angle
g_2	2.7	0.0	Average of the square of the cosine of the scattering angle
$\hat{S}_{IR}$ +++	4.15	0.356	Determines the dust temperature and the shape of the IR spectrum

\+ Equation number

++ Auer and Mihalas (1972) Spectrum, $S_0/4\pi r_*^2 = 1.667 \times 10^{24}$ UV photons $cm^{-2} sec^{-1}$, $r_* = 5.66 \times 10^{11}$ cm (Panagia 1973)

+++ For $J = 0$

the physical parameters that I deduce from my observations?

Finally, we will discuss the effects of the variation of the albedo on the observed IR spectrum again using type II models for clarity of interpretation. However, it is usually the infrared luminosity of a source that is known observationally rather than the central source luminosity. Hence, these results are only a qualitative guide to the effects of albedo.

7.2.1 Mean Intensity and Eddington Factor

On Figure 4, we have plotted the variation of log $[J_\nu(\tau)/J_\nu(0)]$ versus τ/τ_1 for $\nu = \nu_0^+$ (these photons can photoionize hydrogen), $\nu = \nu_0^-$ (these photons cannot photoionize hydrogen), $\nu = 0.25\nu_0$(Ba-C) and $\nu = 1.06\nu_0$ (H 1^2S recombination "line"). The difference between the shapes of the continuum curves ($\nu = \nu_0^\pm$) and the line curves ($\nu = 1.06\nu_0$) is due to the difference in the "source functions" of the two types of photons. The source of continuum photons is, for isotropic scattering, $K_\nu^s J_\nu(\tau)$ which is a strongly decreasing function of τ whereas the source of lines is, for hydrogen, $xnn_e\alpha_H$ which is almost constant inside the Strömgren sphere for uniform densities.

For UV photons ($\nu = \nu_0^+$ and $\nu = 1.06\nu_0$), it can be seen from the figure that as albedo increases the relative intensity is lower near the center of the nebula and higher as τ approaches τ_1. Thus the effect of albedo is to "transport" photons from the center of the nebula to the outer regions. This is primarily a result of the fact that we are keeping the extinction coefficient constant while the albedo is increased and we are, therefore, also increasing the dust absorption mean free path. For type I models if we increase the albedo while keeping all other parameters fixed, $J_\nu^D(\tau)$ will increase at the same radius because the absorption coefficient is decreasing. This effect is most apparent in the value of τ_1 (i.e. the size of the Strömgren sphere).

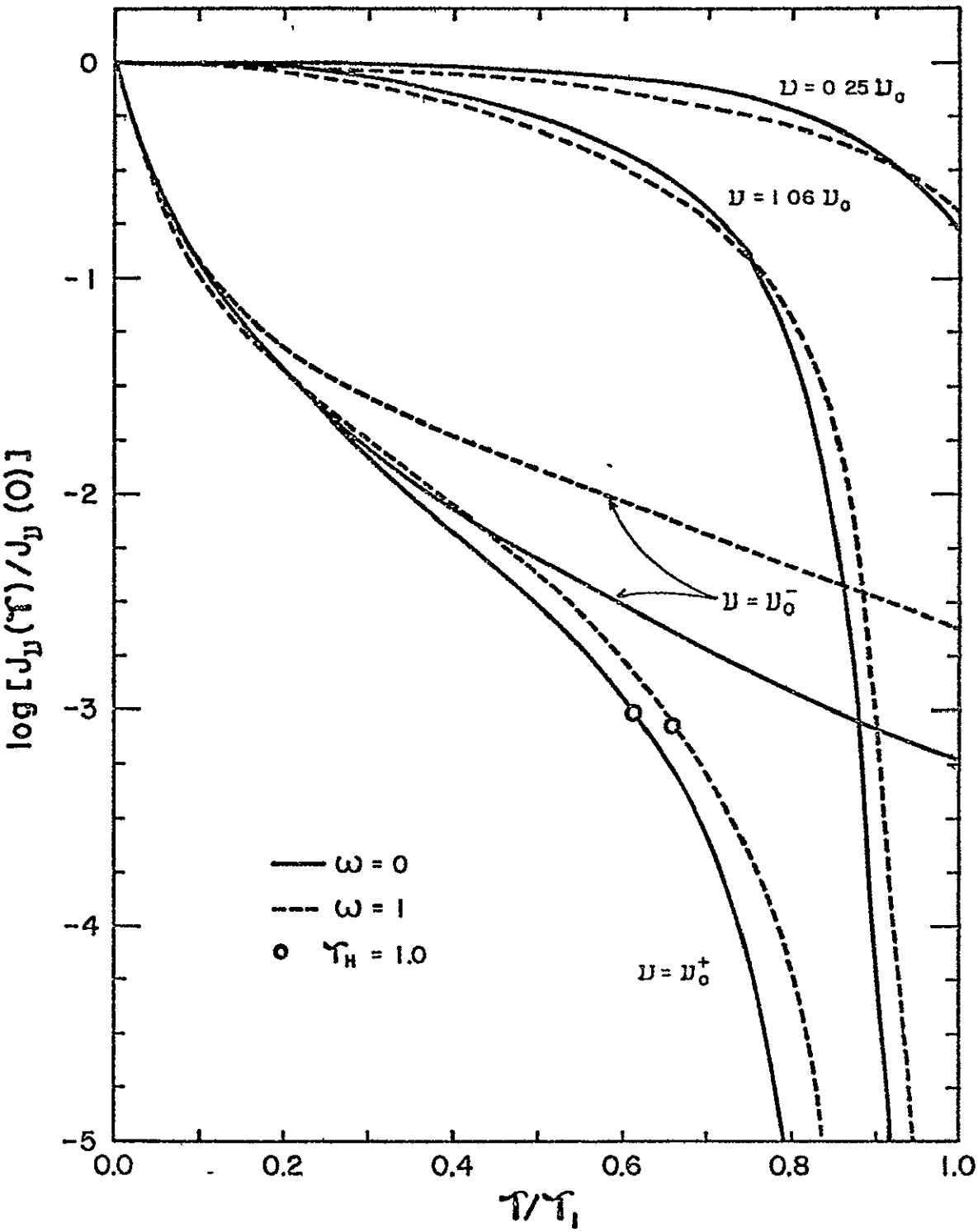

Fig. 4. Variation of the Mean Intensity Versus Optical Depth. Variation of Log $[J_\nu(\tau)/J_\nu(0)]$ for $\omega = 0$ (solid lines), $\omega = 1$ (dashed lines) and for $\nu = \nu_0^+$ (H ionizing photons), $\nu = \nu_0^-$ (non-ionizing photons), $\nu = 1.06\nu_0$ (H 1^1S recombination "line") and $\nu = 0.25\nu_0$ (Balmer continuum "line"). Circles indicate the radii where $\tau_H = 1$.

For these type II models with Y =) and $\hat{S}_0$=4.13, τ_1=1.675 for $\omega_\nu \equiv 0$ and $\tau_1 = 2.388$ for $\omega_\nu \equiv 1$. Hence for the same central source luminosity, variation of the UV albedo from 0 to 1 makes the volume of the Strömgren sphere 2.75 times larger.

When the albedo is zero, only stellar photons contribute to the mean intensity at $\nu = \nu_0^{\pm}$. Thus the difference between the two curves is due to gas absorption of $\nu = \nu_0^{+}$ photons. On the $\nu = \nu_0^{+}$ curves we have indicated the points in the nebula where the optical depth of neutral hydrogen at $\nu = \nu_0^{+}$, τ_H, is equal to unity. τ_H is defined as

$$\tau_H(r) = \int_{r_0}^{r} (1 - x)\, n(r')\, \sigma_0 dr' . \qquad (7.1)$$

Interior to that point, the $\nu = \nu_0^{\pm}$ curves converge because the gas is optically thin. At the Strömgren radius, $\tau_H \sim 10^3$ in all of our models.

Because the gas does not absorb $\nu = \nu_0^{-}$ photons, the large difference between the $\nu = \nu_0^{-}$ curves for $\omega = 0$ and 1 is due entirely to the properties of the dust. When $\omega_\nu = 0$, $r^2 H_{\nu_0}(r) \propto e^{-\tau}$ where τ is the dust extinction (and absorption) optical depth. However, when $\omega_\nu = 1$, $r^2 H_{\nu_0}(r) = r^2(H^*_{\nu_0} + H^D_{\nu_0})$ = constant. Thus we see that the effects of albedo on continuum mean intensities are much greater for photons that are not absorbed by gas. In addition, the "source function" for diffuse continuum photons is proportional to $\omega J_\nu(\tau)$ and hence the mean intensity is strongly dependent on the albedo. This is not true, however, for lines as can be seen by comparing the $\nu = 0.25\nu_0$ curves for $\omega = 0$ and $\omega = 1$. In this

case, the variation of the mean intensity is almost independent of albedo because the "source function" is roughly constant.

Although we have not plotted the variation of the mean intensity for "hard" UV photons ($\nu > 4\nu_0$), we should mention here that the ionization at the Strömgren radius is sustained by these penetrating photons (whose gas opacity is small over most of the nebula) and by recombination photons.

The Eddington factor, calculated self-consistently by the QDM, depends on the boundary conditions and on the source of the photons. Our boundary conditions assume that there is no source of photons from outside of the nebula. Thus diffuse continuum photons must all be traveling "outward only" near the outer boundary and $f_\nu(\tau) \to 1$. However, for lines, which are emitted isotropically and whose emission does not depend directly on $J_\nu^D(\tau)$, $f_\nu(\tau)$ stays close to the isotropic value of $\frac{1}{3}$ throughout the nebula. On Figure 5, we present the Eddington factor from the standard model for the diffuse continuum at the Lyman limit and for hydrogen $n = 1$ and Balmer continuum recombination lines. It can be seen that even for intermediate values of ω_ν and τ ($\tau \approx 1.5$ for the standard model), the diffuse continuum becomes sharply forward peaked at the outer boundary, and the Eddington approximation should differ from the QDM solution in this region. The modified Eddington approximation (see section 5.4) does a better job of approximating the variation of the Eddington factor for both the continuum and the lines.

Physically, the reason that UV continuum photons become so forward peaked at τ_1 is that those photons which are not traveling

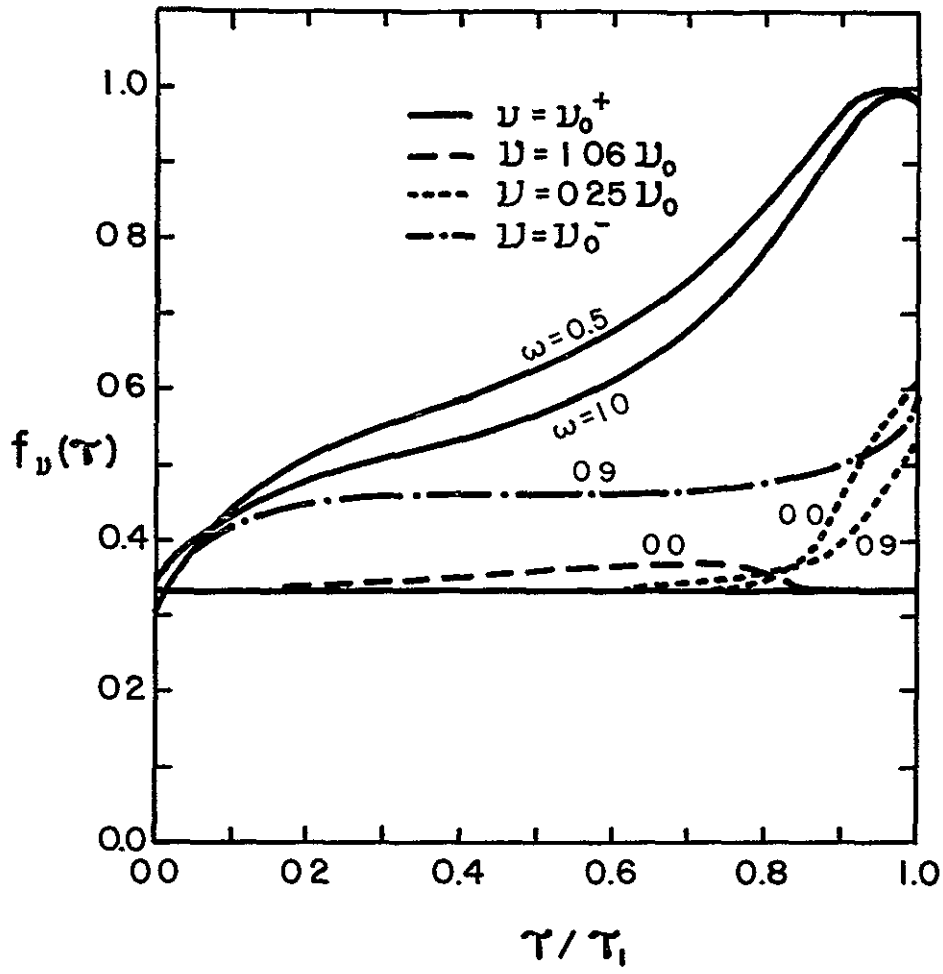

Fig. 5. Eddington Factor. Eddington factor versus τ/τ_1 for various albedos and for the frequencies of Fig. 4.

radially outward have a longer path length in the gas and are hence preferentially absorbed by the gas. It should be remembered, however, from Figure 4 that the intensity of these photons is so low at τ_1 compared to UV lines that they do not contribute to either gas ionization or dust heating. Because lineshave a constant source function, they can maintain isotropy throughout most of the nebula. The OP line, which is not absorbed by gas, does "see" the edge of the nebula and becomes somewhat forward peaked right at the Strömgren radius. On the other hand, because of the large gas optical depth, the $\nu = 1.06\nu_0$ line does not "see" the boundary and remains nearly isotropic throughout. The Lyman-α line, for which we have not plotted the Eddington factor, maintains $f_\nu(\tau) \equiv \frac{1}{3}$ throughout the nebula.

Finally we note that the variation of the Eddington factor is almost indepedent of albedo.

7.2.2 Ionization Structures

The overall ionization structures of hydrogen, helium and the trace elements are presented in Table IV. These type I models, calculated using the Eddington approximation, have the same central source spectrum and Strömgren radius while the albedo and frequency dependence of the dust extinction coefficient (Eq 2 25) are varied. We have used a power-law dependence for $f_d(\nu)$

$$f_d(\nu) = (\nu/\nu_0)^\delta \qquad (7.2)$$

where δ is constant for both UV and OP photons Models A, B and C have $\omega_\nu \equiv 0$ and $\delta = 0$, 1 and 2 respectively. Model D is a nebula

TABLE IV

IONIZATION STRUCTURE OF MODEL NEBULAE

Models

Parameter	A	B	C	D	E	F
$\hat{S}_0$	4.128	9.0	13 0	1.69×10^{11}	2.5	1.3
δ	0	1	2	0	0	0
ω_ν	0	0	0	0	0.5	1.0
f_{gas}	0.298	0.158	0.102	0.927	0.495	0.961
L_{He+}	1.015	0.889	0.383	1.019	1.015	1.014
$\langle x \rangle$	0.973	0.995	0.991	0.977	0.974	0.976
$\langle y^+ \rangle$	0.988	0.884	0.380	0 995	0.989	0.989
$\langle O^+ \rangle$	0.035	0.254	0.793	0 036	0.030	0.027
$\langle O^{+2} \rangle$	0.952	0.740	0.196	0.953	0.957	0.962
$\langle C^+ \rangle$	0.043	0.157	0.506	0.021	0.039	0.036
$\langle C^{+2} \rangle$	0.426	0.642	0.466	0.451	0.398	0.375
$\langle C^{+3} \rangle$	0.525	0.199	0 024	0.505	0.558	0.586
$\langle N^+ \rangle$	0.043	0.224	0.691	0.032	0.038	0.035
$\langle N^{+2} \rangle$	0 818	0.719	0.286	0.845	0.818	0.819
$\langle N^{+3} \rangle$	0.135	0.054	0.0091	0 107	0.140	0.142
$\langle S^+ \rangle$	0.0097	0.036	0.155	0.0021	0.0090	0.0083
$\langle S^{+2} \rangle$	0.068	0.314	0.680	0.069	0.059	0.051
$\langle S^{+3} \rangle$	0 733	0.577	0.150	0.767	0.734	0.735
$\langle S^{+4} \rangle$	0.188	0.071	0.011	0.156	0.198	0 205
$\langle Ne^+ \rangle$	0.133	0.479	0.899	0.136	0.117	0.104
$\langle Ne^{+2} \rangle$	0.864	0.516	0.083	0.864	0.881	0.893

TABLE IV (Cont.)

Models

Parameter	A	B	C	D	E	F
$\langle Ar^{+} \rangle$	0.0056	0.117	0.612	0.0017	0.0051	0.0046
$\langle Ar^{+2} \rangle$	0 294	0.543	0.315	0.306	0.266	0.243
$\langle Ar^{+3} \rangle$	0.698	0.337	0.052	0.692	0.727	0.750

without dust. Models E and F have $\delta = 0$ and $\omega_\nu \equiv 0.5$ and 1.0 (independent of frequency) respectively. The functions f_{gas} and L_{He^+} are calculated with Eqs. (3.34) through (3.36) and in all of these models, $L_{He^{++}} \approx 10^{-8}$. The average ionizations are calculated using Eq. (3.37) and we have not listed ions for which $\langle X^{+P} \rangle < 10^{-4}$.

In models A and D through F, $L_{He^+} \geq 1.0$, in agreement with the results of Hjellming (1966) but not with Hummer and Seaton (1964). Sarazin (1977), who finds $L_{He^+} < 1.0$, incorrectly concludes that this is an effect of the on-the-spot approximation. Our parametric studies have shown that the details of the ionization structure at the Strömgren radius depend most strongly on the spectrum of $J_\nu(\tau \approx \tau_1)$. However, as Sarazin states, the question is academic because static photoionization models are not valid at the Strömgren radius where an ionization front and associate shock waves exist. We note also that L_{He^+} does not depend on ω_ν. Because $\omega_\nu \leq 1$, this conclusion is independent of the frequency dependence of the albedo. As δ increases dust competes more effectively for He ionizing photons and the He Strömgren radius moves inward relative to r_1. The function f_{gas}, on the other hand, depends strongly on both δ and ω which, unfortunately, reduces its reliability in determining τ_1 observationally (see section 3.8).

There are two classes of ions whose average ionization depends on ω_ν. This dependence is defined arbitrarily as a variation of $\langle X^{+P} \rangle$ greater that 10% between models A and F. Class I ions (O^+, C^+, N^+, S^+, Ne^+ and Ar^+) all occur only at the Strömgren radius

where the variation in the spectrum of $J_\nu(\tau)$ is the greatest from models A to F. As we discussed in the last section, the effect of albedo is to strongly enhance the intensity of UV photons near τ_1. Hence the effect of increasing albedo is to enhance the lines from higher stages of ionization at the expense of the lines from lower stages of ionization.

Class II ions (C^{+2}, C^{+3}, S^{+2}, Ar^{+2}) occur in ionization structures that are not dominated by the X^{+2} ion. Dominance of the second ion is defined roughly as $\langle X^{+2} \rangle \geq 0.8$. Physically changes in $\langle X^{+P} \rangle$ can only affect $\langle X^{+P+1} \rangle$ if the $P+1$ ion does not dominate. The ionization structure of carbon is not dominated by any ion so all stages of ionization are affected by ω_ν. All of the effects are, however, much smaller than those of the variation of δ.

Although our central source temperature is for an HII region and not planetary nebulae, we can comment on the CIV/CIII ratio that has been a problem for models of NGC 7027 in particular (Bohlin, Marionni, and Stecher 1975 and Péquignot, Aldrovandi, and Stasinska 1977). Depending on the details of model, the model CIV/CIII ratio [I(1549Å/I(1909Å)] has been from 5 to 10 times larger than the observed ratio. Our calculations show that increasing the albedo enhances the abundance of CIV relative to CIII. However, increasing δ has the opposite effect. It would appear that some combination of positive δ and resonance scattering of the permitted CIV λ 1549 line to increase its absorption by dust could help solve this problem.

In Figure 6 we have plotted the ionization structures of H, He, O, C, N and S for models A through F. The Ne and Ar ionization structures have not been plotted. The Ne structure is qualitatively like that of

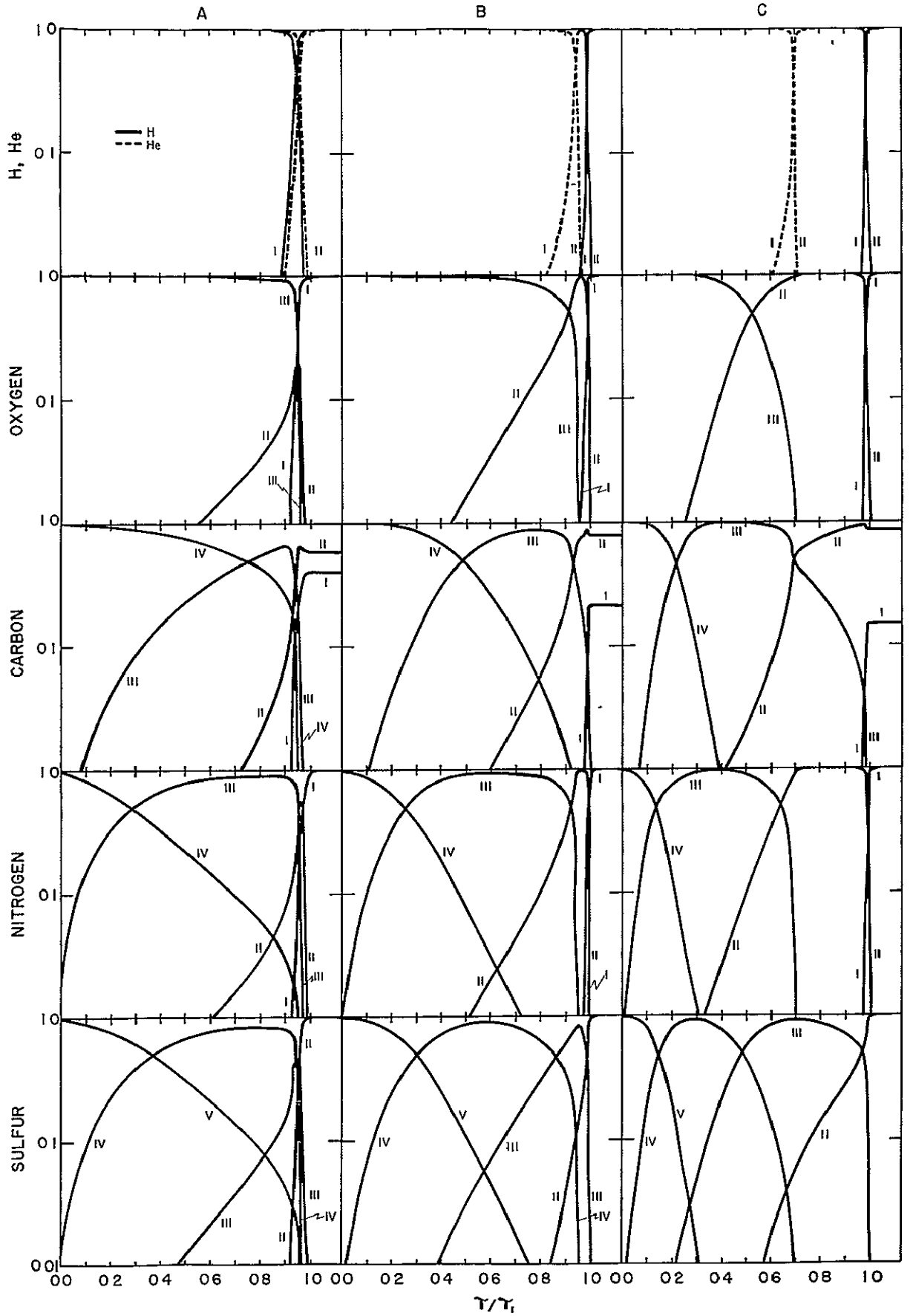

Fig. 6a. Ionization Structures of H, He, O, C, N, and S. Model A is the standard model, Model B has $\delta = 1$ and Model C has $\delta = 2$.

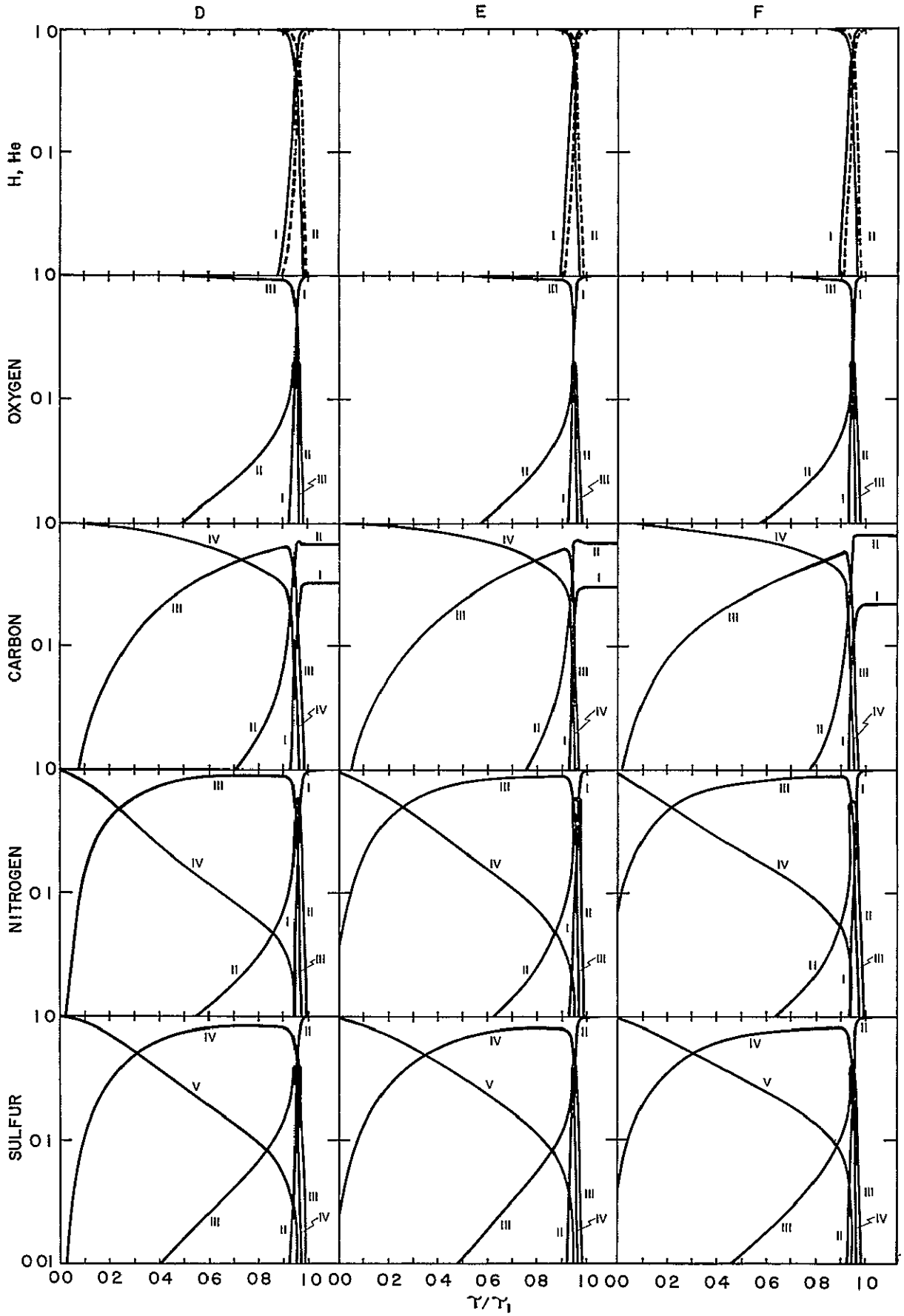

Fig. 6b. Ionization Structures of H, He, O, C, N, and S. Model D has no dust, Model E has $\omega_\nu = 0.5$ and Model F has $\omega_\nu = 1.0$.

0. However, the Ar structure is unique as can be seen in table IV. It is almost dominated by $\langle Ar^{+3} \rangle$ and there is a monatomic decrease in $\langle Ar^{+P} \rangle$ as P decreases for the $\delta = 0$ models (C also exhibits this behavior). The ionization structures are plotted versus τ/τ_1 and there is no material with $\tau > \tau_1$ (see section 2.6).

The ionization potentials of C^0 and S^0 are below 13.6eV so that they are not neutral at the H Strömgren radius. S^0 does not exist in our models but C^0 and C^+ co-exist at τ_1. For clarity in Figure 6, C^0 and C^+ abudances are extended as straight lines for $\tau > \tau_1$. The C ionization structure is the only one we have plotted that is sensitive to the electron density. The discontinuities in the C^{+2} structure in models B and C occur at the He Strömgren radius

Sarazin (1977) plots on his Figure 1 the ionization structures of H, He, N, O and S for a Salpeter initial-mass function central source whose spectrum is similar to an O6 star ($T^* \sim 42{,}000^oK$, ZAMS). This spectrum is slightly hotter and broader in the UV than our standard model central source. Sarazin finds a monotonic increase in the He transiton zone widths* with increasing δ. Our results indicate that this behavior is not monotonic. This result is, however, highly dependent on the details of the central source spectrum and, to some extent, the method of solution. We find that albedo has little effect on the width of the transition zones. Sarazin's zone II ions (N^{+2}, O^{+2}, S^{+3}, C^{+3}, Ne^{+2}, Ar^{+3}) are all dominant and have the largest average ionization in model A. The average ionization of these ions decrease with increasing δ. The average ionizations increase slightly, however, with increasing albedo.

---

* Sarazin uses a slightly smaller value of ϵ ($\epsilon \sim 1.4 \times 10^{-4}$) for his models in Figure 1 which accounts, in part, for his wider transition zones.

Balick (1975) has calculated average ionizations using the on-the-spot approximation, $T^* = 40{,}000^{\circ}K$, and $n = 10^3 cm^{-3}$ for uniform nebula and various forms for $f_d(\nu)$ including a linear form ($\delta = 1$). He then varies ϵ and studies the behavior of $\langle X^{+P} \rangle$. He finds that only an extreme step form of $f_d(\nu)$ [$f_d(\nu) = 1$ for $\nu_0 \leq \nu < 1.807\nu_0$, $f_d(\nu) = 10$ for $1.807\nu_0 \leq \nu \leq \infty$] can reproduce Mezger's (Mezger et al, 1974) observations of $L_{He^+} \sim 0.1$ for several galactic HII regions. Our parametric studies have shown that we need $3 \leq \alpha \leq 4$ to produce $L_{He^+} \sim 0.1$ with our standard model.

Balick and Sneden (1977) have calculated model HII regions using the on-the-spot approximation with up-to-date model atmosphere central source spectrums that include metal opacities. These atmospheres have considerably less high energy UV flux than those of Auer and Mihalas (1972) or black bodies. Therefore, emitted low excitation lines will be enhanced relative to high excitation lines if more realistic stellar spectra are used.

7.2.3 Infrared Emission

In order to study the effects of albedo on the dust temperature structure, we will use the simplifying assumptions of generalized Mie theory (with $J = 1$) and optically thin IR emission. With these approximations the IR spectrum is a probe of the entire dust temperature structure. We will use type II models so that the luminosity of the central source is constant.

Figure 7 shows the IR spectrum for our standard model with $\omega_\nu = 0$ and $\omega_\nu = 0.9$ independent of frequency. The spectrum was calculated using Eq. (4.21). The albedo therefore applies only to the UV and OP photons that heat the dust. Again we assume that there is no material outside of the Strömgren radius of the gas. If radiative transfer of IR photons had been calculated, then because

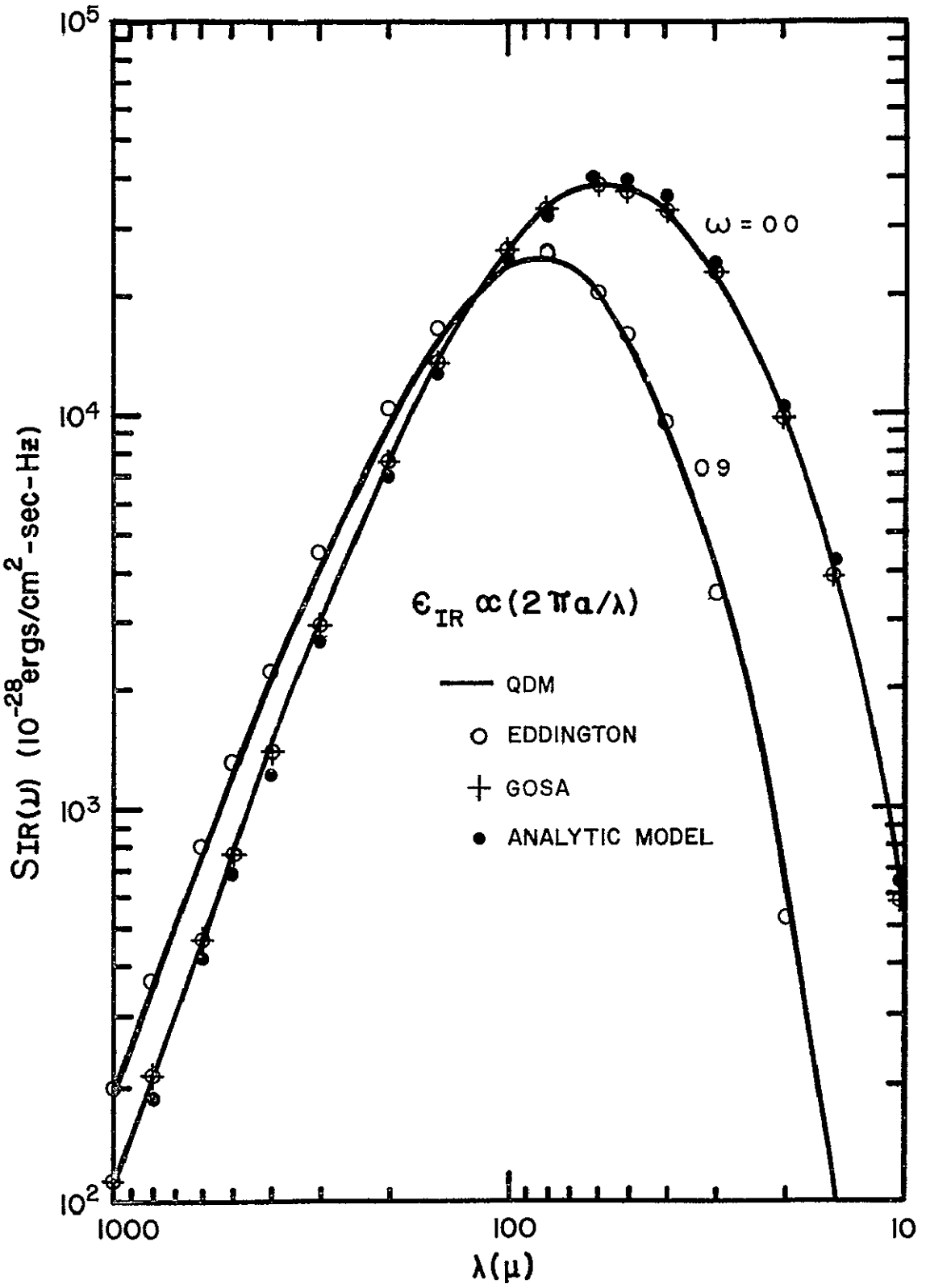

Fig. 7. Infrared Spectra for Various Solutions of Radiative Transfer. Spectra for ω_ν = 0 and 0.9 for UV and OP photons are plotted assuming generalized Mie theory ($\jmath$ = 1) and optically thin dust in the infrared.

most of the spectrum would be optically thin due to the λ^{-1} dependence of $\kappa_\nu(r)$ in the infrared, the main effects show up in the near infrared where the unattenuated Rayleigh-Jeans tail of the central source adds significantly to $S_{IR}(\nu)$.

There are three important effects illustrated by Figure 7. First, as the albedo increases the luminosity of the IR spectrum decreases (i.e. $\kappa^a_\nu(r)$ is smaller for a given extinction coefficient so that the dust absorbs less energy). Second, the spectrum is shifted towards longer wavelengths and is reduced in width (i.e. the spectrum looks more like that of a diluted black body) As we have seen, dust scattering transports photons outward and thus tends to make the mean intensity more uniform as a function of radius (see. Fig.4). Hence the effects of albedo are 1) to reduce the maximum dust temperature which occurs at the center of the nebula (i.e. $T_{d,max}$ 182^oK for $\omega_\nu = 0$ and $T_{d,max} = 117^oK$ for $\omega_\nu = 0.9$) and, 2) to reduce the variation in dust temperature throughout the nebula (i.e. $T_{d,max}/T_{d,min} = 4.75$ for $\omega_\nu = 0$ and $T_{d,max}/T_{d,min} = 4.02$ for $\omega_\nu = 0.9$). The first of these effects is due primarily to the $(1 - \omega_\nu)$ term in the right-hand side of Eq. (4.4) while the second of these effects is due primarily to radiative transfer. Thus we see that as albedo increases, the dust temperature at the same relative radius decreases and, as a result, $S_{IR}(\nu)$ for the near and mid infrared is substantially lower than the zero albedo model. Third, because τ_1 is larger for the non-zero model, there is more material with low dust temperatures which radiates the "excess" far IR flux.

7.3 Comparison of Solutions of Radiative Transfer

In this section we will make detailed comparisons of the solutions of radiative transfer that were discussed in chapter 5 with the QDM solutions and with the Eddington approximation solutions. We will concentrate on observable parameters such as f_{gas}, L_{He^+}, the average ionizations and the IR spectrum. However, the hydrogen ionization

structure will be examined to extract the differences in the properties of the approximations.

7.3.1 Diffusion Approximation

On Figure 8a we plot the emergent luminosity normalized to the luminosity of the central source for pure dust nebulae with isotropic scattering as a function of the total extinction optical depth ($f_d(\nu) \equiv 1$). The diffusion approximation (see section 5.3) does a very good job of predicting the emergent luminosity when the albedo is large and $\tau_1 \geq 2$. The free surface diffusion approximation is almost exact for $\omega_0 \geq 0.9$, whereas the infinite diffusion approximation is 10 to 40% low even for $\omega_0 \geq 0.95$.

The diffusion approximation is not valid at the boundaries and the free surface boundary condition uses a calculation similar to QDM to correct the emergent luminosity. We therefore expect good agreement when the other assumptions of the diffusion approximation are met (see section 5.3). A more exacting test of the accuracy of the approximation is a comparison of $L(\tau)/L^*$ when all assumptions are met. Figure 8b plots the transmitted luminosity as a function of τ for $\tau_1 = 10$ and $\omega_\nu = 0.9$, 0.95, 0.99, and 1.0.

The QDM solution for $\omega_\nu = 1.0$ is a test of the overall accuracy of the differential equation solvers of program SCATER. We mentioned in section 6.5 that flux was not strictly conserved in this case. Over most of the volume of the nebula, the flux is 1.5% high, a result we attribute to the linear approximations made in doing angular integrals. This error increases to 3% at the center of the nebula

C-2

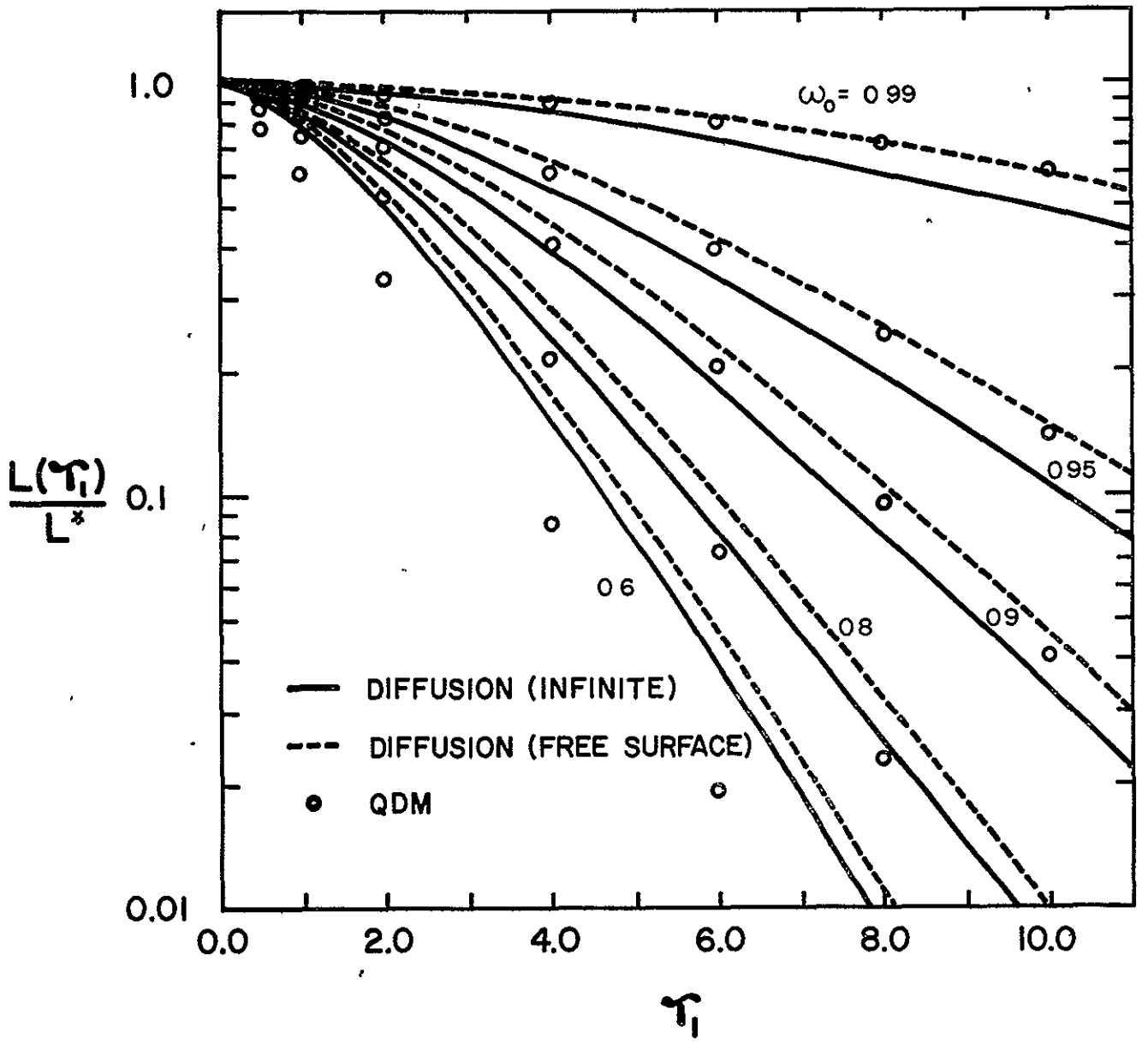

Fig. 8a. Emergent Luminosity Versus τ_1 For Various ω and For the Diffusion Approximation and the QDM. The solid lines are for infinite nebulae and the dashed lines are for nebulae with a free surface.

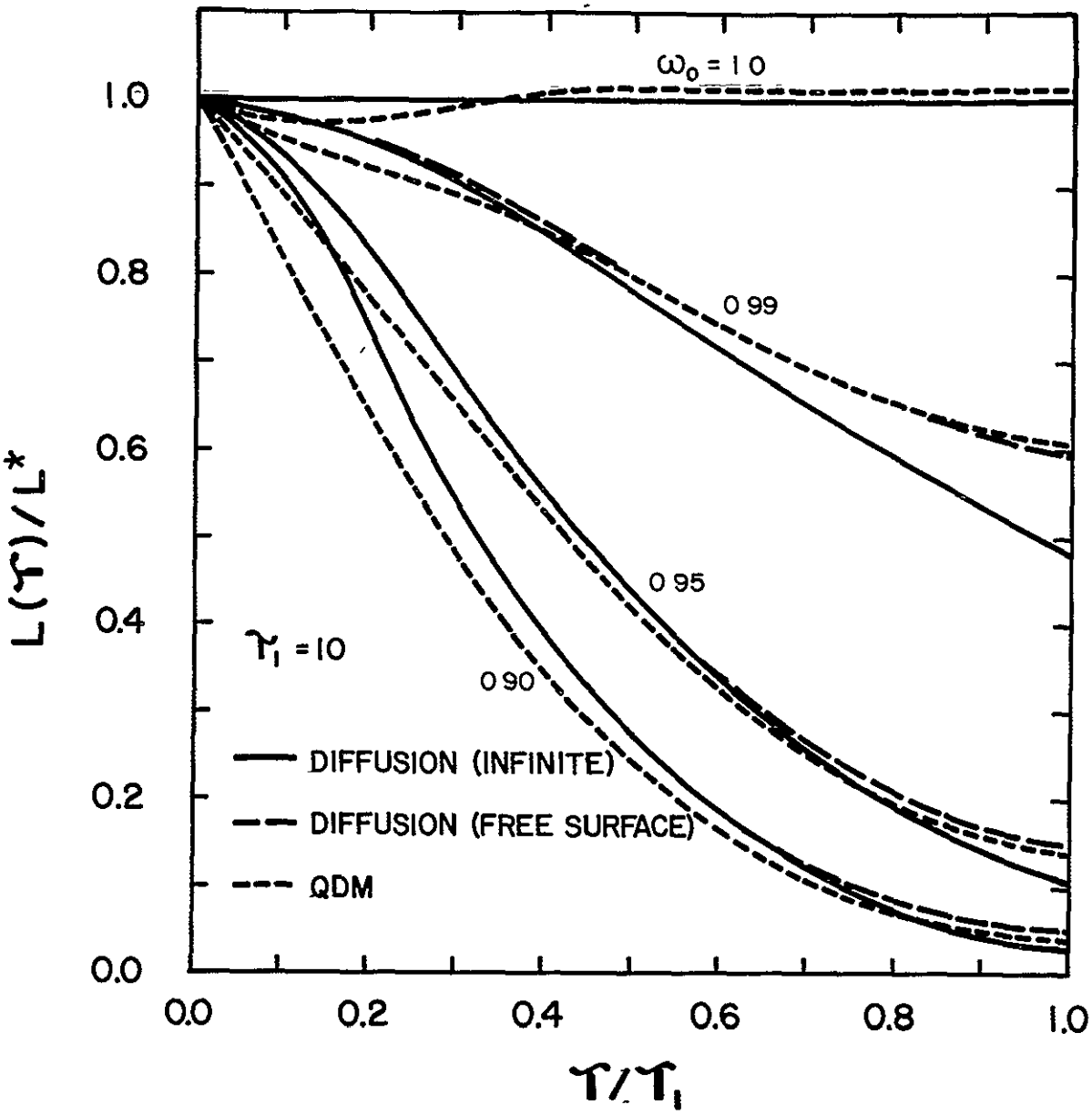

Fig. 8b. Comparison of Luminosity Versus τ for the Diffusion Approximation and for the QDM. $\tau_1 = 10$ for all models.

where the angular grid is coarse (i.e. there are only 10 grid points at $r = r_0$ whereas there are 110 at $r = r_1$ if all of the radial arrays are used) and where the r^{-2} dependence of $\hat{J}_\nu^D(\tau)$ results in less accurate radial integration.

As ω_ν decreases, the diffusion approximation becomes more accurate over most of the volume of the nebula. For $\omega_\nu < 0.99$, the infinite and free surface approximations differ only at the outer boundary, and agree with the QDM solution to within 10% over most of the volume. When $\omega_\nu = 0.99$, the infinite and free surface solutions differ by 20% while the QDM and free surface solutions agree to within 0.5%. Part of the large differences between the QDM and diffusion solutions at the center of the nebula must be attributed to the inaccuracies of program SCATER.

7.3.2 Average Ionizations of Type I Models

The accuracy of any approximate solution of radiative transfer must be assessed in terms of observable quantities. To do this, we will define the QDM solution to be an "exact" solution. We will calculate models A and F (see section 7.2.2) using the Eddington approximation, the modified Eddington approximation, and GOSA (model A only). Table V lists the observable parameters for these models and for the various solutions.

For model A average ionizations, both the Eddington approximation and GOSA differ from QDM by less than 1.5% for all ions, and f_{gas} varies by less than 2% among the solutions. For model F however, the average ionizations can vary by as much as 45% in one case (Ar^+). For dominant ions (see section 7.2.2), the Eddington approximation values

TABLE V

IONIZATION STRUCTURE OF MODEL NEBULAE

COMPARISON OF SOLUTIONS OF RADIATIVE TRANSFER

Parameter	Models[++] A	A	A	F	F	F
Solution	EDD[+]	GOSA[*]	QDM[±]	EDD[+]	QDM[±]	MEA[±±]
$\hat{S}_0$	4.128	4.128	4.128	1.300	1.300	1.300
δ	0	0	0	0	0	0
ω_ν	0	0	0	1.0	1.0	1.0
f_{gas}	0.298	0.291	0.298	0.961	0.936	0.961
L_{He}	1.015	1.016	1.016	1.014	1.016	1.015
$\langle x \rangle$	0.973	0.972	0.973	0.976	0.970	0.973
$\langle y \rangle$	0.988	0.988	0.988	0.989	0.986	0.988
$\langle O^{+} \rangle$	0.035	0.034	0.035	0.027	0.032	0.030
$\langle O^{+2} \rangle$	0.952	0.953	0.952	0.962	0.953	0.957
$\langle C^{+} \rangle$	0.043	0.043	0.044	0.036	0.046	0.042
$\langle C^{+2} \rangle$	0.426	0.420	0.425	0.375	0.385	0.375
$\langle C^{+3} \rangle$	0.525	0.531	0.525	0.586	0.564	0.580
$\langle N^{+} \rangle$	0.043	0.042	0.043	0.035	0.043	0.040
$\langle N^{+2} \rangle$	0.818	0.816	0.817	0.819	0.809	0.801
$\langle N^{+3} \rangle$	0.135	0.138	0.135	0.142	0.142	0.154
$\langle S^{+} \rangle$	0.0097	0.0098	0.0098	0.0083	0.012	0.0097
$\langle S^{+2} \rangle$	0.068	0.066	0.068	0.051	0.062	0.058
$\langle S^{+3} \rangle$	0.733	0.732	0.733	0.735	0.723	0.715
$\langle S^{+4} \rangle$	0.188	0.192	0.189	0.205	0.202	0.217
$\langle Ne^{+} \rangle$	0.133	0.130	0.133	0.104	0.121	0.115
$\langle Ne^{+2} \rangle$	0.864	0.867	0.864	0.893	0.876	0.882

Models[++]

Parameter	A	A	A	F	F	F
Solution	EDD[+]	GOSA[*]	QDM[±]	EDD[+]	QDM[±]	MEA[±±]
$\langle Ar^{+} \rangle$	0.0056	0.0055	0.0056	0.0046	0.0064	0.0054
$\langle Ar^{+2} \rangle$	0.294	0.288	0.294	0.243	0.266	0.257
$\langle Ar^{+3} \rangle$	0.698	0.704	0.698	0.750	0.725	0.736

[*]GOSA: Generalized On-the-Spot Approximation (Section 5.2.1)

[+]EDD. Eddington Approximation

[±]QDM. Quasi-Diffusion Method

[±±]MEA. Modified Eddington Approximation (Section 5.4)

[++]Models A_{EDD} and F_{EDD} are reproduced from Table IV for comparison.

agree with the QDM values to within 10% in all cases. In general, the modified Eddington approximation (MEA) does better than the Eddington approximation, especially for those ions whose average ionizations are small. Only for $\langle C^{+2} \rangle$, $\langle N^{+3} \rangle$, and $\langle S^{+4} \rangle$ does the MEA fail to do a better job of reproducing the average ionizations.

7.3.3 Ionization Structure of Type II Models

The detailed ionization structure of hydrogen is presented in Figure 9 for type II models. The solid lines are for QDM models with ω_ν = 0, 0.5, 0.8 and 1.0 in the UV. In addition we plot (1 - x) for the GOSA, the Eddington approximation and the analytic model. For simplicity helium has not been included in these calculations although all the other parameters are the same as our standard model.

For ω_ν = 0 we can make a direct comparison of all our models. As can be seen from Figure 9, (1 - x) calculated with GOSA and Eddington approximation agree with QDM's calculation over most of the nebula. The Eddington approximation agrees to within 5% over all of the nebula and to within 2% except where (1 - x) $\sim$ 0.1. GOSA agrees to within 10% when (1 - x) $\gtrsim$ 0.1 but varies by as much as 40% when (1 - x) $\approx$ 1.0 All three models produce exactly the same value of τ_1 (i.e. they all find the Strömgren radius condition [Eq. 3.32] satisfied at the same radial grid point). The analytic model which uses OSA (diffuse UV photons are absorbed on-the-spot by the gas) underestimates the value of (1 - x) because dust does absorb a large fraction of diffuse UV photons. The analytic model also underestimates the value of τ_1 by 10% primarily because it uses frequency averaged intensities and cross sections. Hence the analytic model cannot account for the fact

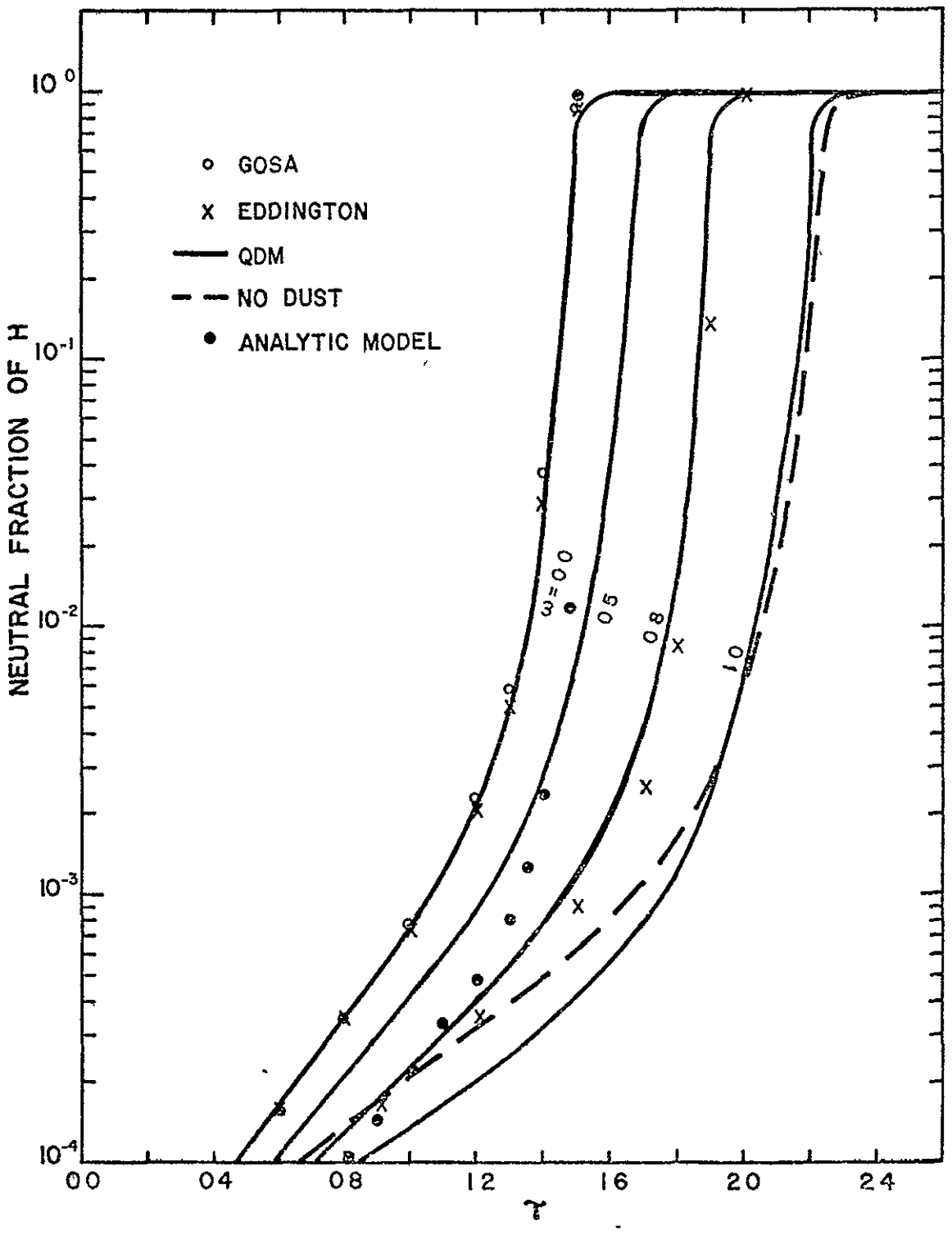

Fig. 9. Neutral Fraction of Hydrogen Versus τ for Various ω and Solutions of Radiative Transfer. A model without dust (dashed line) calculated with the QDM is presented for comparison with the $\omega_\nu = 1$ model.

that hard UV photons penetrate farther into the gas than do photons with $\nu \approx \nu_0$. The rounding of 1 - x at the Strömgren radius is due to ionizations by recombination lines and by penetrating hard UV photons.

As the albedo increases the Eddington approximation becomes less accurate when compared to the QDM solution of (1 - x) because the Eddington approximation does not account for the forward peaking of the scattered continuum. The Eddington approximation model calculates a larger value of $J_\nu^D(\tau)$ over most of the nebula and hence a smaller value of (1 - x). It should be remembered from the last section that despite these differences in the internal structure, observable quantities agree well between the two models.

We have also plotted 1 - x for a dusty model with $\omega_\nu \equiv 1$ and a dustless model [dashed line with $d\tau = (2 \times 10^{-4}) n(r) \sigma_0 dr$] with the same luminosity and gas density. The difference in (1 - x) between the two models is due primarily to the difference in the stellar flux as a function of radius. The dusty model quickly scatters the stellar photons into diffuse (and more isotropic) photons, increasing the mean intensity near the center of the nebula and thus reducing (1 - x) relative to the dustless model. At the Strömgren radius the dustless model has a smaller (1 - x) and therefore a larger τ_1 because the stellar flux is considerably larger than at a corresponding point in the dusty model. Hence in the dustless model the stellar photons penetrate farther into the nebula before they are absorbed by the gas.

7.3.4 Variation of f_{gas} with Albedo

The fraction of UV photons "destroyed" by gas, f_{gas}, depends primarily on the value of τ_1 for our standard models because of the

"sharpness" of the ionization fronts. We therefore expect that all models of radiative transfer that accurately calculate τ_1 will also accurately calculate f_{gas}. On Figure 10 we plot the variation of f_{gas} (calculated with Eq. 3.34) with albedo for the QDM, Eddington approximation, GOSA and analytic models. As expected the Eddington approximation calculation of f_{gas} agrees very well with the QDM calculation. In addition, both GOSA and analytic models accurately calculate f_{gas} when $\omega_\nu \equiv 0$.

Although we have not plotted L_{He^+}, the ratio of the intensity of helium to hydrogen recombination line (Eq. 3.36), we find similarly excellent agreement among the various models because this quantity also depends primarily on the value of τ_1.

7.3.5 Infrared Emission

On Figure 7 we have plotted the infrared spectrum for our Standard models and for the QDM solution, the Eddington approximation, GOSA, and the analytic model. For $\omega_\nu = 0$ all approximate solutions reproduce the shape and the strength of the spectrum.

The analytic model is least accurate for two reasons. First, the volume integral of Eq. (2.21) is calculated in a more approximate way in the analytic model. Second, the analytic model underestimates τ_1 by 10%, and hence underestimates the far infrared flux that is radiated by low temperature dust at the edge of the nebula.

Agreement between the Eddington approximation, GOSA and the QDM spectra for $\omega_\nu = 0$ is almost exact because, for this model, most dust heating is by stellar photons in the OP and UV ranges. However, for $\omega_\nu > 0$, the Eddington approximation underestimates J_ν^D at the center

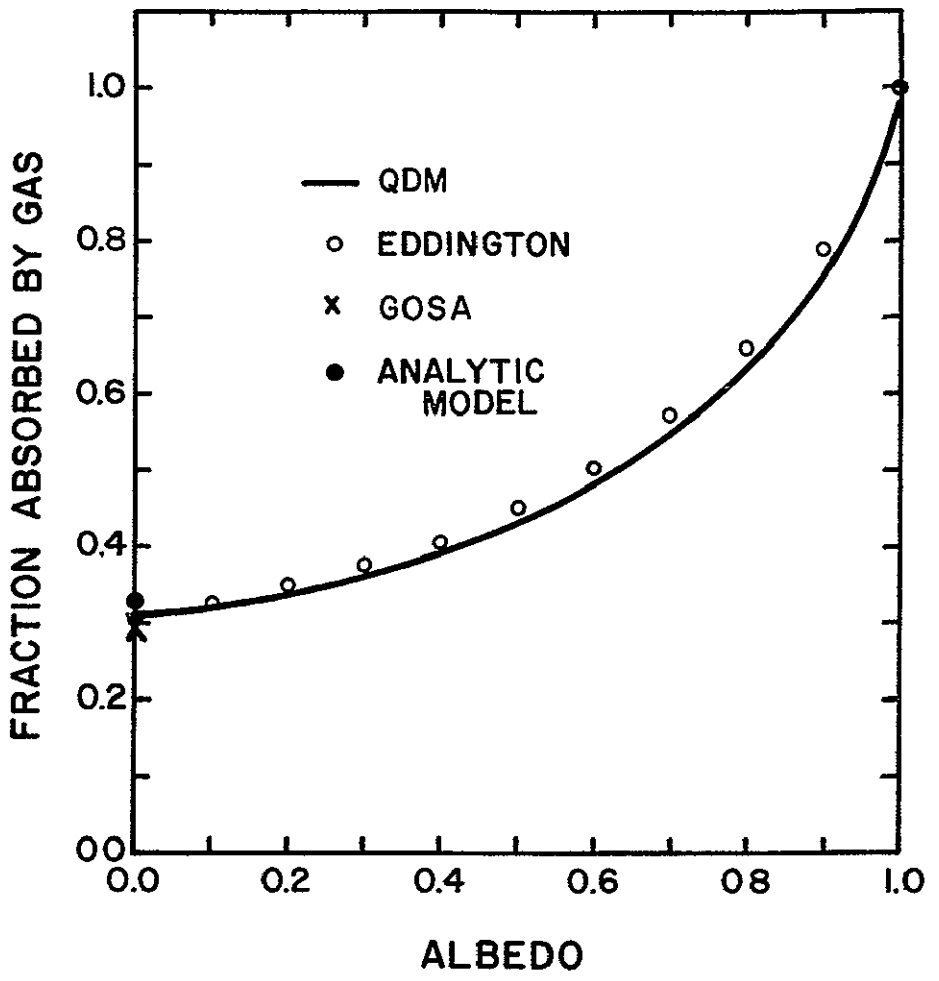

Fig. 10. Variation of f_{gas} Versus ω for Various Solutions of Radiative Transfer.

of the nebula and overestimates J_ν^D at the Strömgren radius. Hence the near infrared is too low compared to the QDM and the far infrared is too high. Even so, L_{IR} (Eq. 4.23) agrees to within 0.2% between the Eddington and QDM spectra.

In general, these comparisons are academic because of the 20 to 50% errors in the published IR broadband photometric data.

7.3.6 Accuracy of Semi-Analytic Solution

The semi-analytic solutions described briefly in section 5.2.2 and appendix B and completely in Papers I and II are extremely useful for calculating f_{gas} and L_{He^+} because they are simple to calculate. The models use frequency averaged intensities and fluxes, however, so that they cannot be expected to accurately describe the details of the ionization structures at the Strömgren radius.

We have run several GOSA calculations using program SCATER with various power law forms for the frequency dependence of the dust extinction coefficient in the UV ranging from $(\nu/\nu_0)^{-3}$ to $(\nu/\nu_0)^{+4}$, with τ_1 in the range $1 \leq \tau_1 \leq 3$, with $\gamma_0 = 0.04$ and 0.108 (see Eq. B.1), and with $Y = 0.1$. We have also calculated the semi-analytic models with values of α (see Eq. B.4) calculated by using the corresponding power law from for $\sigma_d(\nu)$ averaged over the spectrum of the central source [i.e. in Eq. B.2, replace $\sigma_H(\nu)$ with $\sigma_d(\nu)$ and use $J_\nu^*(r_0)$].

When we compare these solutions, we find that for $\alpha \leq 0$ ($\delta \leq 0$ in Eq. 7.2) L_{He^+} agrees to within 10% and f_{gas} to within 20% in all cases. However, when $\alpha > 0$ ($\delta > 0$) L_{He^+} usually agree to within 50% but f_{gas} can differ by as much as 150%. The

reason for these large errors is that the semi-analytic models fail to predict the sharp decrease in τ_1 as a positive δ (defined above) increases. Physically what is happening is that because the semi-analytic model treats all UV photons alike, it fails to account for the "penetrating power" of hard UV photons (remember that the gas opacity drops rapidly as ν increases). If these photons are preferentially absorbed by dust, then the Strömgren radius must move inward. Even so, L_{He^+} is fairly accurate because it is calculated as the ratio of two functions of τ_1 (see Eq. B.33). f_{gas}, on the other hand, is proportional to a single function of τ_1 (Eq. B.31).

Finally, we can define an effective optical depth, τ_{eff}, which when used in Eq. (B.31), produces the same value of f_{gas} that is calculated by program SCATER. If we do this as a function of the UV albedo for our standard model parameters, we get the curves shown in Figure 11. Here we have plotted τ_{eff}/τ_{abs} where $\tau_{abs} \equiv (1-\omega)\tau_1$ versus ω. We see that these curves bear little resemblance to those of Figure 7 in paper I. If, however, one were to continue the lengthy and costly process of calculating type I models ($\hat{S}_o$ must be adjusted to keep τ_1 constant as ω increases), then Figure 11 could be used to adjust the values of τ_1 deduced from observations (section 3.8) for an assumed albedo.

7.4 Conclusions and Concluding Remarks

We have considered the effects of dust scattering on the internal structure and observable quantities of dusty nebulae. We have also compared our solutions with more approximate solutions of radiative transfer. When doing these comparison we consider the QDM solution

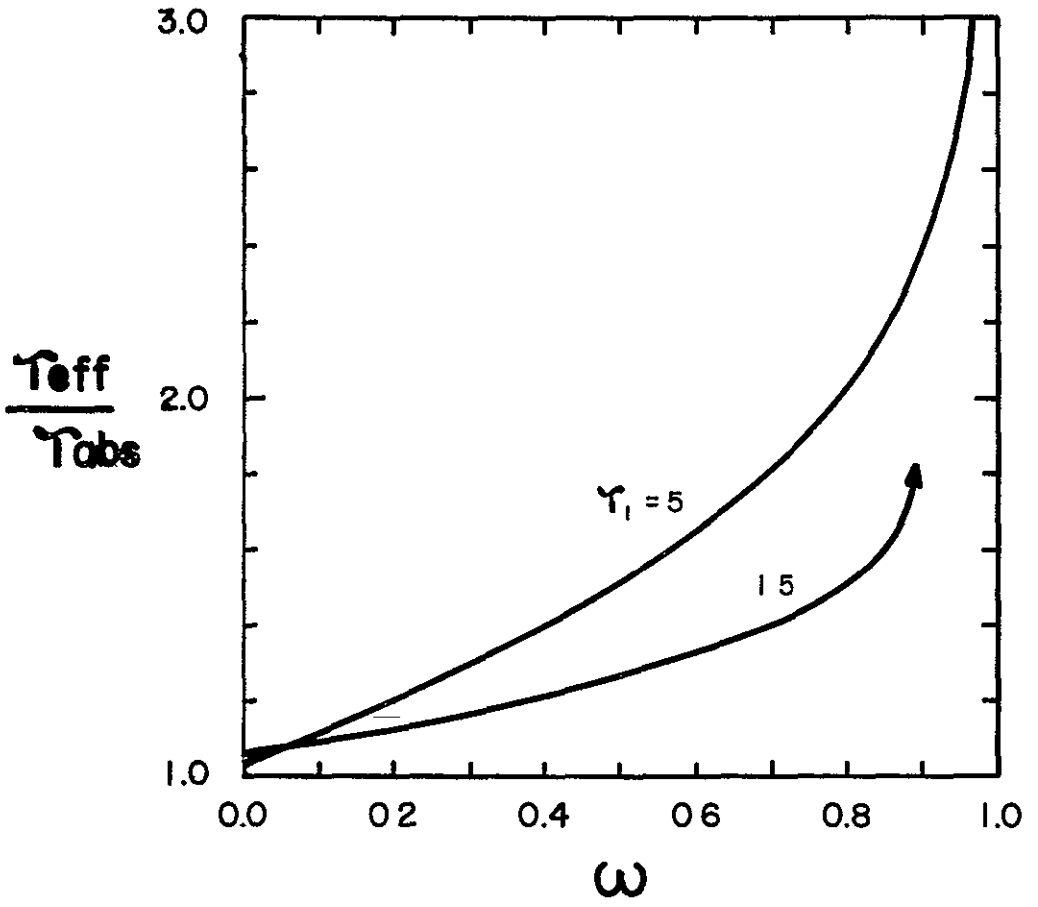

Fig. 11. Effective Optical Depth Versus ω

to be "exact". Particular emphasis has been given to ionization structures of the gas and to the emitted infrared spectrum. The major new results and conclusions of this study are listed below.

1. UV and OP recombination line intensities (even those not resonantly scattered by the gas) remain fairly isotropic throughout the nebula while the scattered continuum intensities become outwardly peaked.
2. The radial variation of the Eddington factor is fairly independent of albedo.
3. L_{He+} does not depend on the albedo of dust. It does depend weakly on τ_1 and strongly on the frequency dependence of the dust extinction coefficient and on the spectrum of the central source.
4. f_{gas} depends strongly on both the albedo and the frequency dependence of the dust extinction coefficient.
5. Dust scattering has the following effects on the ionization structures of hydrogen, helium and the trace elements.
   a) Dust scattering enhances the UV mean intensity near the Strömgren radius.
   b) Therefore near the Strömgren radius increasing albedo enhances lines from higher stages of ionization at the expense of lines from lower stages of ionization.
   c) Interior to the Strömgren radius, dust scattering can strongly affect only ionization structures that are not dominated by a single ion. Carbon and Argon were the only elements we included that were strongly affected by dust scattering.

d) In all cases the effects of the variation of the albedo were much smaller than the effects of the variation of the frequency dependence of the dust UV extinction coefficient.

6. Increasing the albedo of dust in the frequency ranges primarily responsible for dust heating has the following two major effects.

   a) The total infrared luminosity and the dust temperature at the same relative radius are reduced because the dust absorption coefficient is reduced for a given extinction coefficient.

   b) The variation of the dust temperature from the inner to the outer radius of the nebula is reduced, thus making the observed IR spectrum narrower.

7. The diffusion approximation with the "free surface" boundary condition can accurately predict both the emergent luminosity and the internal variation of the flux when the assumptions of the approximation (large scattering optical depth) are met.

8. When the UV albedo is zero the average ionizations of all elements calculated using GOSA or the Eddington approximation agree with the values calculated by QDM to within 1.5%. f_{gas} varies by less than 2% among the different solutions.

9. When $\omega_\nu \equiv 1$ for UV photons the Eddington approximation average ionizations agree with the QDM values to within 10% for all dominant ions. Variations between the solutions as large as 45% can be found when the average ionizations are small. In general, the modified Eddington approximation predicts values closer to those of QDM.

10. f_{gas} and the IR spectrum are accurately calculated by the Eddington approximation.

11. The semi-analytic solutions calculate L_{He^+} and f_{gas} to within 10% and 20% respectively if dust does not preferentially absorb hard UV photons. When this does happen, L_{He^+} is accurate to within 50% but f_{gas} can be off my more than a factor of 2.

Finally, a few words should be said about the conclusions we did not or could not make. As has often been the case of previous generations of graduate students, this thesis is being completed at this time because a new and completely different career awaits in the very near future. Hence several things must be left undone.

Although program SCATER has been used in close collaboration with the author by Alan Tokunaga of NASA-Ames Research Center in an attempt to fit the IR spectra of S140, this work is still too preliminary to include here. Regretfully, we have not had time to use SCATER to fit both the OP and IR spectra of an HII region.

In addition, we have not had time to include radiative transfer of OP and IR forbidden lines. This work would require first a self-consistent electron temperature calculation and then calculation of the populations of the collisionally excited states from which these forbidden lines come.

Appendix A

DIFFERENCE EQUATIONS

The JAY [Eq. (2.19)] and RAY [Eq. (2.42)] equations are both of the form

$$\mathcal{D}Y = A\left[\frac{d}{dx}\ \frac{B}{C}\frac{d}{dx}(DY)\right] \approx EY + F \qquad (A.1)$$

where the known functions A through F are, in general, dependent on frequency, x , and Y . The boundary conditions are of the form

$$G\frac{d}{dx}(DY)\Big|_{x=x_B} = (HY + I)\Big|_{x=x_B} \qquad (A.2)$$

for both the inner and outer boundaries of the JAY and RAY equations.

The range of x is divided into n grid points with $x_1 < x_2 < \ldots\ldots < x_{i-1} < x_i < x_{i+1} < \ldots < x_n$. Using a three-point central difference approximation for the $\mathcal{D}Y$ term evaluated at the i^{th} grid point gives

$$\mathcal{D}_i Y_i = A_i \frac{\left[\frac{B_{i+1}}{C_{i+1}} + \frac{B_i}{C_i}\right]\left[\frac{D_{i+1}Y_{i+1} - D_i Y_i}{x_{i+1} - x_i}\right] - \left[\frac{B_i}{C_i} + \frac{B_{i-1}}{C_{i-1}}\right]\left[\frac{D_i Y_i - D_{i-1}Y_{i-1}}{x_i - x_{i-1}}\right]}{x_{i+1} - x_{i-1}} \qquad (A.3)$$

Substituting Eq (A.3) into Eq (A.1) gives the set of difference equations that approximate Eq. (A 1).

$$(T_1+T_2)D_{i-1}Y_{i-1} - [(T_1+ T_2+ T_3+ T_4) D_i+ T_5E_i] Y_i$$
$$+ (T_3+ T_4) D_{i+1}Y_{i+1} = \bar{T}_5F_i \tag{A.4}$$

where

$$\begin{aligned} T_1 &= W_{1,i} C_{i+1} C_i B_{i-1} A_i \\ T_2 &= W_{1,i} C_{i+1} C_{i-1} B_i A_i \\ T_3 &= W_{2,i} C_i C_{i-1} B_{i+1} A_i \\ T_4 &= W_{2,i} C_{i+1} C_{i-1} B_i A_i \\ T_5 &= W_{3,i} C_{i+1} C_i C_{i-1} \end{aligned} \tag{A.5}$$

for $i = 2, 3, \ldots\ldots, n-1$. The weighting functions $W_{j,i}$ are defined as

$$\begin{aligned} W_{1,i} &= x_{i+1} - x_i \\ W_{2,i} &= x_i - x_{i-1} \\ W_{3,i} &= (x_{i+1}-x_i)\ (x_{i+1}-x_{i-1})\ (x_i-x_{i-1}) \end{aligned} \tag{A.6}$$

Note that the W functions depend only on the grid spacing and hence can be calculated when the grid is defined and/or changed and stored for later use. Using the Eq. (2.33) and Eq. (2.45) forms of the JAY and RAY equations respectively, the W functions depend only on $\tau(r)$ and can be used for both equations. For the RAY equation μ is tabularized as a function R and B.

At the boundaries DY is expanded in a second-order Taylor series

in a manner described by Auer (1967). Eq. (A.2) is used to evaluate the first-order derivative of DY and Eq. (A.1) is used to evaluate the second-order derivative. At the inner boundary we get the following relationship between Y_1 and Y_2

$$[A_1B_1C_2D_1G_1 + \gamma_1H_1 + \delta_1E_1]\ Y_1 - A_1B_1C_2D_2G_1Y_2 = -\gamma_1I_1 - \delta_1F_1 \qquad \text{(A.7)}$$

(Inner B.C.)

where

$$\gamma_1 = \tfrac{1}{2}A_1(x_2-x_1)\ (3B_1C_2 - B_2C_1)$$
$$\delta_1 = \tfrac{1}{2}(x_2 - x_1)^2\ C_1C_2G_1\ . \qquad \text{(A.8)}$$

At the outer boundary,

$$-A_nB_nC_{n-1}D_{n-1}G_nY_{n-1} + [A_nB_nC_{n-1}D_nG_n - \gamma_nH_n + \delta_nF_n]\ Y_n = -\delta_nF_n + \delta_nI_n \qquad \text{(A.9)}$$

(Outer B.C.)

where

$$\gamma_n = \tfrac{1}{2}A_n(x_n - x_{n-1})\ (3B_nC_{n-1} - B_{n-1}C_n)$$
$$\delta_n = \tfrac{1}{2}(x_n - x_{n-1})^2\ C_nC_{n-1}G_n\ . \qquad \text{(A.10)}$$

The inner boundary of the RAY equation requires more care because μ is identically zero on the symmetry line. Thus we use Eqs. (2.52) and (2.53) at the inner boundary.

Eqs. (A.4), (A.7) and (A.9) form a diagonally dominant tridiagonal system of linear equations that are easily solved using the Gausian elimination method (Greenspan 1970).

Finally, the W weights can be used to calculate radial derivatives of a general function f(x) using a three-point approximation.

$$\left.\frac{df(x)}{dx}\right|_{x = x_i} \approx - \frac{W_{2,i}^2 f(x_{i-1}) + (W_{2,i}^2 - W_{1,i}^2) f(x_i) + W_{1,i}^2 f(x_{i+1})}{W_{3,i}} \quad . \quad (A.11)$$

APPENDIX B

SEMI-ANALYTIC MODELS

B.1 Introduction

In this appendix we discuss the ionization structure of hydrogen and helium. This discussion is a condensed form of Petrosian and Dana (1975, Paper I) and Dana and Petrosian (1976, Paper II) For a general form of the frequency dependence of the dust extinction coefficient in the UV, we derive coupled differential equations which can easily be solved numerically for the Strömgren radii of hydrogen and helium. We present approximate analytic expressions for the evaluation of the variation of the fraction of ionizing radiation absorbed by gas, f_{gas}, and the ratio of the volume emission measures of HeII to HII regions, L_{He^+}, with the spectrum of the ionizing source, helium abundance and absorption properties of dust As before we assume spherically symmetric nebulae and we use frequency averaged cross sections and intensities. We will apply these models to dusty HII regions excited by O or B stars so that no doubly ionized helium exists. Equivalently, we could apply these models to the regions of the nebulae outside of the HeIII Strömgren sphere.

B.2 Equations of Transfer for UV Photons

We shall be dealing with fluxes and intensities integrated over frequency. We must distinguish between photons capable of ionizing only hydrogen and those capable of ionizing both hydrogen and helium

We therefore define net fluxes through spherical shells

$$S_1(r) = \int_{\nu_0}^{1.807\nu_0} d\nu\ S_\nu(r),\quad S_2(r) = \int_{1.807\nu_0}^{4\nu_0} d\nu\ S_\nu(r), \tag{B.1}$$

$$S(r) = S_1(r) + S_2(r),\quad \gamma(r) \equiv S_2(r)/S(r),\quad \gamma_0 = \gamma(r_0)$$

and similar expressions for the intensities $I(r)$ and $J(r)$. We use $4\nu_0$ as the maximum frequency because photons with $\nu > 4\nu_0$ will be absorbed in a small HeIII region interior to the region of validity of these models.

Average hydrogen cross sections for $\nu < 1.807\nu_0$ and for $\nu > 1.807\nu_0$ are defined as

$$\sigma_{H,1}\ J_1(r) = \int_{\nu_0}^{1.807\nu_0} d\nu\ \sigma_H(\nu)\ J_\nu(r), \tag{B.2}$$

$$\sigma_{H,2}\ J_2(r) = \int_{1.807\nu_0}^{4\nu_0} d\nu\ \sigma_H(\nu)\ J_\nu(r),$$

so that the total average hydrogen cross section is

$$\sigma_H = \sigma_{H,1}\ \frac{1 + (1-\beta)J_2/J_1}{1 + J_2/J_1}\ , \tag{B.3}$$

$$\beta \equiv 1 - \sigma_{H,2}/\sigma_{H,1}\ .$$

Similarly, for dust we define $\sigma_{d,1}$ and $\sigma_{d,2}$ so that

$$\sigma_d = \sigma_{d,1} \frac{1 + (1+\alpha)J_2/J_1}{1 + J_2/J_1} \quad , \quad 1 + \alpha \equiv \sigma_{d,2}/\sigma_{d,1} \quad . \qquad (B.4)$$

In these models we will characterize the dust by its optical depth averaged over the frequency range $\nu_0 \leq \nu < 1.807\nu_0$. Hence the dust extinction cross section at the Lyman limit is replaced by $\sigma_{d,1}$ in our formulas for $\hat{S}_0$ (Eq. 3.24), ε (Eq 3 28) and for the optical depth functions τ and R.

For helium we have one average cross section σ_{He} (the He^+ notation is unnecessary because He^{++} does not exist in this model) defined as

$$\sigma_{He} J_2(r) = \int_{1.807\nu_0}^{4\nu_0} d\nu \, \sigma_{He}(\nu) \, J_\nu(r) \qquad (B.5)$$

We now define separate average cross sections σ_x^* and σ_x^D for the stellar and diffuse radiation. For σ_x^* the average intensities J_1 and J_2 can be replaced by S_2^* and S_1^*, respectively.

We will use the on-the-spot approximation (i.e. diffuse UV recombination photons are absorbed by the gas where they are emitted) and set the dust albedo $\omega_\nu \equiv 0$. With these approximations the diffuse UV radiation satisfies the relations

$$(1 - x)n(r)\sigma^{D}_{H,1}\, 4\pi\, J^{D}_{1}(r) = xn(r)n_e\, \alpha^{1}_{H} + \zeta_1 Yyn(r)n_e\, \alpha^{B}_{He}$$

$$(1 - y)Yn(r)\, \sigma^{D}_{He}\, (1 + \rho)4\pi J^{D}_{2}(r) = Yyn(r)n_e \alpha^{1}_{He} \qquad \text{(B.6)}$$

where ζ_1 is the fraction of photons from recombinations to excited states of helium that are capable of ionizing hydrogen ($\zeta_1 = 0.96$ with the approximations of Section 3.4) and

$$\rho = \sigma^{D}_{H,2} / Y\sigma^{D}_{He} \approx (1 - x)\sigma_H(1.807\nu_0)/[Y(1 - y)\sigma_{He,0}] \qquad \text{(B 7)}$$

is the fraction of recombination photons to the ground state of helium that are absorbed by hydrogen*. Upon substitution of equations (B.6) into the ionization equilibrium equation (Eq. 3 2 with $\delta = \delta' = 0$), the dimensionless ionization equations (Eq. 3.29) become

$$(1 - x) = (x + Yy)[x - y\tilde{Y}(\zeta_1 + \zeta_2)]\, A_H R^2 \mathcal{G}_g[1 - \beta^* \gamma(\tau)] \,/\, \hat{S}^*(\tau)$$

$$(1 - y) = y(x + Yy)[1 + \zeta_2]\, A_{He} R^2 \mathcal{G}g/[\gamma(\tau)\hat{S}^*(\tau)] \qquad \text{(B.8)}$$

---

*In most OSA calculations this fraction (and consequently the quantity ζ_2 in Eq. B.8) is set equal to zero. If this were the case, the absorption of J_2 photons by hydrogen could also be neglected. As we shall see below, neglecting ρ or ζ_2 with respect to unity will cause up to a 30 percent underestimation of γ_0 or a similar overestimation of Y.

where*

$$A_H = \epsilon/[\hat{S}_0(\sigma^*_{H,1}/\sigma_0)]$$
$$A_{He} = \epsilon\alpha^B_{He} \,/\, [\hat{S}_0\alpha^B_H(\sigma^*_{He}/\sigma_0)] \tag{B.9}$$

and we have defined

$$\tilde{Y} = Y\alpha^B_{He}/\alpha^B_H \,, \quad \zeta_2 = \alpha^1_{He}\,\rho/[\alpha^B_{He}(1+\rho)]. \tag{B.10}$$

Substitution of these equations into the equations governing radiative transfer of stellar photons $(dS^*_1/dr = -\kappa_{tot,1}S^*_1)$ gives

$$dS^*_1/dr = -\kappa^*_{d,1}\,S^*_1 - 4\pi r^2 n(r) n_e \alpha^B_H\,[x + \hat{Y}y(\zeta_1 + \zeta_2)]\sigma^*_{H,1}S^*_1/\sigma^*_H S^* \tag{B.11}$$

$$dS^*_2/dr = -\kappa^*_{d,2}\,S^*_2 - 4\pi r^2 n(r) n_e \alpha^B_H \Big\{ (1+\zeta_2)y\tilde{Y} + [x - \tilde{Y}y(\zeta_1+\zeta_2)]\,\sigma^*_{H,2}S^*_2/\sigma^*_H S^* \Big\} \,. \tag{B.12}$$

Addition of these two equations gives

$$dS^*/dr = -\kappa^*_d S^* - 4\pi r^2 n(r) n_e \alpha^B_H\,[x + y\tilde{Y}(1-\zeta_1)] \,, \tag{B.13}$$

which for $\zeta_1 = 1$ is identical to Eq. (25) of paper I for nebulae with dust and hydrogen only (note also that $\kappa^*_d/\kappa^*_{d,1} = 1 + \alpha^*\gamma$ depends on γ).

---

*Note that $\sigma^*_H = \sigma^*_{H,1}\,(1 - \beta^*\gamma)$

From here on we shall be dealing only with stellar photons. Therefore we shall eliminate the asterisk notation in what follows. If we eliminate S_1 and S_2 in favor of S and γ in Eqs (B.11) and (B.12), the general equations for stellar photons are

$$\begin{aligned} d\hat{S}/d\tau &= -(1 + \alpha\gamma)\hat{S} - \hat{\Sigma}(\tau) \\ d\gamma/d\tau &= -\alpha\gamma(1 - \gamma) + (1 - \gamma)(\beta\gamma - \gamma')(1 - \beta\gamma)^{-1}\,\hat{\Sigma}(\tau)/\hat{S} \end{aligned} \tag{B.14}$$

where

$$d\tau = \kappa_{d,1}\,dr, \quad \hat{S}(\tau) = \hat{S}^{*}(\tau)/S_0$$

$$\hat{\Sigma}(\tau) = [x + y\tilde{Y}(1 - \zeta_1)](x + y\gamma)[R^2\alpha_g^2/\alpha_d]\hat{S}_0 \tag{B.15}$$

$$\gamma' = \frac{y\tilde{Y}(1 + \zeta_2)}{x + y\tilde{Y}(1 - \zeta_1)} \quad .$$

We shall ignore $(1 - x)$ and $(1 - y)$ with respect to unity in Eqs. (B.11) - (B.15) (e.g. paper I). This is true everywhere (in particular for large dust optical depths) except very near the ionization fronts. This amounts to setting $x = 1$ and $y = 1$ inside of their respective Strömgren spheres in Eqs. (B.11) - (B.15).

B.3 Pure Hydrogen Nebulae

For nebulae without helium ($y = Y = \alpha = \beta = 0$), Eqs. (B 8) and (B.14) reduce to

$$(1 - x) = x^2 A_H R^2 G_g / \hat{S}(\tau) \qquad \text{(B 16)}$$

$$d\hat{S}/d\tau = -\hat{S} - x^2 (R^2 G_g^2 / G_d)/\hat{S}_0 \qquad \text{(B 17)}$$

These equations are equivalent to Eqs. (23) and (25) of paper I.[1] Eq (B.17) is easily solved to give

$$\hat{S}(\tau) = e^{-\tau}[1 - g(\tau)/\hat{S}_0] \qquad \text{(B.18)}$$

where

$$g(\tau) = \int_0^\tau dt\ x^2 R^2(t) G_g^2(t) e^t / G_d(t) \qquad \text{(B.19)}$$

and we have used the normalization of $\hat{S}(\tau)$ (Eqn. 2.30) as the initial condition of Eq. (B.17). In practice x is set equal to 1 inside of the hydrogen Strömgren sphere and $g(\tau)$ becomes a simple function of τ once the radial dependence of the dust and gas densities [$G_d(r)$ and $G_g(r)$] have been specified. For uniform nebulae,

$$g(t) = e^t \tilde{g}(t + R_0) - \tilde{g}(R_0)$$

$$\tilde{g}(x) = x^2 - 2x + 2 \qquad \text{(B.20)}$$

where R_0 is the inner radius of the nebula in optical depth units (Eqn. 2.24).

Equation (B.18) points out the role of $\hat{S}_0$ in determining the optical depth of a nebula. The Strömgren radius is defined in this model when $\hat{S}(\tau) = 0$. This occurs when $g(\tau_1) = \hat{S}_0$. (Note that $g(\tau)$ is a monotonically increasing function of τ for the power law density variations of section 2.4). Although this is the only model where τ_1 can be determined analytically, $\hat{S}_0$ plays an analogous role in all of our models including the QDM model.

The ionization of hydrogen can now be calculated from Eqs. (B.16) and (B.18). Interior to the Strömgren radius, $(1 - x)$ is given by the right-hand side (with $x = 1$) of Eq. (B.16). At the Strömgren sphere, however, the quadratic form of Eq. (B.16) must be solved to give

$$(1 - x) = [1 + A(\tau)] - \sqrt{[1 + A(\tau)]^2 - 1} \qquad \text{(B.21)}$$

where

$$A(\tau) = \hat{S}(\tau)/2A_H R^2 G_g \ . \qquad \text{(B.22)}$$

For nebulae without dust, Eq. (B.19) with $\kappa_d = 0$, gives

$$d\hat{S}/d\tau_H = -x^2 R^2 G_g/\hat{S}_0 \ , \quad d\tau_H = n(r)\sigma_{H,1} dr \qquad \text{(B.23)}$$

and $\hat{S}_0$ is given by Eq. (3.24) with $n_d(r_0)\sigma_{d,0} = n(r_0)\sigma_{H,1}$. The solution to Eq. (B.23) is

$$\hat{S}(\tau_H) = 1 - \xi(\tau_H)/\hat{S}_0 \qquad (B.24)$$

where

$$\xi(\tau_H) = \int_0^{\tau_H} dt x^2 R^2(t) G_g(t) \qquad (B.25)$$

and τ_H is the optical depth of neutral hydrogen at the Lyman limit. Again, the role of $\hat{S}_0$ is apparent from Eq. (B.24). For uniform nebulae (with x = 1 inside of Strömgren sphere),

$$\xi(\tau_H) = \tfrac{1}{3}(\tau_H + R_0)^3 - \tfrac{1}{3}R_0^3 \quad . \qquad (B.26)$$

The ionization structure is given by Eq. (B.21).

B.4 Nebulae with Hydrogen and Helium

Since to our knowledge there are no approximate solutions for nebulae with hydrogen and helium but without dust, we consider this case first. With $\kappa_d = 0$, Eqs. (B.14) and (B.15) reduce to

$$\hat{S}(\tau_H) = 1 - \tilde{\xi}(\tau_H)/\hat{S}_0 \quad , \qquad (B.27)$$

$$\frac{d\gamma}{d\hat{S}} = \frac{-1}{\hat{S}} \frac{(1 - \gamma)(\beta\gamma - \gamma')}{(1 - \beta\gamma)}$$

where

$$\tilde{\xi}(\tau_H) = \int_0^{\tau_H} dt[x + y\tilde{Y}(1 - \zeta_1)](x + Yy)R^2(t)Q_g(t) \qquad (B.28)$$

To evaluate Eq (B.28), x and y are set equal to 1 inside of their respective Strömgren spheres and are set equal to 0 outside.

The parameters β and Y' in Eq (B.28) vary throughout the nebula The variation of β is due to the change in the spectrum of UV photons. However, since the photoionization cross section of hydrogen decreases rapidly with frequency $(\sigma_H(\nu) \propto \nu^{-3})$, $\beta \approx 1 - (1/1.807)^3 \sim 0.8$ and changes by a few percent for a variety of plausible spectra (cf. Table VI) We therefore neglect the variation of β. The parameter Y', on the other hand, varies because of the variation of ζ_2, which is primarily due to the change of the ratio $(1 - x)/(1 - y)$ in Eq (B.7). In general, if $\gamma_0 < Y$, then $\zeta_2 \ll 1$ and it can be ignored However, for $\gamma_0 > Y$, $\zeta_2 > 0.1$ in the inner regions and near the edge of the nebula where $\gamma \to 1$, $\zeta_2 \to \alpha^1_{He}/\alpha^B_{He} \sim 0.6$ (for $T_e = 10^4$ ^oK). As we shall see below, even in this case the variation of ζ_2 is negligible. Thus we shall assume that Y' is also constant.

Equation (B.27) is now readily solved·

$$\hat{S}(\tau_H) = \left(\frac{1-\gamma(\tau_H)}{1-\gamma_0}\right)^{\frac{1-\beta}{\beta-Y'}} \left(\frac{\beta\gamma_0 - Y'}{\beta\gamma(\tau_H) - Y'}\right)^{\frac{1-Y'}{\beta-Y'}} \qquad (B.29)$$

Figure 12 shows the variation of γ with $\hat{S}$ for various values of γ_0 (solid lines) For $\beta\gamma_0 = Y'$, $\gamma = \gamma_0 =$ constant. For $\beta\gamma_0 < Y'$, γ (and therefore $\hat{S}_2$) becomes zero at

TABLE VI

AVERAGE CROSS SECTIONS AND STELLAR PARAMETERS

$T(^{o}K)^{\dagger}$	γ_0	β	$\sigma_{H,1}/\sigma_0$	σ_{He}/σ_0
90300.	0.500	0.837	0.452	0.688
62200.	0.300	0.808	0.487	0.832
50000.	0.194	0.793	0.514	0.900
40000.	0.108	0.787	0.555	0.959
40000.††	0.268	0.831	0.528	0.802
37500.	0.0887	0.786	0.564	0.979
30900.	0.0445	0.785	0.602	1.023
30000.††	0.0013	0.790	0.747	1.123
$n = 2^{*}$	0.553	0.916	0.507	0.410
$n = 4^{*}$	0.169	0.855	0.585	0.754

*Averaged over power law distribution $S_\nu = S_0(\nu_0/\nu)^n$.

†Averaged over black body distribution $B_\nu(T)$.

††Averaged over model atmosphere (Auer and Mihalas 1972)

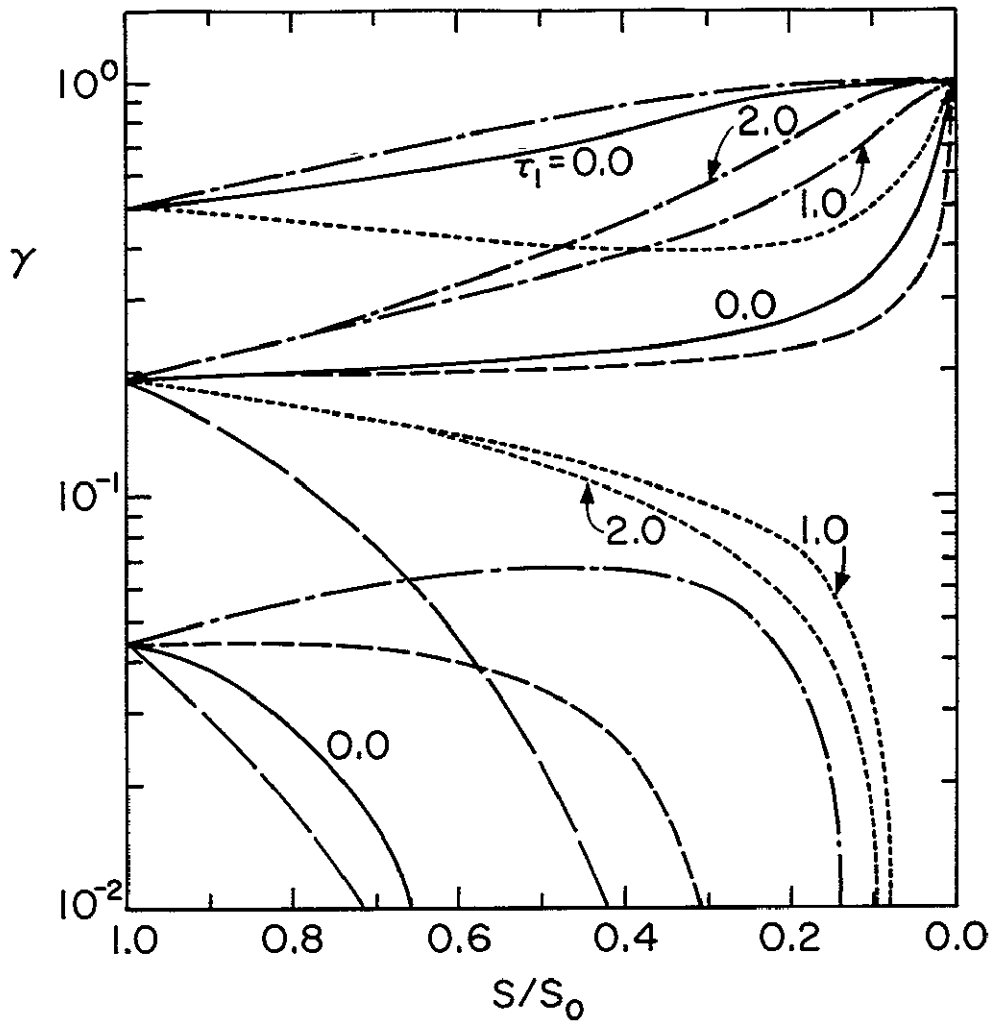

Fig. 12. Variation of $\gamma(\tau)$ Versus $S(\tau)$ for Various τ_1 and γ_0. The values γ_0=0.50, 0.194 and 0.0445 correspond to black body stellar temperatures of 90,300, 50,000 and 30,900 °K respectively. The solid lines are for nebulae without dust (τ_1=0). Four different dust cross sections were used. α= -1 (dash-dot line), α = 0 (short dash), α = 1 (dot), α = 5 (long dash), where 1 + α = $\sigma_{d,2}/\sigma_{d,1}$. Two cases where τ_1=2 are plotted and labeled.

All other cases are for τ_1= 1. All curves are for uniform gas and dust distributions.

$$\hat{S} = \hat{S}_{cr} = (1-\beta\gamma_0/Y')^{(1-Y')/(\beta-Y')}(1-\gamma_0)^{(\beta-1)/(\beta-Y')} \qquad (B.30)$$

or at $r = r_2$ where r_2 is obtained from Eq. (B 28) with $\xi = \xi_2 \equiv 1 - \hat{S}_{cr}$. Thus in these cases the helium Strömgren sphere is inside of the hydrogen Strömgren sphere. For $\beta\gamma_0 > Y'$, γ increases toward the outer edge and approaches unity at the hydrogen Strömgren radius where $\hat{S} = 0$. As is evident, the shape of these curves is determined primarily by the value of γ_0 (actually by the value of $\beta\gamma_0/Y'$).

Once the variations of $\hat{S}$ and γ are known, the ionization structure can be calculated with Eqs (B 8) - (B.10). Since $1 0 < (\zeta_1 + \zeta_2) \leq 1.4$, Eq. (B.8) can be approximated as $(1-x) = A(\tau)x^2$ ($A(\tau)$ is equal to A_H times the radial functions on the right-hand side of Eq. B.8) A few values of $\sigma_{H,1}/\sigma_0$ and σ_{He}/σ_0 are given in Table VI. The slow variation of these quantities due to changes in the spectrum of UV radiation throughout the nebula are neglected in this treatment.

Equation (B.8) can now be solved for (1-y) using the above values of x and assuming ζ_2 = constant. This assumption is clearly justified because $R^2\mathcal{G}_g(1-\beta\gamma)/\hat{S}$ varies much more rapidly than any expected variation of ζ_2. The results of these calculations are shown in Figure 13a for various values of γ_0, Y = 0.1, and uniform nebulae. We also show the variation of ζ_2. As is evident, the assumption of constancy of ζ_2 is a good approximation for small values of γ_0. For small values of γ_0, $\zeta_2 \ll 1$ so that $Y' \approx \tilde{Y} \approx 1.05Y$ (for $T_e = 10^4$ °K, c.f. Burgess and Seaton 1960). For large values of

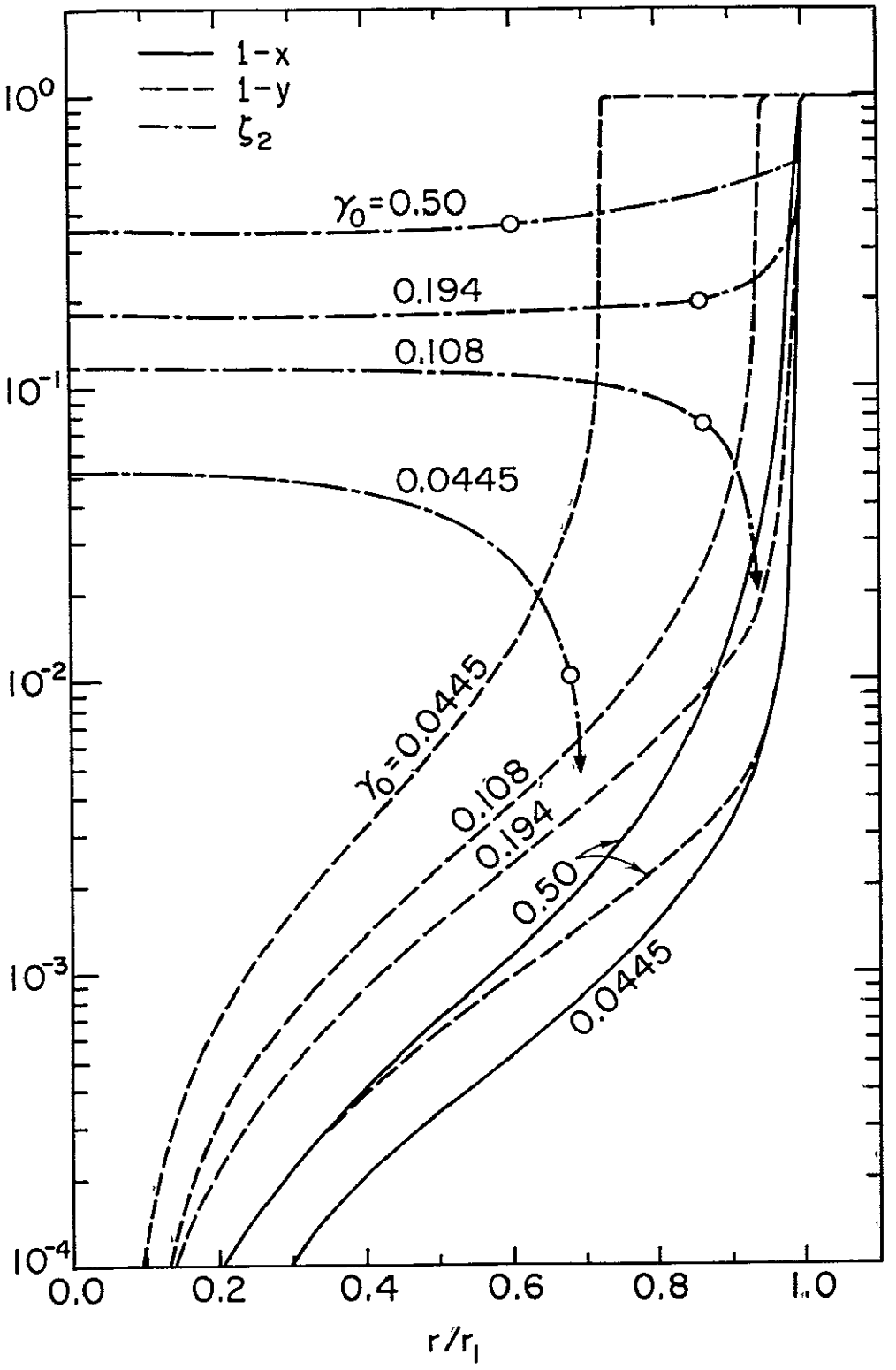

Fig. 13a. Ionization Structure of Hydrogen and Helium. The neutral fraction of hydrogen (solid lines) and helium (dashed lines) and ζ_2 (dash-dot) for uniform dustless nebulae as a function of normalized radius r/r_1. The open circles denote the volume average of ζ_2. Y = 0.1.

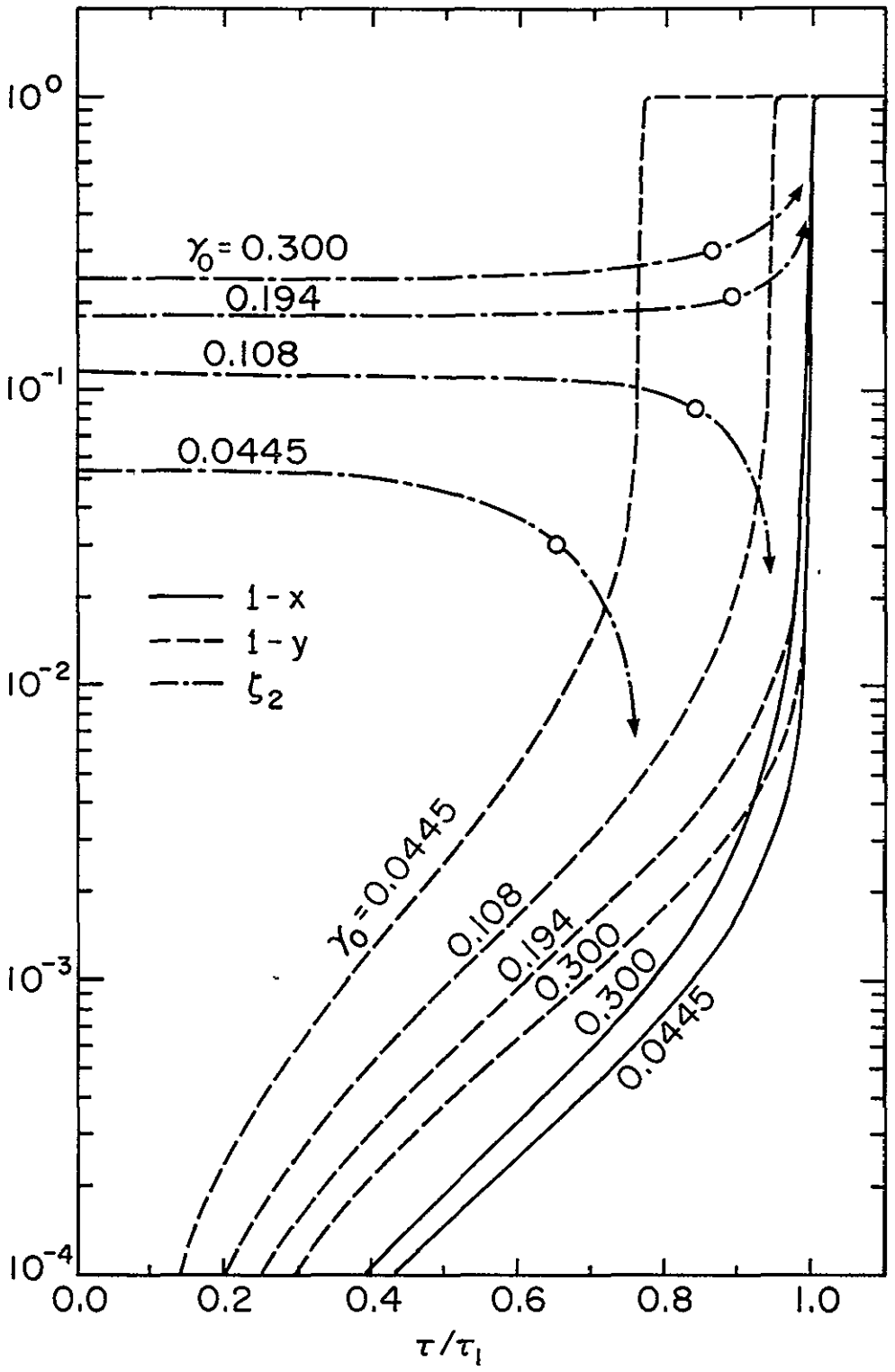

Fig. 13b. Ionization Structure of Hydrogen and Helium. The neutral fraction of hydrogen and helium and ζ_2 as functions of τ/τ_1 for uniform dusty nebulae with a constant dust cross section ($\alpha = 0$). $\tau_1 \approx 1.0$ and Y = 0.1 for all cases. The symbols are the same as in Fig. 13a.

γ_0, ζ_2 varies slowly but is no longer negligible compared to unity. Therefore, neglecting ζ_2 as is commonly done, will result in an incorrect determination of the value of γ_0/Y' from observations. For example, for a given value of Y and observed value of r_2/r_1 (r_1 is the H Strömgren radius and r_2 is the He Strömgren radius), the required value of γ_0 is underestimated when ζ_2 is neglected. In general, for small values of r_2/r_1, ζ_2 is negligible and is rarely exceeds 0.4.

For nebulae with dust and with hydrogen and helium, simple analytic solutions to the coupled differential equations (B.14) are possible only if α is negligible or zero, i.e. only if $\sigma_d(\nu)$ varies slowly so that $\sigma_{d,1} \approx \sigma_{d,2}$. In this case we have plotted on Figure 12 the variation of γ with $\hat{S}$ (dashed lines). Using these results, we have calculated (1-x), (1-y) and ζ_2 for uniform nebulae, $\epsilon = 2 \times 10^{-4}$, and $\tau_1 \approx 1.0$. These results are presented in Figure 13b. Comparison of Figures 13a and 13b show that for a given size r_1 of the nebula, introducing dust increases the fractional ionization of both hydrogen and helium. This is primarily due to the increased value of S_0, and thus of $\hat{S}(\tau)$ throughout the nebula.

When $\alpha \neq 0$, simple analytic solutions are not possible. However, Eq. (B.14) can readily be solved numerically. On Figure 12 we present γ versus $\hat{S}$ for a few values of α. In general we find that the shapes of the (1-x) and (1-y) curves are nearly independent of the details of the problem and are determined primarily by the values of $\hat{S}_0$ and γ_0. Consequently, we do not present the ionization structures for $\alpha \neq 0$.

B.5 Observable Parameters

Since we treat fluxes integrated over frequency, we lose most of the information on the variation of the spectrum of UV radiation throughout the nebula. Consequently, we cannot calculate the ionization structures of the trace elements with these semi-analytic models. The main result of these solutions is the ionization structure of hydrogen and helium. Hence we can calculate f_{gas} and L_{He} (we have neglected doubly ionized helium so L_{He} refers only to He^+)

The fraction of ionizing radiation absorbed ("destroyed", cf. section 3.8) by gas is

$$f_{gas} = \frac{4\pi\alpha_H^B}{S_0}\int_{r_0}^{r_1} dr(x + Yy)[X - \tilde{Y}y(1 - \zeta_1)]r^2n^2(r)$$
$$= \hat{S}_0^{-1}\int_0^{\tau_1} dt[x + \tilde{Y}y(1 - \zeta_1)](x + Yy)R^2(t)G_g^2(t)/G_d(t) \quad . \tag{B.31}$$

For $\zeta_1 \approx 1$, Eq. (B.31) reduces to

$$f_{gas} = [f(\tau_1) + Yf(\tau_2)]/\hat{S}_0 \tag{B.32}$$

where

$$f(\tau) = \int_0^{\tau} dtR^2(t)G_g^2(t)/G_d(t) \tag{B.33}$$

and τ_2 is the dust optical depth at the helium Strömgren radius.

The ratio of the intensity of helium to hydrogen recombination

lines (Eq. 3.36) is equal to

$$L_{He} = (1 + Y)f(\tau_2)/\hat{S}_0 f_{gas} \qquad (B.34)$$

As explained previously (Petrosian 1973, 1974), for a given value of γ_0/Y the presence of dust with $\sigma_d(\nu) \approx$ constant (i.e. $\alpha = 0$) increases the value of L_{He} with increasing values of the total dust optical depth τ_1. For negative values of α ($\sigma_{d,1} > \sigma_{d,2}$), fewer He ionizing photons compared with H ionizing photons are absorbed by the dust and L_{He} is larger The reverse occurs for positive values of α. It should be noted the L_{He} depends on γ_0/Y but is insensitive to the value of Y. L_{He} is also fairly independent of non-uniformities or inhomogeneities in the dust and gas distribution as long as the dust-to-gas ratio is constant. However, L_{He} changes for dust and gas distributions that are not the same.

Note that because we have used the approximations $x = 1$ for $r \leq r_1$ and $y = 1$ for $r \leq r_2$ the ratio $L_{He} \leq 1$.

REFERENCES

Aldrovandi, S. M. V. and Péquignot, D., 1973, Astr. Ap., 25, 137.

Auer, L. H., 1967, Ap. J. (Letters), 150, L53.

Auer, L. H., 1971, J. Quant. Spectrosc. and Rad. Trans., 11, 573.

Auer, L. H. and Mihalas, D., 1970, M.N.R.A.S., 149, 65.

Auer, L.H. and Mihalas, D., 1972, Ap. J. Suppl., No. 205, 24, 193.

Balick, B., 1975, Ap. J., 201, 705.

Balick, B. and Sneder, C., 1976, Ap. J., 208, 336.

Bohlin, R. C., Marionni, P. A. and Stecher, T. P., 1975, Ap. J., 202, 415.

Burgess, A. and Seaton, M. J., 1960, M.N.R.A.S., 121, 471.

Chandrasekhar, S., 1960, Radiative Transfer (New York: Dover) p. 23.

Dana, R. A. and Petrosian, V., 1976, Ap. J., 208, 354 (Paper II).

Davison, B., 1957, Neutron Transport Theory (Oxford: Clarendon Press).

Dycke, H. M. and Simon, T., 1977, Ap. J., 211, 421.

Flower, D. R., 1968, Planetary Nebulae (IAU Symposium No. 34), ed. D. E. Osterbrock and C. R. O'Dell (Dordrecht: Reidel), p. 205.

Greenspan, D., 1970, Introduction to Numerical Analysis and Applications (Chicago: Markham), p. 53.

Henrey, R. J. W., 1970, Ap. J., 161, 1153.

Hjellming, R. M., 1966, Ap. J., 143, 420.

Hummer, D. G. and Rybicki, G. B., 1971, M.N.R A.S., 152, 1.

Hummer, D. G. and Seaton, M. J., 1963, M.N.R.A.S., 125, 437.

Hummer, D. G. and Seaton, M. J., 1964, M.N.R.A.S., 127, 217.

Jameson, R. F., Longmore, A. J., McLinn, J. A. and Woolf, N. J., 1974, Ap. J., 190, 353.

Kirkpatrick, R. C., 1972, Ap. J., 176, 381.

Kirkpatrick, R. C., 1977, private communication.

Kleinmann, D. E., Gillett, F. C. and Wright, E. L., 1976, Ap. J., 208, 42.

Knacke, R. F. and Thomson, R. K., 1973, Pub. A.S.P., 85, 341.

Krügel, E., 1975, Astr. Ap., 38, 129.

Lamarsh, J. R., 1966, Nuclear Reactor Theory (Reading, Massachusetts Addison-Wesley).

Leung, C. M., 1975, Ap. J., 199, 340.

Mathis, J. S., 1970, Ap. J., 159, 263.

Mathis, J. S., 1971, Ap. J., 167, 261.

Mathis, J. S., 1972, Ap. J., 176, 651.

Mezger, P. G., Smith, L. F. and Churchwell, E., 1974, Astr. and Ap., 32, 269.

Natta, A. and Panagia, N., 1976, Astr. Ap., 50, 191.

Osterbrock, D. E., 1974, Astrophysics of Gaseous Nebulae (San Francisco: Freeman) (AGN).

Panagia, N., 1973, A. J., 78, 929.

Péquignot, D., Aldrovandi, S. M. V. and Stasinska, G., 1977, preprint.

Petrosian, V., 1973, in IAU Symposium 52, Interstellar Dust and Related Topics, ed. J. M. Greenberg and H. C. van de Hulst (Dordrecht: Reidel), p. 445.

Petrosian, V., 1974, in HII Regions and the Galatic Center, Proc. 8th ESLAB Symposium, ed. A. F. M. Moorwood (Froscati: ESROSP-105), p. 173.

Petrosian, V., Silk, J. and Field, G. B., 1972, Ap. J. (Letters), 177, L69.

Petrosian, V. and Dana, R. A., 1975, Ap. J., 196, 733 (Paper I).

Rieke, G. H. and Low, F. J., 1975, Ap. J. (Letters), 199, L13.

Righini, G., Simon, M. and Joyce, R. R., 1976, Ap. J., 207, 119.

Rubin, R. H., 1968, Ap. J., 153, 761.

Sarazin, C. L., 1977, Ap. J., 211, 772.

Seaton, M. J., 1960, Rept. Progr. Phys., 23, 313.

Simon, T. and Dycke, H. M., 1975, M.N.R.A.S., 172, 19P.

Spitzer, J., Jr., 1968, Diffuse Matter in Space (New York: Interscience).

Tarter, C. B., 1967, Ph.D. Thesis, Cornell University.

Telesco, C. M., Harper, D. A. and Loewenstein, R. F., 1976, Ap. J. (Letters), 203, L53.

Telesco, C. M. and Harper, D. A., 1977, Ap. J., 211, 475.

Thronson, H., 1977, Ph.D. Thesis, University of Chicago.

Weisheit, J. C., 1974, Ap. J., 190, 735.

Weisheit, J. C. and Collins, L. A., 1976, Ap. J., 210, 299.

Yorke, H. W., 1977, paper presented at the Symposium on Recent Results in Infrared Astrophysics, January 1977, NASA-Ames Research Center.